

**AFRL-IF-RS-TR-2005-351**  
**Final Technical Report**  
**October 2005**



## **A MICRO HYDROGEN AIR FUEL CELL**

**Case Western Reserve University**

**Sponsored by**  
**Defense Advanced Research Projects Agency**  
**DARPA Order No. J346**

*APPROVED FOR PUBLIC RELEASE; DISTRIBUTION UNLIMITED.*

**The views and conclusions contained in this document are those of the authors and should not be interpreted as necessarily representing the official policies, either expressed or implied, of the Defense Advanced Research Projects Agency or the U.S. Government.**

**AIR FORCE RESEARCH LABORATORY**  
**INFORMATION DIRECTORATE**  
**ROME RESEARCH SITE**  
**ROME, NEW YORK**

## **STINFO FINAL REPORT**

This report has been reviewed by the Air Force Research Laboratory, Information Directorate, Public Affairs Office (IFOIPA) and is releasable to the National Technical Information Service (NTIS). At NTIS it will be releasable to the general public, including foreign nations.

AFRL-IF-RS-TR-2005-351 has been reviewed and is approved for publication

APPROVED:       /s/

WALTER KOZIARZ  
Project Engineer

FOR THE DIRECTOR:       /s/

JAMES A. COLLINS, Deputy Chief  
Advanced Computing Division  
Information Directorate

<b>REPORT DOCUMENTATION PAGE</b>			<i>Form Approved</i> <i>OMB No. 074-0188</i>	
Public reporting burden for this collection of information is estimated to average 1 hour per response, including the time for reviewing instructions, searching existing data sources, gathering and maintaining the data needed, and completing and reviewing this collection of information. Send comments regarding this burden estimate or any other aspect of this collection of information, including suggestions for reducing this burden to Washington Headquarters Services, Directorate for Information Operations and Reports, 1215 Jefferson Davis Highway, Suite 1204, Arlington, VA 22202-4302, and to the Office of Management and Budget, Paperwork Reduction Project (0704-0188), Washington, DC 20503				
<b>1. AGENCY USE ONLY (Leave blank)</b>		<b>2. REPORT DATE</b> OCTOBER 2005	<b>3. REPORT TYPE AND DATES COVERED</b> Final Jul 97 – Sep 04	
<b>4. TITLE AND SUBTITLE</b> A MICRO HYDROGEN AIR FUEL CELL			<b>5. FUNDING NUMBERS</b> C - F30602-97-2-0311 PE - 63739E PR - E117 TA - 00 WU - 31	
<b>6. AUTHOR(S)</b> Robert F. Savinell and Jesse S. Wainright				
<b>7. PERFORMING ORGANIZATION NAME(S) AND ADDRESS(ES)</b> Case Western Reserve University 10900 Euclid Avenue Cleveland Ohio 44106			<b>8. PERFORMING ORGANIZATION REPORT NUMBER</b>  N/A	
<b>9. SPONSORING / MONITORING AGENCY NAME(S) AND ADDRESS(ES)</b> Defense Advanced Research Projects Agency AFRL/IFTC 3701 North Fairfax Drive 525 Brooks Road Arlington Virginia 22203-1714 Rome New York 13441-4505			<b>10. SPONSORING / MONITORING AGENCY REPORT NUMBER</b>  AFRL-IF-RS-TR-2005-351	
<b>11. SUPPLEMENTARY NOTES</b>  AFRL Project Engineer: Walter Koziarz/IFTC/(315) 330-2536/ Walter.Koziarz@rl.af.mil				
<b>12a. DISTRIBUTION / AVAILABILITY STATEMENT</b> APPROVED FOR PUBLIC RELEASE; DISTRIBUTION UNLIMITED.				<b>12b. DISTRIBUTION CODE</b>
<b>13. ABSTRACT (Maximum 200 Words)</b> The object of this project is to produce a microfabricated hydrogen-air fuel cell by combining microfabrication techniques, polymer electrolyte fuel cell technology, and metal hydride fuel storage. The result will be a device capable of providing on-board electrical power for microelectronic circuits, sensors, and actuators with energy storage and power delivery capabilities considerably greater than that of thin-film batteries. Integrated packages of fuel cells (up to three cells in series) and fuel storage/hydrogen generation have been successfully fabricated and tested. Each of the major milestones has been achieved and the fabrication yields and device performance have been improved. We have also been looking for insertion opportunities and partners with which to develop this technology. Recently, we have signed an agreement of collaboration with The Ashlawn Group, LLC, of Alexandria, VA to develop this technology to provide power for "smart" munitions.				
<b>14. SUBJECT TERMS</b> Fuel Cell, MEMS, Micro-Machined, Hydrogen-Air, Micro Power Generation, Micro-Electromechanical Systems			<b>15. NUMBER OF PAGES</b> 119	
			<b>16. PRICE CODE</b>	
<b>17. SECURITY CLASSIFICATION OF REPORT</b>  UNCLASSIFIED	<b>18. SECURITY CLASSIFICATION OF THIS PAGE</b>  UNCLASSIFIED	<b>19. SECURITY CLASSIFICATION OF ABSTRACT</b>  UNCLASSIFIED	<b>20. LIMITATION OF ABSTRACT</b>  UL	

## Table of Contents

Executive Summary.....	1
Introduction.....	2
Experimental.....	2
Conclusions.....	7
Recommendation.....	8
Summary of Publications and Presentations.....	8
Personnel Summary.....	10
Appendix A: Selected Technical Progress Reports.....	11
Appendix B: Summary Of Project Tasks And Milestones.....	103
Appendix C: Microfabricated Fuel Cells.....	106

## **List of Figures**

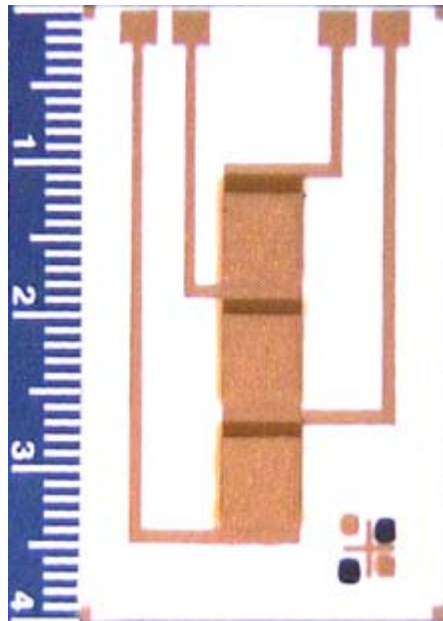
Figure 1: Cross Section View of Microfuel Cell. (Not to scale) * Polymer Electrolyte Membrane (PEM).....	4
Figure 2: Polarization curves obtained with air at 50 and 20%RH. Anode feed: dry Hydrogen Room Temperature.....	5
Figure 3 Exploded view of microfuel cell construction.....	7

## **List of Tables**

Table A: Summary of thick film printer setup for micro fuel cell fabrication.....	3
Table B: Mask Properties and typical Thicknesses of the printed layers.....	3

## EXECUTIVE SUMMARY

The objective of this project is to produce a microfabricated hydrogen-air fuel cell by combining microfabrication techniques, polymer electrolyte fuel cell technology, and metal hydride fuel storage. The result will be a device capable of providing on-board electrical power for microelectronic circuits, sensors, and actuators with energy storage and power delivery capabilities considerably greater than that of thin-film batteries. Integrated packages of fuel cells (up to three cells in series) and fuel storage/hydrogen generation have been successfully fabricated and tested. Each of the major milestones has been achieved and the fabrication yields and device performance have been improved. We have also been looking for insertion opportunities and partners with which to develop this technology. Recently, we have signed an agreement of collaboration with The Ashlawn Group, LLC, of Alexandria, VA to develop this technology to provide power for 'smart' munitions.



**Microfabricated 1.5V fuel cell stack. All components thick film printed.**

## INTRODUCTION

Efficient small-scale power generation is critical to realizing the full benefit of many portable electronic devices. Wireless electronic devices, e.g., micro sensors and micro electromechanical or microfluidic systems, require electrical power for operation and data transmission. The availability of on-board power with appropriate sized power and energy capabilities, coupled with wireless data transmission, will open numerous possibilities for self-sustaining devices for remote or difficult to access locations. The power and energy needs for small portable devices may vary considerably depending on their design and function. Small microfabricated fuel cells open the door for energy delivery devices with independent sizing of power and energy capacity, while having the capability to supply short pulses of peak power without significant adverse effect on energy utilization. Finally, such fuel cells have the potential for energy densities significantly greater than present and predicted battery technology.

This final report presents concepts and results arising from a program at Case Western Reserve University to develop a small and completely microfabricated polymer-based fuel cell with on-board hydrogen storage. The ultimate goal is to co-fabricate a sensor or sensor suite with sufficient analog/digital circuitry for signal conditioning/processing, wireless communications capability (low-power RF) and a power source on a single wafer. The anticipated power requirements are for extended periods of very low (sub - milliwatt) power draws to power the sensor, with random or periodic pulses of 10-100s of milliwatts required for signal processing or data transmission. Potential operational lifetimes are from hours to days (surveillance at a particular location) to years (machinery monitoring). Development of a microfabricated power source is an enabling technology for the autonomous sensor concept. It is envisioned that this power delivery device would operate in a passive mode, without active control of temperature, humidity, reactant pressure or flow rate. This greatly simplifies the construction and operation of the fuel cell. The power density achievable in passive operation will naturally be less than that obtained in conventional fuel cells. However, the applications envisioned do not require high power densities.

## EXPERIMENTAL

This project involved the development of materials and methods for fabricating a miniature fuel cell on a solid substrate, with on-board hydrogen storage. The experimental elements of the project include:

- Formulating inks to print current collectors, anodes and cathodes. Testing the formulations for printing capability, and resulting transport and electrochemical properties.
- Developing techniques to pattern Nafion as an electrolyte under required processing constraints. Testing of electrochemical properties.
- Design and testing of concepts to produce a multi-layer fuel cell device.
- Testing and diagnosing fabricated fuel cells for performance and performance limitations.
- Synthesizing novel polymers and testing for electrochemical and mechanical properties.

- Design and testing an integrated borohydride hydrogen storage system.
- Synthesizing novel metal hydrides and testing for hydrogen storage capacity, cycleability, and equilibrium pressure. Incorporating into the fuel cell structure and testing.

The numerous techniques used in this research, of course, have evolved over the years of this project and specific details have been reported in the semi-annual progress reports. Therefore, selected important progress reports are included here in Appendix A. Tables A and B summarize the procedures used to fabricate the microfuel cells. In Figure 1, a cross section view of the device is shown.

Table A: Summary of thick film printer setup for micro fuel cell fabrication

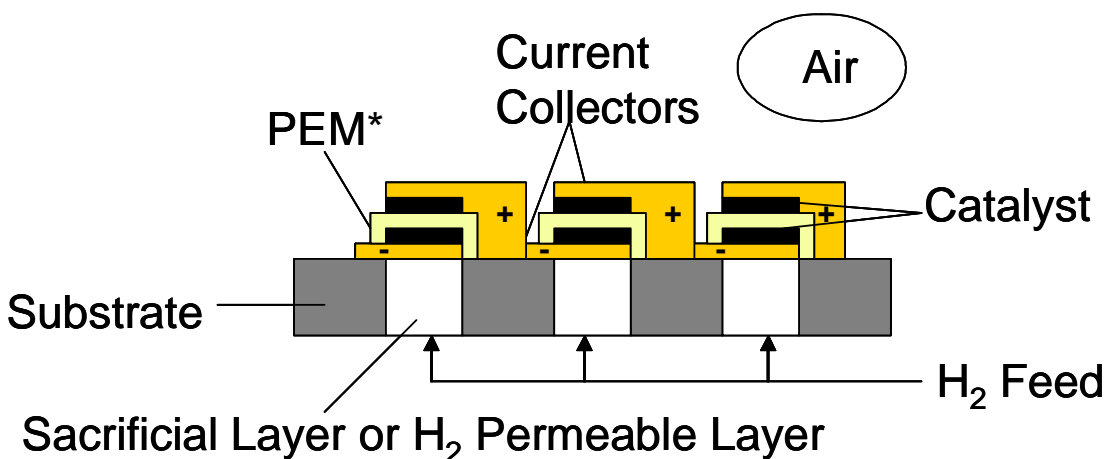
Layer	Snap-off Height	Squeegee Downstop	Squeegee Pressure	Ink	Cure Temp	Cure Time
Default	10 mil	-15 mil	6 lbs.			
Anode Current Collector	10 mil	-15 mil	15 lbs.	Ercon Gold	110°C	10 minutes
Anode	10 mil	1 mil	6 lbs.	DEG based Catalyst	varies	45 minutes
Electrolyte	15 mil	0 mil	6 lbs.	40% Nafion in EG	110°C	20 minutes
Cathode	10 mil	1 mil	6 lbs.	DEG based Catalyst	110°C	10 minutes
Cathode Current Collector	10 mil	-15 mil	6 lbs.	Ercon Gold	110°C	10 minutes

Table B: Mask Properties and typical Thicknesses of the printed layers

Layer	Mask Type	Mask Properties	Thickness (μm)
Anode Current Collector	Screen	280	15-20
Anode	Stencil	1 mil	10-15
Electrolyte	Stencil	4 mil	35-40
Cathode	Stencil	1 mil	10-15
Cathode Current Collector	Screen	280	15-20

The electrochemical testing included potential sweeps (open circuit potential to 0V (short circuit) at 2 mV/s) and impedance scans for all of the fuel cells. The potential sweeps resulted in a polarization curve, and the impedance scans yielded the value of the membrane resistance. These tests were performed at room temperature with air at a controlled relative humidity over the cathodes. The anodes were typically fed dry or 100%RH hydrogen at 5 sccm. Hydrogen pump tests were also performed for some of the cells. These tests are performed with the anode and cathode under hydrogen, and they show the performance of the electrodes. They are very useful in determining the limiting electrode of a fuel cell by enabling the examination of the kinetic performance of each electrode separately.





**Figure 1:** Cross Section View of Microfuel Cell. (Not to scale)

\* Polymer Electrolyte Membrane (PEM)

## RESULTS

Since this project was intended to develop materials and methodologies to fabricate a miniature hydrogen-air fuel cell, the results represent a series of experimental approaches. The details of these approaches and the subsequent results are reported in details through inclusion in Appendix A selected progress reports prepared during the performance of this work. Since the earlier stages of the work were very exploratory, only one report per year of the program is reproduced here. However, the details reported give an indication of the numerous approaches, some successful and others not so successful, and also provide information so others can reproduce, or avoid mistakes, on their own. All the technical reports of the last two years are included because most of the relevant progress occurred, as expected for this type of work, during this time period.

A summary of the status of the fuel cell development is presented here.

Typical results obtained in the last 12 months of this program show that the maximum power output has been increased to  $\approx 7 \text{ mW/cm}^2$  using dry hydrogen and air at 50%RH at room temperature as shown in Figure 2. (Note that Nafion is still used as the electrolyte since new polyimide materials did not meet the requirements of this application.) The highest power density realized under these conditions was  $7.5 \text{ mW/cm}^2$ . The earlier cells were limited by hydrogen access to the anode, which resulted in a limiting current density of  $\approx 15 \text{ mA/cm}^2$ . Fabricating the cells directly on top of the metal hydride material allows sufficient hydrogen accessibility that the cells are now limited by other factors - oxygen access to the cathode and the electrolyte resistance.

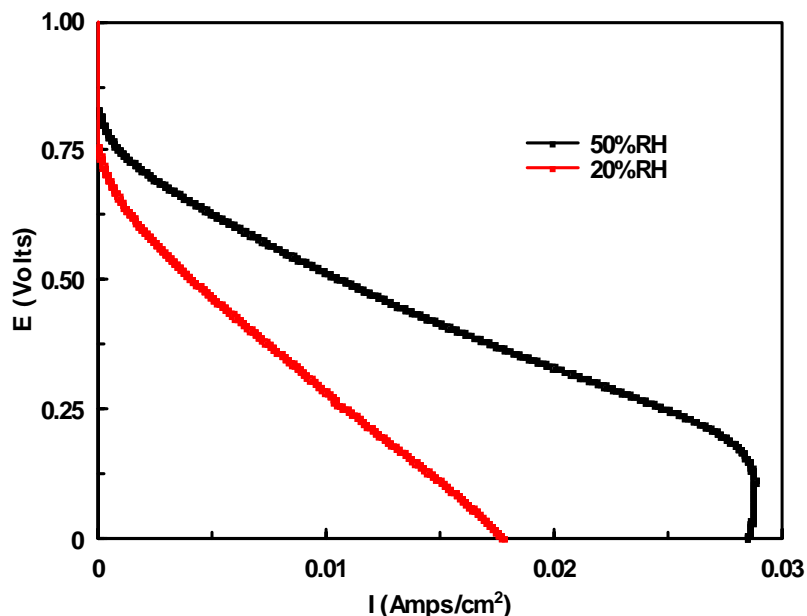


**Figure 2** Polarization curves obtained with air at 50 and 20%RH. Anode feed: dry hydrogen. Room temperature.

Earlier versions of a on-board fuel storage included a successful liquid borohydride system for on-demand delivery of hydrogen to the fuel cell. Although this approach was successful, it was felt that a solid hydrogen storage system might be of higher interest for this type of technology. Therefore, most recent attention was given to developing a on-board metal hydride fuel storage system.. The first generation of improved hydride materials were based on a modified  $\text{LaAl}_x\text{Ni}_{5-x}$  hydride, and made into thick film printable ink using a water-soluble binder. In addition, several second-generation inks, using the same hydride material, but incorporating a non-water-soluble binder have been developed. The first generation inks have now been cycled over 5000 times without loss in hydrogen storage capacity, or a change in the hydrogen sorption/desorption rate. In addition, these inks remained adherent to the substrate (alumina) throughout the cycle tests and have been found to retain their activity even after exposure to ambient humidity air for 55 weeks. The second-generation inks have been developed to expand the fabrication possibilities and to further improve the performance of the hydride storage in the humid fuel cell environment. This effort has also been successful, a non-water-soluble binder has been found that retains the desirable properties of the first generation system; very low binder content (<1 wt%) for high energy density storage, rapid sorption/desorption rates for hydrogen, and the ink can be prepared, printed and cured in ambient air without loss of hydrogen storage activity.

A major cause of fuel cell failure during production is the shorting of the anode catalyst layer to the cathode layer catalyst. The electrolyte layer between the two catalysts is supposed to prevent them from making low resistance electrical contact (see **Figure 3** for structure of the fuel cell). The high fabrication yields and good performance of similar capacitor structures fabricated

on smooth substrates have confirmed that our fabrication issue with the microfabricated fuel cells is primarily related to their substrate. Depositing the hydride material into the through holes in the alumina results in a substrate that is to some extent rough and un-even. In addition, while the adhesion of the gold current collector layer to the alumina is good, its adhesion to the hydride material is considerably weaker. These factors result in much lower fabrication yields – the roughness/un-evenness of the substrate is magnified as each subsequent layer is deposited, and failures due to delamination are also more likely. Although this method of fabrication produces the highest power output as described above, the fabrication yields remain on the order of 50%.

A specific task of this project during the last year of this project is to find insertion opportunities for this technology into military applications. In the past six months we have reached a collaboration agreement with The Ashlawn Group, LLC, of Alexandria, VA to develop this technology to provide power for ‘smart’ munitions. Ashlawn has considerable experience working in the munitions area for the US Army. The agreement covers development of printed fuel cell technology for munitions using CWRU technology developed under this effort. Our goal is to replace the thermal batteries currently used in ‘smart’ munitions. Ashlawn will develop the hydrogen storage and packaging for the microfabricated fuel cell consistent with requirements for munitions, i.e., 10 year shelf life, instantaneous activation, and able to withstand high G accelerations.

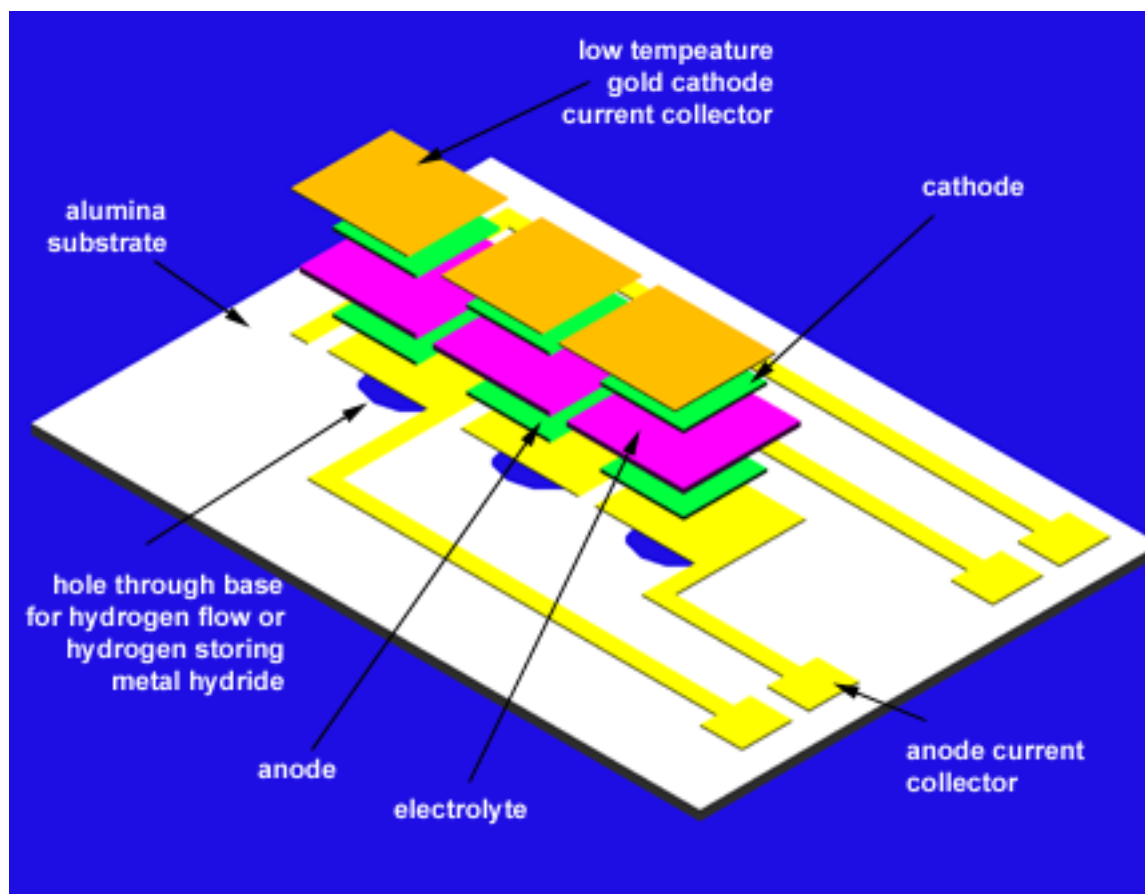


**Figure 3** Exploded view of microfuel cell construction.

Finally, to be consistent with DARPA reporting requirements during this project, in Appendix B are given the detailed task descriptions, status, and technical highlights related to the tasks statements.

## CONCLUSIONS

A small fuel cell stack, operating with on-board hydrogen storage and ambient air, microfabricated using multi-layering of inks and thick-film techniques to form current collectors, electrodes, and electrolytes has been demonstrated. A prototype three-cell stack, of  $0.25 \text{ cm}^2$  each was operated at a power density of  $7 \text{ mW/cm}^2$ . This research developed electrode and membrane inks and printing techniques to fabricate the fuel cells. Two on-board hydrogen storage systems were developed: one based on liquid sodium borohydride solution, and the other based on a solid-state  $\text{LaAl}_x\text{Ni}_{5-x}$  alloy material modified for reversibly high-capacity hydrogen storage (energy density of hydride ink:  $1200 - 1800 \text{ mAh/cm}^3$ ).

## RECOMMENDATION

Further development of this technology would benefit by directing work towards one or two well-defined applications, which cannot be supported by other forms of already available power delivery technology like batteries or capacitors. Such a “killer-ap” would be one that needs the high energy density of the fuel cell, requires the form of a printed device, and has a significant potential for large-scale use. On-board power for chip-type devices such as sensors, data transmitters, etc are some examples. Another example would be power for smart munitions as being pursued by The Ashlawn Group, LLC. Specific target applications would define the energy and power needs and power delivery-time profiles for the device, and would define packaging and processing constraints as well as aid in selecting the form of energy storage.

In the case of solid-state hydride storage design reported here, further work is needed in improving the yield of un-shorted cells. This may require an intermediate layer placed between the hydride storage layer and the current collector, or anode layer.

Since the fuel cell fabrication techniques developed here are also useful for fabricating ultra-capacitors, it is recommended that hybrid fuel cell/capacitor systems be developed, which could provide high power pulses along with long-term energy delivery at low power levels.

Finally, the search for better ionomers for electrolytes should be continued. The need for acceptable ionic conductivity under low-humidity conditions persists, especially in polymers that can be patterned under the processing constraints of a micro-fabricated fuel cell.

## SUMMARY OF PUBLICATIONS AND PRESENTATIONS

### “Microfabricated Fuel Cells”

J. S. Wainright, R. F. Savinell, CC. Liu and M. Litt, *Electrochimica Acta*, 48, 2869, (2003)

### “Molecular design of polyimides toward high proton conducting materials”

Zhang, Yue; Litt, Morton; Savinell, Robert F.; Wainright, Jesse S.; Vendramini, Jerome  
*American Chemical Society, Polymer Preprints, Division of Polymer Chemistry*, 41, 2, 2000, p.1561.

In November 1998, Dr. Jesse Wainright presented a review of this program at the Institute for Defense Analysis for the kick-off meeting of the TBESC Integrated Product Team (IPT) for MEMS transition to Warrior Systems. The presentation was at the request of Dr. Richard Singer, chair of the IPT.

Participated in the DARPA/MEMS Technical Interchange Meeting on Microscale Power Generation hosted by DynCorp, March 22<sup>nd</sup>, 2000.

An invited talk entitled “Polymer Electrolyte Membranes for High Temperature Fuel Cells”, was presented by Morton Litt, at the Gordon Research Conference on Fuel Cells, Bristol, RI, July 2000.

An invited talk entitled “Perspectives on Micro Fuel Cells”, was presented by Jesse Wainright, at the Gordon Research Conference on Fuel Cells, Bristol, RI, August 2001.

An invited paper entitled “Microfabricated Fuel Cells using Thick Film Printing Techniques” was presented by Jesse Wainright at the Fall 2003 meeting of the Materials Research Society in Boston MA.

A paper entitled “Molecular Design in the Synthesis of Proton-conductive Polyimides (II)”. by Yue Zhang, Morton Litt, Robert F. Savinell, Jesse S. Wainright, and Jerome Vendramini, was presented at the 222nd ACS National Meeting, Washington, D.C., August, 2000.

A paper entitled “Microfabricated Fuel Cells” was presented at the Fall Meeting of the Electrochemical Society, October 2002.

A paper entitled “A microfabricated hydrogen-air fuel cell incorporating a novel polymer electrolyte” was presented at the Fall Meeting of the Electrochemical Society, October 2000, Phoenix AZ.

A paper entitled “Polymer Electrolytes for Micro Fuel Cells” was presented at the Fall Meeting of the Electrochemical Society, October 2000, Phoenix AZ.

A paper entitled “A microfabricated hydrogen-air fuel cell” was presented at the Fall Meeting of the Electrochemical Society, October 1999.

## PERSONNEL SUMMARY

The following staff and students were engaged during the course of this program.

Robert F. Savinell, Professor and P.I. - Fuel cell design and mathematical modeling.  
Chung-Chiun Liu, Professor and Co-P.I. – Microfabrication leader.  
Morton Litt, Professor, Novel polymer synthesis leader.  
Jesse Wainright, Research Professor – Experimental design and testing of fuel cell  
Joseph Payer, Professor, Development of novel hydride storage materials  
Laurie Dudik, Engineer, Mask design and carbon flow field printing.  
Q. Wu, Engineer, Microfabrication of silicon components.  
C.S. Tu, Visiting Professor, Microfabrication of fuel cell components  
Y. Zhang, Graduate student, Polymer synthesis and testing  
Kenneth Yee, BS/MS student, Microfabrication and hydrogen storage testing  
Snezana Gojkovic, Research Associate, Electrochemical characterization  
Hongyan Jiang, Research Associate, Polymer synthesis.  
Don Comfort, BS student, Carbon flow field fabrication.  
Dave Skender, BS student, Polymer testing.  
Liangyuan Chen, Graduate student, Polymer film formation and characterization.  
Debi Conrad, BS student, Pd ink formulation.  
Paul Dean, BS student, Polymer testing.  
Nicole Schilling, undergraduate, micro fuel cell fabrication and testing.  
Mike Burel, undergraduate, capacitor testing.  
Geoff Stephens, undergraduate, polymer testing.  
Hyoung-Juhn Kim, Graduate student, Polymer synthesis.  
Jerome Vendramini, Research Associate, Polymer testing  
Andrew Swann, BS/MS student, microfuel cell fabrication and testing.  
Wanida Pongsaksawad, undergraduate, palladium hydride storage  
Mike Swanson, undergraduate, microfuel cell testing.  
Xi Shan, graduate student, metal hydride synthesis and characterization  
John Staser, undergraduate student, micro fuel cell testing  
Arun Venkatesan, Research Associate, polymer synthesis, polymer film deposition

A total of three Ph.D. degrees and three M.S. degrees were awarded based on this effort.

## APPENDIX A- Selected Technical Progress Reports

### June 1998 Progress Report

#### 1. RESEARCH STATUS

##### Task 1. Micro Fuel Cell Power Unit/ Microfabrication Development

##### Design of the Micro Fuel Cell

###### Fuel Cell Structure

As reported in the last progress report, a laser pre-drilled alumina substrate was obtained from Laser Tech (Minnetonka, Minnesota). This gave a substrate with 125  $\mu\text{m}$  holes through it for the gas channels. The thick film printing steps needed to form an upper well for the fuel cell anode, are already known. It was found that the gold anode current collector could also be formed by thick film printing a metallo-organic gold ink over the well and channels. The metallo-organic ink prints and fires thin enough that it does not block the channels. This eliminated the step of having to sputter chrome/gold onto the wells and channels. Currently methods of printing a thicker back well on the alumina for the hydride storage block are being investigated. The back well will house the palladium hydride fuel storage material. The deepest back well so far obtained is 150  $\mu\text{m}$ , the desired thickness is 250-500  $\mu\text{m}$ .

At this time, there is no indication that the silicon fuel cell structure and the alumina structure have any significant differences. Since the amount of time necessary to build the alumina devices is currently much less than the silicon ones, effort will be concentrated on producing more alumina devices for testing.

##### Demonstration and Testing of Fabrication Steps

###### Deposition of carbon flow distributor – anode

The two requirements for the carbon flow distributor are high electrical conductivity and sufficient porosity to disperse hydrogen over the entire area of the anode. In the last progress report, it was noted that the carbon material (Carbon 2513, Metech, Elverson, Pennsylvania) used to make the carbon flow field was not porous to hydrogen. To address this problem, carbon powder was added to the Metech ink in various amounts as reported previously. The modified inks were successfully applied to the alumina and silicon fuel cell structures. Adding carbon powder to the Metech ink did increase the porosity of the flow distributor, in particular the formulations designated E1 and E2. However, the porosity is not enough for a 1% hydrogen/99% nitrogen feed. In addition, these formulations suffered from poor reproducibility (see section on anode performance below and Appendix A). Several alternative materials and processes have been tried to find a carbon material that is porous enough for the worst case condition (1%  $\text{H}_2$  in  $\text{N}_2$ ) and yet is able to be thick film printed and retains sufficient electrical conductivity. Efforts during the past quarter have focused on:

- Adding various solvents to thin the Metech ink and then adding more carbon powder. This method allowed for higher carbon powder loadings but was unprintable.
- Trying to identify another binder to adhere carbon powder to the substrate. Ethyl Cellulose showed some initial promise but was not printable.
- Finding alternative ways to mix the carbon powder, inks and solvents. A mechanical homogenizer and an ultrasonic dismembrator have been used. They did not seem to increase the reproducibility of the E1 and E2 inks.



- Trying a different commercial carbon ink, Ercon G-449(1). This ink performed in a similar fashion as the Metech ink.

None of these methods yielded a substance that was porous, conductive and thick film printable. A complete list of the different carbon ink formulations is given in Appendix A, Table A1. Additional methods and materials are being investigated. Some of the ideas currently being evaluated are:

- Obtaining carbon rods and mixing them with various binders. The hope is that a porous “mat” like structure will be obtained.
- Mixing small amounts of carbon, just enough to be conductive, with a silicone elastomer. The elastomer chosen is known to be permeable to hydrogen. Although it is known that this will not produce a porous structure, it is hoped that the elastomer will be permeable enough to hydrogen that the lack of pores will not be a problem.

Effort is now also being directed to researching alternative porous materials, such as sol gels, to use in place of the carbon ink type of material.

#### Deposition of DuPont Nafion polymer electrolyte films

An important step in the fabrication of the micro fuel cell power unit will be the deposition of thin (ca. 25  $\mu\text{m}$ ), uniform films of polymer electrolyte with well-defined geometry. In addition, the polymer electrolyte must have sufficient proton conductivity (at least 0.001 S/cm) under conditions of ambient temperature and humidity. Since Nafion is a commercially available polymer electrolyte and there is an extensive body of literature on the properties of the material, we are considering Nafion for this application. At the same time, since it is well known that the conductivity of Nafion is low under low relative humidity conditions, we are developing polymers specifically for this application (see Task 3).

During the past quarter we have continued our study of Nafion films cast from the commercial alcohol/water solvent system. At the beginning of this quarter, we were evaluating films that were cast and then cured at moderate temperatures under humid conditions. Films cast in this manner gave acceptable conductivities at humidities greater than 35%, but longer term testing showed that the conductivity decreased with time, indicating that the structure formed is not stable. Additional trials confirmed this result, and this approach has been set aside.

As a result, we are now considering films deposited from solvents other than the commercial alcohol/water system. Our objectives remain the same, to increase the viscosity of the solution to improve the film casting characteristics and to cast a film whose structure enhances the proton conductivity at low relative humidities. During the past quarter, we have focussed on dimethyl sulfoxide (DMSO) as an alternative solvent. The procedure for making these solutions is as follows: DMSO is added in an appropriate amount to a volume of Nafion solution in alcohol/water. The combined solution is then heated at 80°C to evaporate the majority of the alcohol and water, leaving behind a solution of Nafion in DMSO, which has a considerably higher boiling point. Five percent solutions of Nafion in DMSO have been made repeatedly, and initial attempts indicate that ten percent solutions can also be made, which should increase the solution viscosity. The conductivity of Nafion films cast from a 5% solution in DMSO is shown in **Figure 3.1** below. As seen previously, the conductivity is acceptable at relative humidities of 35% and up, however, the conductivity at 15%RH has not been improved by this casting method.

#### Deposition of platinum fuel cell catalysts/anode and cathode testing

Previously we have considered sputtering a thin layer of platinum to form the anode and cathode catalyst layers. This approach has some potential drawbacks, including 1) low surface area (which can be overcome by electroplating Pt onto the sputtered layer as discussed in previous reports) and 2) the fact that the polymer electrolyte onto which the cathode layer is deposited may be adversely effected by exposure to vacuum and the sputtering process. As an alternative,

we are also considering depositing the catalyst layers by thick film printing of catalyst/ionomer inks. These inks are a recent innovation in the fuel cell community (M.S. Wilson and S. Gottesfeld, *J. Electrochem. Soc.*, **139**, L28, 1992, M.S. Wilson, S. Valerio and S. Gottesfeld, *Electrochim. Acta*, **40**, 355, 1995). From a fuel cell point of view, these inks offer the advantage of an intimate mixing of the catalyst with the polymer electrolyte leading to higher catalyst utilization than can be achieved with a sputtered Pt electrode.

The technical challenge in this area is to adapt the successful ink formulations found in the literature to the situation at hand. Specifically, we need to maintain a high degree of electrode performance under low relative humidity conditions (the literature formulations are optimized for operation at 100%RH) and to make the ink compatible with conventional thick film printing. In addition, the typical process for manufacturing electrode/membrane assemblies is to bond the electrodes to a polymer electrolyte membrane using a press at elevated temperatures. Typical pressing conditions are 130°C and 1000 psi for acid form Nafion membranes. For the microfabricated fuel cell, it will be necessary to obtain intimate contact between the electrodes and the polymer electrolyte without hot pressing.

Our initial trials using catalyst inks used standard compositions taken from the literature. This proved unsuccessful as the adherence of the ink to the carbon flow distributor was poor, and the ink viscosity was too low. By varying the polymer electrolyte content in the ink, thicker inks, which produced adherent catalyst layers, were found. A carbon to electrolyte ratio of ca. 1:1 by weight appears to be reasonable. Three inks were then formulated using catalysts (E-Tek Inc.) with different Pt loadings on the carbon support (XC72, Cabot Inc.) in order to evaluate the activity of the electrode as a function of Pt content. The carbon to electrolyte ratio was held roughly constant. The compositions of these inks are given in **Table 1.1**.

**TABLE 1.1** Catalyst Ink Compositions

Catalyst used	Composition wt% Pt/C/Nafion	Typical Pt loading of electrodes* mg/cm <sup>2</sup>
20 wt % Pt on XC72	11/44/45	0.15
40 wt% Pt on XC72	25/38/37	0.3
60 wt% Pt on XC72	42/28/30	0.5

\* - each electrode formed from approximately 5 uL of ink (catalyst plus Nafion plus solvent) dispersed over 5mm x 5mm electrode area. Loadings determined by weighing the substrates before applying the catalyst ink, and after drying the ink.

In order to compare the intrinsic catalytic activity of these inks, polarization curves for hydrogen oxidation were obtained using a pure hydrogen feed at one atmosphere pressure. With this feed, limitations due to transport of hydrogen should be minor. The electrolyte used was 0.1 M H<sub>2</sub>SO<sub>4</sub>. Polarization curves for two electrodes of each ink are shown in **Figure 1.1**. These results show that each of these inks has reasonable activity for hydrogen oxidation. Under these conditions we would expect the anode potential to be not more than 10 mV vs RHE at a current density of 10 mA/cm<sup>2</sup>. Each of the polarization curves shown meets this criteria. It can also be seen in Figure 1.1 that 4 of the 6 electrodes had very similar performance. The relatively poorer performance of the other

two electrodes can be traced to hydrogen transport limitations, as evidenced by the data shown in **Figure 1.2**. In this figure the performance of the same six electrodes is shown, using 1% H<sub>2</sub> in N<sub>2</sub> as the feed. For each, a limiting current is obtained, due to the diffusion of hydrogen through nitrogen in the pores of the anode flow distributor. The two electrodes that had the somewhat poorer performance on pure H<sub>2</sub>, also had the lowest limiting currents on 1% H<sub>2</sub>. The limiting currents vary over a wide range, despite the fact that the flow distributor is the same in each case, the E2 carbon ink. Similar experiments with additional electrodes (14 - E1 trials, 22 - E2 trials) showed that the limiting currents for both the E1 and E2 inks ranged from 1 to 10 mA/cm<sup>2</sup>. These results are detailed in Appendix A, Table A2. In addition to the fact that the limiting currents are not consistent, all of the limiting currents measured to date are too low. Our design goal is a limiting current of 40 mA/cm<sup>2</sup> for a 1% H<sub>2</sub> in N<sub>2</sub> feed. If we can achieve this goal, the fuel cell should be capable of operating at the desired 10 mA/cm<sup>2</sup> with an acceptable cell voltage under the worst case condition for the fuel supply.

The catalyst ink containing the 20 wt% Pt on XC72 was also evaluated as an air cathode. The flow distributor was the E2 carbon ink. The polarization curve for this electrode is shown in **Figure 1.3**. The cathode performance is very promising, especially considering the relatively low Pt content of the electrode, 0.16 mg/cm<sup>2</sup>. A cathode potential of 783 mV vs RHE was obtained at 8 mA/cm<sup>2</sup>. Our goal for the cathode is a potential of 800 mV at 10 mA/cm<sup>2</sup>.

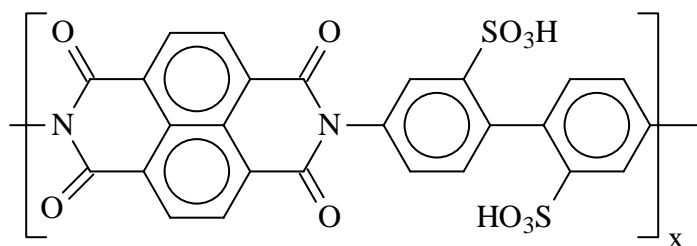
## Task 2. Performance and diagnostic testing of micro fuel cell power unit.

Scheduled to start in year two.

## Task 3. Novel polymer synthesis and characterization

Novel proton conducting polymers are being sought that have reasonable proton conductivity at low humidity, good mechanical properties, low permeability and dimensional stability. We are currently investigating polyimide block copolymers, in which one of the blocks contains a sulfonic acid functionality to provide proton conductivity and a non-ionic block will provide dimensional stability. Monomers with bulky side groups will be incorporated into the polymer backbone. Because these polyimides are linear, rigid rod polymers, bulky groups that push the backbones apart will keep them apart for the whole chain length. This creates a nanoscale pore lined with sulfonic acid groups. Such pores should adsorb water very strongly even at relatively low humidities. (The best example of this is synthetic zeolite. When dry, it equilibrates with water vapor at 10<sup>-6</sup> mm pressure.) For the best case, the water content should be almost independent of relative humidity, and the same should be true for the proton conductivity.

The structure shown below is that of the polyimide homopolymer containing the functional monomer 4,4'-diamino-2,2'-biphenyl disulfonic acid (DAPS).

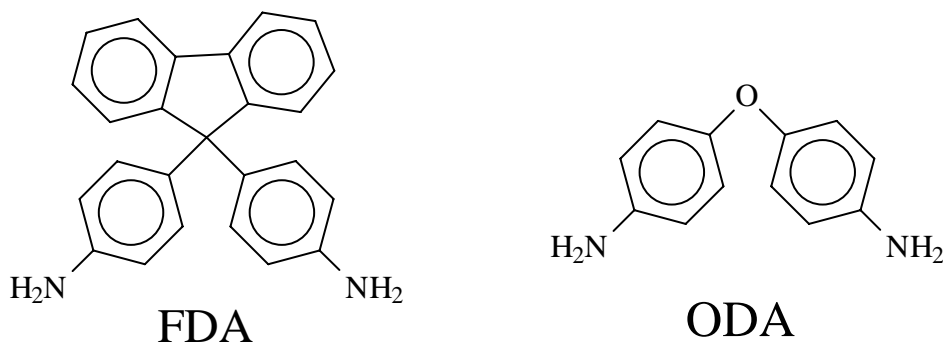


Homopolymer -NTDA/DAPS

The homopolymer has excellent conductivity (to be discussed later) but the conductivity still depends on the relative humidity more than desired. The first attempt at copolymerization, using the monomer 1,4-diaminoanthraquinone (DAA), was unsuccessful. This compound has strong

electron-withdrawing groups next to the diamino benzene ring. In addition, the steric hindrance of the carbonyl group may have prevented the diamine from reacting. Side reactions were found in the synthesis of the model oligomer from diaminoanthraquinone and naphthalene tetracarboxylic dianhydride. The amide could not be converted fully to imide.

We concluded that the DAA monomer was not suitable for this work, and turned to another monomer: 4,4'-(9-fluorenylidene) diamine (FDA), shown below. In addition to being a bulky diamine, FDA imparts a zigzag conformation to the final copolymer with a rigid-rod chain between each bend. This conformation comes from the bond angle (about 112°) between the two benzene rings that the amine groups connect to. Consequently, the polymer chains cannot pack themselves tightly in any direction and there is space that water can occupy. FDA copolymerizes well and random copolymers have already been made with five, ten and twenty percent co-monomer, labeled RF5, RF10 and RF20 respectively.



Bulky Diamine Monomers

The nomenclature rationale is that the first letter tells whether the copolymer is random (R) or block (B). The second letter defines the co-monomer, F for FDA, O for ODA and D for DAPP (defined below). The number at the end for a random copolymer is the percentage of co-monomer. For a block copolymer, the two numbers are the average block sizes, the first for the disulfonic acid block and the second for the co-monomer block.

Two block copolymers were made following the literature example using oxydianiline (ODA) as the co-monomer. One copolymer, BO3/4, had a sulfonic acid block length of three and an ODA block length of four. The second co-monomer, BO4/4, had block lengths of four for each sequence. In addition, a block copolymer was made with FDA as the co-monomer, BF3/4. Here block lengths were three for the sulfonic acid and four for the non-polar component. The structures are summarized in **Table 3.1**.

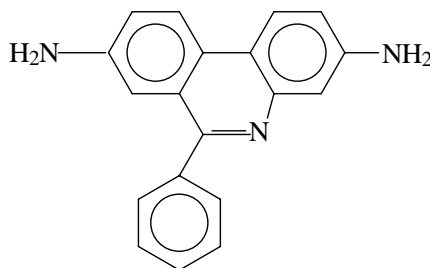
**Table 3.1** Structure of polyimides tested.

Sample ID	Chemical structure
H	-(NTDA) <sub>0.5</sub> -(DAPS) <sub>0.5</sub> -
BO3/4	-[(NTDA) <sub>0.28</sub> -(DAPS) <sub>0.22</sub> ]-[(ODA) <sub>0.28</sub> -(NTDA) <sub>0.22</sub> ]-
BO4/4	-[(NTDA) <sub>0.31</sub> -(DAPS) <sub>0.25</sub> ]-[(ODA) <sub>0.25</sub> -(NTDA) <sub>0.19</sub> ]-
RF20	-(NTDA) <sub>0.50</sub> -(DAPS) <sub>0.40</sub> -(FDA) <sub>0.10</sub> -
RF10	-(NTDA) <sub>0.50</sub> -(DAPS) <sub>0.45</sub> -(FDA) <sub>0.05</sub> -

RF5 BF3/4	$-(\text{NTDA})_{0.50}-(\text{DAPS})_{0.45}-(\text{FDA})_{0.025}-$ $-[(\text{NTDA})_{0.28}-(\text{DAPS})_{0.22}] - [(\text{FDA})_{0.28}-(\text{NTDA})_{0.22}]-$
--------------	--

Note: monomer ratios normalized to add up to 1.0

A third comonomer, diamino phenyl phenanthridine, DAPP was also used. Its structure is shown below.



DAPP

This monomer maintains the linear, rigid rod, liquid crystal nature of the polymer chain. However, the phenyl ring protrudes from the backbone and pushes the chains apart to some degree. In addition, the monomer is basic. The phenanthridine system has an aromatic nitrogen and is about as basic as pyridine. It forms salts with the sulfonic acids present in the rest of the molecule.

The polyimides containing DAPP were prepared by one-step solution polymerization. The mole ratio of monomers NTDA:DAPS:DAPP was selected as 100:100:0, 100:90:10 and 100:80:20 to make a systematic comparison. A second random polymer was also prepared using delayed addition of DAPP. Viscosities and water loss were measured for these polymers and are listed in **Table 3.2**. The water uptake measurements in this Table are only a first approximation; there was some *m*-cresol (solvent used for film casting) remaining in the polymer films.

**Table 3.2.** Viscosity and water uptake (TGA) for DAPP copolymers.

Polymer	NTDA:DAPS:DAPP	Inherent Viscosity <sup>a</sup>	Water uptake (%) measured by weight loss below 300 °C	Water molecules per SO <sub>3</sub> group
H	100:100:0	1.91	24.5	3.9
RD10	100:90:10	2.02	19.1	3.4
RD20-1	100:80:20	1.61	12.4 <sup>b</sup> , 18.3 <sup>c</sup> , 2.8 <sup>d</sup>	3.6 <sup>e</sup> , 0.55 <sup>d</sup>
RD20-2 <sup>e</sup>	100:80:20	1.90	22.3 <sup>c</sup>	4.4

<sup>a</sup> Measured in DMSO at 25 °C, solution concentration is 0.5 g/dL.

<sup>b</sup> Salt form, equilibrated in laboratory atmosphere. <sup>c</sup> Acid form, equilibrated in laboratory atmosphere. <sup>d</sup> Acid form, dried in nitrogen flow overnight; <sup>e</sup> DAPP monomer was added after NTDA and DAPS had reacted for 12 h.

The DAPP co-polyimides are soluble in DMSO, *m*-cresol, NMP, and in DMF. After heating at 180 °C under vacuum for 8 h, the copolyimides became less soluble in *m*-cresol and DMF. The decrease of solubility is mostly due to cyclization and possibly cross-linking reactions. At this moment, DMSO is the best solvent.

## Characterization:

**Water Uptake:** Three methods: thermogravimetry (TGA), Differential Scanning Calorimetry (DSC) and weighing, were found to be suitable to measure the water uptake capacity of free standing polyimide films. The water uptake of polyimide films in lab air was obtained using TGA by monitoring the weight loss, centered at ca. 130°C, at a heating rate of 20°C/min; the data are shown in **Tables 3.2 and 3.3**.

It is interesting to note that the introduction of 10 and 20 mol% FDA or DAPP into the random copolyimide (Tables 3.2 and 3.3) does not affect the water uptake (as measured by percent weight gain) significantly at low relative humidity. In fact, in comparison to the homopolymer, the number of water molecules per acid group is increased by addition of FDA or DAPP. On the other hand, the block copolyimide containing FDA shows lower water uptake and water molecules per acid group than the corresponding block copolyimide containing ODA. These differences suggest a difference in chain packing of polyimides in solid state, which will be investigated starting in the next quarter.

**Table 3.3.** Water uptake of free standing polyimide films equilibrated with lab air (~30% RH), measured by TGA.

Sample ID	Water uptake in % <sup>a</sup> and (H <sub>2</sub> O/SO <sub>3</sub> ratio), from (TGA) Weight Gain	
homopolymer	18.6 (3.0)	21 (3.4)
BO3/4	16.3 (5.2)	
BO4/4	11.5 (3.2)	17 (4.8)
RF20	20.6 (4.1)	24 (4.8)
RF10	23.6 (4.2)	
BF3/4	7.1 (2.7)	

<sup>a</sup> Water uptake when equilibrated with lab air ~50% RH.

The influence of relative humidity on the water uptake of three polyimides was examined over the region of 15 to 100%RH. The free standing polyimide films were vacuum dried at 80°C for 72 hr and then for 12 hr at 25°C. Quick equilibrium was achieved by placing the films in a vacuum desiccator containing an aqueous solution of LiCl with the desired vapor pressure, evacuating it to 20 mm Hg for 1 minute and then sealing it. The weight percent water uptake and corresponding mole ratio of water to sulfonic acid is listed in **Table 3.4**.

**Table 3.4.** Influence of relative humidity on the water uptake capacity, shown as overall weight percent increase and moles of water per sulfonic acid group.

RH (%)	homopolymer		BO4/4		RF20	
	Wt %	H <sub>2</sub> O/SO <sub>3</sub>	Wt %	H <sub>2</sub> O/SO <sub>3</sub>	Wt %	H <sub>2</sub> O/SO <sub>3</sub>
15	15.1	2.4	9.4	2.6	13.8	2.8
35	16.9	2.7	13.3	3.7	18.6	3.7
50	20.5	3.3	16.1	4.5	24.3	4.9
75	27.0	4.3	18.9	5.3	30.9	6.2
100	60.8	9.7	28.1	7.9	55.8	11.2

The number of water molecules per acid group for the homopolymer (H) parallels Nafion except at 100% RH, where Nafion is higher. The random copolymer, RF20, is higher than the homopolymer, the greatest increase is in the mid RH region where it is as much as 50% higher. The block copolymer, BO4/4, also shows an increase in number water molecules per acid group over the homopolymer in the midrange of humidities, but the total water absorption is lower.

**Conductivity:** Initial conductivity measurements as a function of relative humidity have been made on many of these polymers. Examples of the room temperature data are presented in **Figure 3.1**. The figure also includes our measurements on Nafion 117 done under the same conditions as the polyimides. These agree with literature values.

To some degree, we have validated our guiding hypothesis. The random copolymers absorb as much or more water as the homopolymer. The number of water molecules per sulfonic molecules can be 50% higher for the copolymers in the humidity mid-range. This increase shows up in the conductivities as well. Although the copolymer equivalent weights are higher than that of the homopolymer, their conductivities are as high or higher over the whole humidity range. The random copolymer with 5% FDA is our best result to date, with a conductivity similar to Nafion from 100% down to 35% RH, and with substantially higher conductivity at 15%RH. This is an important result, as it is the best evidence that structures can be formed that will retain water under low humidity conditions where the commercial material cannot function. The block polymer with ODA (BO3/4) shows the conductivity independence on relative humidity that we were looking for, but at too low a conductivity. It is paralleled by a smaller change in water absorption as a function of RH than was found for the other polyimides (Table 3.4).

#### **Task 4. Novel polymer incorporation into micro fuel cell.**

Scheduled to start in year two.

#### **Task 5. Palladium thick film deposition and characterization**

The on-board fuel storage will be a palladium hydride system as described previously. A thick film deposition will be used to apply the palladium in high surface area form. The requirements for the thick film ink include: high porosity (to enable rapid hydrogen sorption/desorption rates), a low temperature cure (for compatibility with other materials present in the micro fuel cell) and the ability to lay down relatively thick deposits (0.1 to 1.0 mm thick, so that sufficient storage capacity can be deposited in a single pass). We are currently evaluating methods to reduce the amount of silicone binder in our Pd thick film inks to increase the amount of hydrogen stored per unit volume.

## **2. DIFFICULTIES/PROBLEMS**

- Producing highly conductive, but dimensionally stable polymer films for fuel cell electrolyte with low hydrogen and oxygen permeability to prevent fuel loss and maintain energy storage.
- Demonstration of high permeability anode flow distributor in fuel cell structure.
- Strategies are needed to increase the volumetric energy density of the Pd/H storage block.

## June 1999 Progress Report

### 1. RESEARCH STATUS

#### Task 1. Micro Fuel Cell Power Unit/ Microfabrication Development

##### Design of the Micro Fuel Cell

No new data to report.

##### Demonstration and Testing of Fabrication Steps

###### Deposition of carbon fuel distributor – anode

The two requirements for the carbon fuel distributor are high electrical conductivity and sufficient porosity to disperse hydrogen over the entire area of the anode. Several alternative materials and processes have been tried to find a carbon material that is porous enough for the worst case condition (1% H<sub>2</sub> in N<sub>2</sub>) and yet is able to be thick film printed and retains sufficient electrical conductivity. During the past six months we have investigated two approaches: 1) loading various carbon inks with copper powder (1-2 μm dia.) and 2) combining carbon particles with an inorganic binder and cellulose.

The copper containing inks can be printed, and the copper dissolved out electrochemically, ideally leaving behind a porous, conductive, carbon matrix. At this point we have evaluated these inks based on 1) the amount of copper that could be incorporated without loss of printability, and 2) the ease of copper dissolution. The best results for this system were obtained with a formulation based on a commercial carbon ink from Metech. However, based on the difficulties encountered with the Metech ink during the fuel cell trials we have set this approach aside. The fuel cell trials showed very low hydrogen permeability in the anode fuel distributor. Follow-up experiments showed that the permeability decreased with increasing time at elevated temperature. Each curing step, following deposition of the anode, electrolyte, cathode and cathode current collector, apparently lowered the permeability of the anode fuel distributor.

Each curing step listed above is performed at 120°C. In the second approach, we have used an inorganic binder which when cured is completely stable at 120°C. Cellulose was added as a pore former, when the binder is cured (400°C), the cellulose is burned out to increase the porosity. A comparison of the previous system and the system with the inorganic binder is shown in Figure 1A. On pure hydrogen, the new system is a slight improvement over the old, the polarization is ca. 5 mV lower in the region of interest around 10 mA/cm<sup>2</sup>. However, unlike the previous system, the new ink should be stable during the curing of the rest of the components of the fuel cell.



## Anode Polarization 1st Generation vs 2nd Generation Flow Distributor

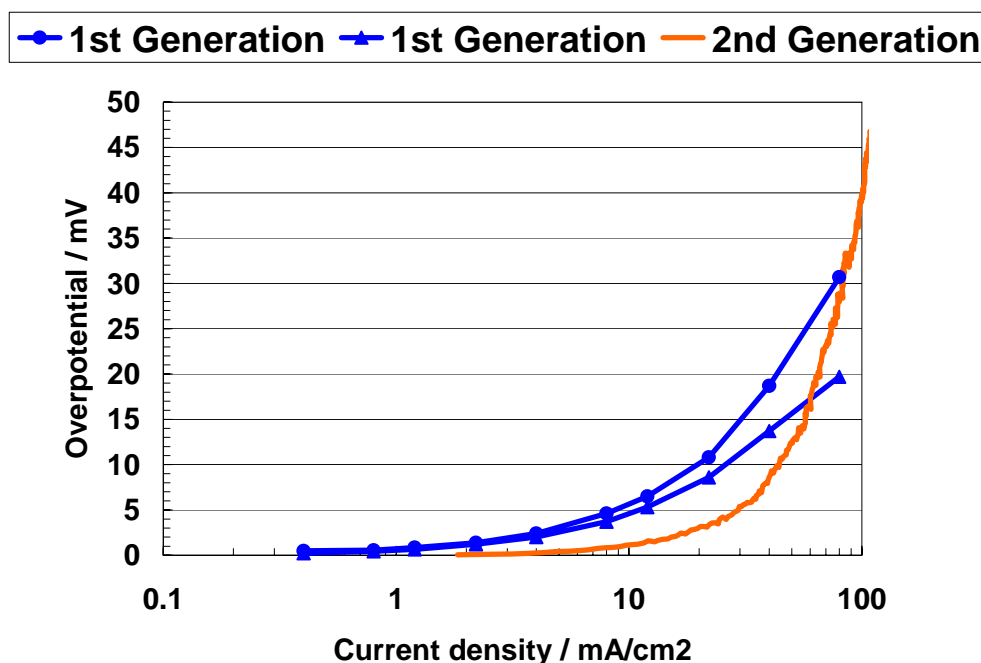


**Figure 1A.** Anode polarization curves for pure hydrogen. 1<sup>st</sup> generation anode flow distributor – modified Metech ink. 2<sup>nd</sup> generation flow distributor – inorganic binder, carbon and cellulose. Polarization curves measured in half cell configuration using 0.5 M H<sub>2</sub>SO<sub>4</sub>.

### Deposition of DuPont Nafion polymer electrolyte films

An important step in the fabrication of the micro fuel cell power unit will be the deposition of thin (ca. 25  $\mu\text{m}$ ), uniform films of polymer electrolyte with well-defined geometry. In addition, the polymer electrolyte must have sufficient proton conductivity (at least 0.001 S/cm) under conditions of ambient temperature and humidity. Since Nafion is a commercially available polymer electrolyte and there is an extensive body of literature on the properties of the material, we are considering Nafion for this application. At the same time, since it is well known that the conductivity of Nafion is low under low relative humidity conditions, we are developing polymers specifically for this application (see Task 3).

During the past quarter we have continued our study of Nafion films cast from solvents other than the commercial alcohol/water system. Our objectives remain the same, to increase the viscosity of the solution to improve the film casting characteristics and to cast a film whose structure enhances the proton conductivity at low relative humidities. During the past two quarters, we have focused on ethylene glycol(EG) as an alternative solvent. The procedure for making these solutions is as follows: EG is added in an appropriate amount to a volume of Nafion solution in alcohol/water. The combined solution is then heated at 80°C to evaporate the majority of the alcohol and water, leaving behind a solution of Nafion in EG, which has a higher boiling point. Previously we made five and ten percent solutions of Nafion in EG. Casting from EG increases the conductivity considerably, unlike any of the other solvents considered. All of

our previous results with Nafion had acceptable conductivity ( $> 1$  mS/cm) only at relative humidities at or above 35%. The films cast from EG are more conductive at all relative humidities, and meet the conductivity target at 15% RH.

However, the printing/film casting characteristics of the 5% Nafion solutions in EG were poor. Two or more coats were needed to yield membrane thicknesses on the order of 25  $\mu\text{m}$ . Fuel cells constructed using the 5% solution were often shorted due to insufficient thickness/uniformity of the electrolyte layer (see below). Consequently, we have begun working with higher concentration solutions. The procedure used to make the solution is the same as for the 5% solution, only the amount of EG added has been changed. Solution concentrations between 20 and 34 wt% have been successfully obtained. This has improved the casting properties considerably, and the success rate for manufacturing complete fuel cells has improved (see below). The conductivity of the films cast from the more concentration solutions is generally  $\frac{1}{2}$  that of films cast from the original 5% solutions (**Table 1.1**). However, the improved processing behavior is more important at this time.

**Table 1.1** Conductivity of Nafion films cast from ethylene glycol

Relative humidity	Conductivity – films cast from 5% solution	Conductivity – films cast from 25% solution
15	0.0019 S/cm	$9 \times 10^{-4}$ S/cm
35	0.0073	0.0067
50	0.042	0.01
75	0.07	0.042
90	0.18	0.10

## Task 2. Performance and diagnostic testing of micro fuel cell power unit.

Several complete fuel cell structures were fabricated and tested. The basic sequence of fabrication steps is given below:

### Fabrication Procedure – Sequence of deposition steps and materials used

- anode current collector (gold)
- glassy insulation layer ( $\text{SiO}_2$ )
- anode flow distributor (modified Metech carbon)
- anode catalyst (Pt/C, Nafion)
- polymer electrolyte (Nafion or RF5)
- cathode catalyst (Pt/C, Nafion)
- cathode current collector (cathode ink, or un-modified Metech carbon)

More detail on the construction and appearance of these cells is given in **Table 2.1**. Three different failure modes were observed, as reported in the comments in Table 2.1. The failure modes were as follows:

### Explanation of Failure Modes in Table 2.1

Cracks – cracks in the anode flow distributor, resulting in loss of material out of the slots in the alumina substrate. These cracks occurred at any point in the process.

Shorts – all electrical shorts appear to be the result of gaps in the polymer electrolyte layer, with one exception – when the cathode current collector was misaligned.

Delamination – two types of delamination occurred. With the RF5 electrolyte, the anode would delaminate from the flow distributor when the polymer electrolyte layer was cured. With the Nafion electrolyte, the cathode would delaminate from the polymer electrolyte when the cathode was cured.

**Table 2.1** Full Fuel Cell Trials – each trial is a set of three cells  
All sets in X series have hand printed anodes  
All sets in A series have machine printed anodes, except A4 (hand printed)

Designation	Electrolyte Fabrication Notes	Comments
X1	Nafion/EG 5%	all cells shorted
X2	Nafion/EG 5%	two cells shorted
X3	Nafion/EG 5%	two cells shorted
X4	RF5/DMSO 5%	one cell shorted
X5	RF5/DMSO 5%	all cells delaminated
X6	RF5/DMSO 5%	all cells good
X7	RF5/DMSO 5%	
X8	Nafion/EG 34% Metech cathode current collector	2 cells cracked
X9	Nafion/EG 34%	One cell cracked, two cells delaminated
A1	Nafion/EG 5%	All cells shorted by cathode current collector
A2	Nafion/EG 5%	Two cells cracked
A3	Nafion/EG 5%	One cell shorted
A4	Nafion/EG 5%	One cell cracked, one cell shorted
A5	Nafion/EG 5%	Two cells with low open circuit potential
A6	Nafion/EG 34%	Two cells cracked
A7	Nafion/EG 34%	One cell cracked, one cell shorted
A8	Nafion/EG 34%	All cells good
A9	Nafion/EG 34%	Two cells cracked
A10	Nafion/EG 34% Metech cathode current collector	One cell shorted
A11	Nafion/EG 34% Metech cathode current collector	Two cells with very low open circuit potential
A12	Nafion/EG 34% Metech cathode current collector	One cell with very low open circuit potential
A13	Nafion/EG 34% Metech cathode current collector	All cells good
A14	RF5/DMSO 8%	Two cells delaminated
A15	RF5/DMSO 8%	One cell cracked, two cells delaminated
A16	RF5/DMSO 8%	Two cells delaminated

All of the cells that did not fail due to shorts, delamination, or cracks, were tested with hydrogen supplied to the anode fuel distributor at atmospheric pressure, and the cathodes exposed to the laboratory air. The relative humidity in the lab during the tests was 20-22%. The testing consisted of measurement of the open circuit potential, an AC impedance scan (DC potential equal to the open circuit potential, 10 mV RMS AC applied from 20 kHz to 1 Hz), and a slow polarization scan (open circuit potential down to 0 V at 5 mV/s).

The open circuit potential under the test conditions will ideally be 0.9 – 1.0 V. In a few cases, extremely low open circuit potentials (< 25 mV) were recorded, as listed in Table 2.1. These

cells were dropped from further testing. Most of the remaining cells had open circuit potentials between 0.5 and 0.7 V. The highest potential recorded was 0.788 V. The cause of the low open circuit potentials is mixing of the reactants, from hydrogen permeation to the cathode, or oxygen permeation into the anode. The correlation between the amount of reactant crossover and the decrease in the open circuit potential depends on the activity of the electrodes and the relative rates of crossover and reactant supply to the electrodes.

The slow polarization scans on the remaining cells all showed the same behavior – a linear V-I curve. Examples are shown in **Figure 2A**. This was very surprising, as it indicates that the electrochemical reaction kinetics (which do not have linear V-I characteristics over a wide range of voltage) are not the determining factor in the cell performance. The obvious resistive elements in these cells are the electrolyte resistance, and the electrical resistance in the anode and cathode current collectors. Most of the cells were constructed with the cathode catalyst ink used to form the cathode current collector. Since this ink is not designed for optimal electrical conductivity, we expected an increased resistance. To determine the nature of the resistance, the AC impedance scans are used. At high frequencies, the double layer capacitance at each electrode is essentially a short, eliminating the reaction kinetics and mass transfer resistances from the impedance measurement. The remaining impedance is due to those elements in series with the electrodes, the membrane resistance, and the electrical resistance of the current collectors. However, the resistance observed in the polarization scans is much larger than that observed in the high frequency measurements. This implies that the controlling resistance is not due to insufficient conductivity in the membranes or in the current collectors. This conclusion is supported by the fact that when the Metech carbon ink was used as the cathode current collector, essentially no change was observed in the cell performance. Also, very similar results were obtained with the different polymer electrolytes, and when the cells were deliberately humidified (which should greatly decrease the resistance of the polymer layer).

At this point, several cells were run with pressurized hydrogen fed to the anode. With 6 psig  $H_2$ , the open circuit potentials generally increased (highest open circuit value recorded with pressurized  $H_2$  was 850 mV). This suggests that the poor open circuit potentials were due to oxygen permeation into the anode compartment, and not hydrogen permeation to the cathode. Since it is unlikely that oxygen permeation through the polymer electrolyte is significantly greater than hydrogen permeation, this suggests that the problem lies with the hydrogen supply to the anode. Unfortunately, the overall cell performance was not significantly improved with the pressurized hydrogen feed.

To check the hydrogen permeation characteristics of the anode flow distributor, limiting current measurements were performed. With a pure hydrogen feed, the limiting currents should be greater than 100 mA, as shown by our previous measurements on anode structures. However, on two complete fuel cells we measured only 2.1 and 7.5 mA. This confirmed that the anode fuel distributor had lost porosity due to the elevated temperatures used to cure the other layers of the fuel cell structure.

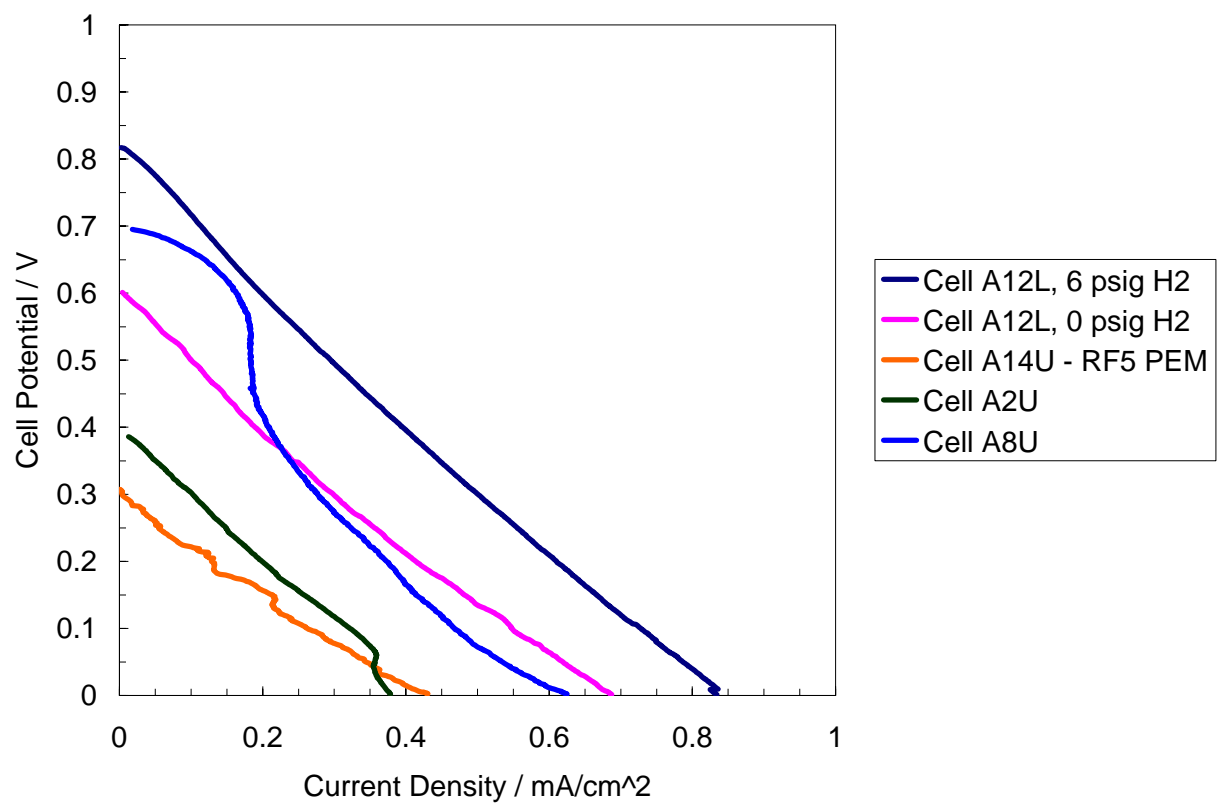


Figure 2A Microfuel cell polarization curves, 5 mV/s from open circuit to 0 V/cell. H<sub>2</sub>/air.

### Task 3. Novel polymer synthesis and characterization

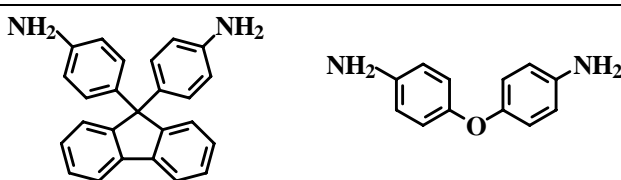
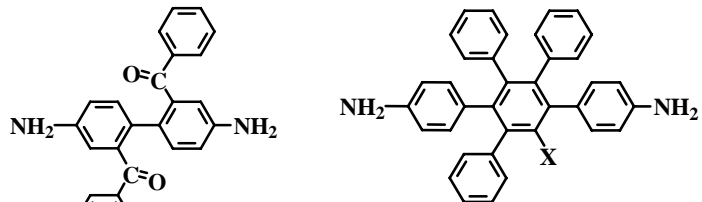
We are seeking novel proton conducting polymers that have reasonable proton conductivity at low humidity, good mechanical properties, low permeability, and dimensional stability. We have synthesized some sulfonic acid containing copolyimides that incorporated bulky diamines. The bulky groups are expected to push the polymer backbones apart and keep them apart along the whole chain length. This should create a nanoscale pore lined with sulfonic acid groups. Such pores should adsorb water very strongly even at relatively low humidity. Previously, we had identified 4,4'-(9-fluorenylidene) diamine (FDA), which when incorporated into random polymer structures at 5, 10, and 20 mole% (designated RF5, RF10 and RF20, respectively) increased the water uptake when compared with the homopolymer. The best samples with FDA are more conductive than Nafion over the whole relative humidity range. This is mainly because FDA imparts a zigzag conformation to the final copolymer with a rigid-rod chain between each bend and is bulky. Consequently, the polymer chains cannot pack themselves tightly in any direction and there is space that water can occupy.

The problem with the homopolymer and the FDA or ODA (4,4'-oxydianiline) copolymers is that they are water sensitive. Random co-polymers and several block co-polymers of these compounds either dissolve or fragment easily in water at elevated temperatures. We have now synthesized sulfonic acid containing co-polyimides that incorporate a series of linear diamines with bulky side groups. These are much more stable in water. We now have a series of copolymers that absorb water well, and conduct at about the same level as RF5. They are all liquid crystal and their interchain distances are larger than that of the homopolymer. We continue to synthesize and characterize bulkier diamines seeking the optimal blend of the desired properties. While we have increased conductivity over previous polymers, there have been no dramatic increases. We are starting a program to synthesize analogous systems, which use a different principle to force the chains apart. Groups will be inserted into the polymers that create jogs in the backbone while keeping the backbone segments co-linear. Depending on the size of these groups, the chains can be shifted by 1.4 to 50Å. The large spacers will dilute the carrier concentration, but may increase carrier mobility.

#### 3.1 Synthesis and characterization of copolymers with bulky side groups

##### 3.1.1) co-polymers with 2,2'-dibenzoyl-benzidine (DBB)

We have been testing another new bulky diamine synthesized in our lab: 2,2'-dibenzoyl-benzidine (DBB). A 5 mole% random copolymer was made. The conductivity of a random copolymer with 5% DBB, i.e., RD5, is as good as the other random copolymers with bulky diamines that were synthesized earlier, **Table 3.1**.

Category	Structure
angled comonomers	 <div style="display: flex; justify-content: space-around;"> <div>FDA</div> <div>ODA</div> </div>
rigid-rod bulky comonomers	 <div style="display: flex; justify-content: space-around;"> <div>DBB</div> <div>X = H, Ph (3P)TDA, (4P)TDA</div> </div>

**Table 3.1.** Conductivity of RD5, compared to previous polyimides and Nafion.

Relative Humidity (%)	Conductivity (S/cm)						
	RD5	RF5	RO5	R(3P)T5	R(4P)T5	Homo-polymer	Nafion
100	0.29 (0.04)	0.24 (0.07)	0.21 (0.14)	0.13 (0.06)	0.17 (0.002)	0.19 (0.07)	0.07
75	0.023 (0.006)	0.042 (0.016)	0.03 (0.008)	0.031 (0.003)	0.042 (0.005)	0.018 (0.003)	0.03
50	0.009 (0.004)	0.012 (0.003)	0.018 (0.002)	0.012 (0.002)	0.006 (4.0E-4)	0.004 (-)	0.013
35	1.2E-3 (6.9E-4)	4.0E-3 (1.4E-3)	5.2E-3 (2.0E-3)	4.2E-3 (1.8E-3)	3.0E-3 (5.0E-4)	1.5E-3 (7.2E-4)	2.0E-3
15	6.9E-4 (2.7E-4)	6.3E-4 (1.0E-4)	9.5E-4 (1.8E-4)	1.1E-3 (9.0E-4)	9.0E-4 (1.4E-4)	3.1E-5 (2.1E-5)	4.8E-5

\*Shown data are averaged results and the standard deviations are in the brackets.

The water uptake capacity of RD5, R(3P)T5 and R(4P)T5 was measured by our normal weighing method. In agreement with the high conductivity, the results indicated that those copolymers absorb more water per sulfonic acid group than the homopolymer does at all relative humidities, **Table 3.2.**



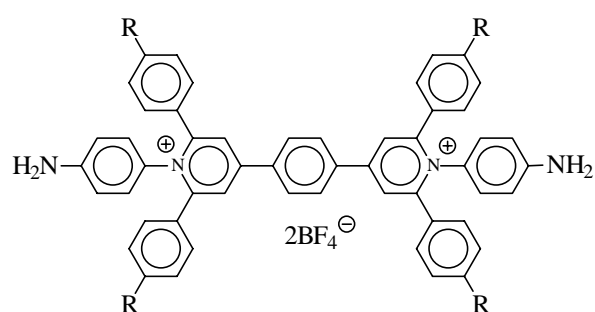
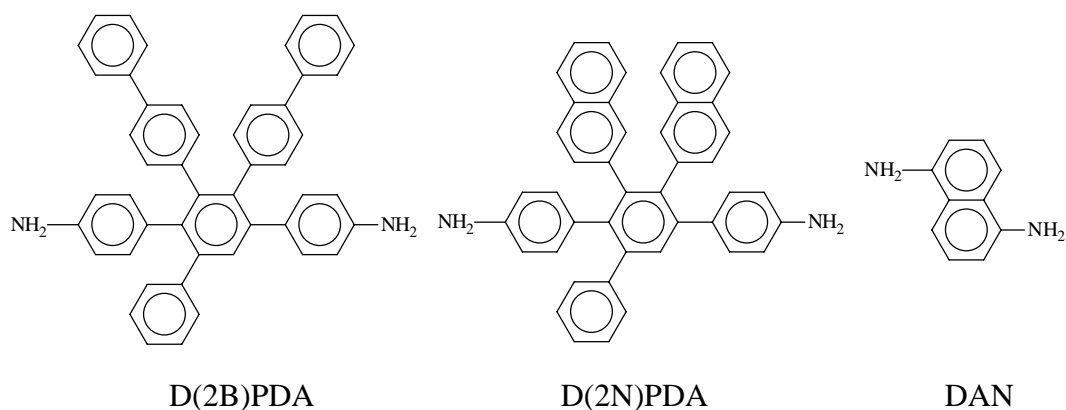
**Table 3.2** Influence of relative humidity on the water uptake, shown as overall moles of water per sulfonic acid group.

Relative Humidity (%)	Moles of water per sulfonic acid group					
	RD5	RF5	RO5	R(3P)T5	R(4P)T5	Homo-polymer
100	10.1	10.1	9.55	10.1	10.5	9.72
75	5.45	6.38	5.04	5.38	5.79	4.32
50	4.09	4.61	4.19	4.39	4.16	3.28
35	3.34	3.84	3.26	3.53	3.38	2.7
15	2.86	3.23	2.38	2.52	2.74	2.42

### 3.1.2) Co-polymers with bulkier side groups

We are designing new polyimides that should show even higher water retention and proton conductivity than the copolymers presented above. In this quarter, we tested five newly synthesized bulky diamines as co-monomers for the polyimide electrolyte: 1,4-bis(4-aminophenyl)-2,3-di-biphenyl-5-phenylbenzene (D(2B)PDA); 1,4-bis(4-aminophenyl)-2,3-dinaphthyl-5-phenylbenzene (D(2N)PDA); 2',6', 3'', 5''tetra (R-phenyl) 4, 1''''-diazapentaphenylene diamine (NHA [R=H], NMA [R=CH<sub>3</sub>] and NEA [R=ethoxy]). The synthesis and polymerization of both D(2B)PDA and D(2N)PDA are new, and have not been previously reported in any literature that we are aware of. The structures of these diamines are shown below. A commercial diamine, 1,5-diaminonaphthalene (DAN), has also been incorporated as a co-monomer. This compound is the first in a new concept for creating nano-scale pores in these electrolytes, as discussed in Section 3.2 below.

The diamines shown below all have a rigid-rod structure; the difference is that D(2B)PDA, D(2N)PDA, NHA, NMA and NEA are linear while the bonds for DAN, while co-linear, are staggered by 1.4Å, creating a jog in the backbone. The copolymers were synthesized with co-monomer ratios of 2.5, 5 and 10%. Intrinsic viscosities with the first three monomers were between 3.2-4.6 dL/g, showing that high molecular weight polymers were obtained. The NHA, NMA and NEA copolymers had IVs of about 2.3 to 2.8. The copolymer with 10% D(2B)PDA formed gel in solution so it was not studied further.



R=H (NHA); R=CH<sub>3</sub> (NMA); R=OCH<sub>2</sub>CH<sub>3</sub> (NEA)

New, bulkier, co-monomers incorporated into polyimides.

**Table 3.3 and Figure 3A** summarize the conductivities of these new copolymers, with Nafion and homopolymer as references. All the new copolymers have good conductivities throughout the entire relative humidity region. One copolymer, R([2B]PP)<sub>5</sub>, shows the highest conductivity at low RH that we have measured; it is  $1.4 \times 10^{-3}$  S/cm at 15%RH, twenty five times higher than that of Nafion.

The data for the RNMA series are presented in Fig. 3A since these had the highest conductivity in this series. RNHA had somewhat lower conductivity (smaller cross-section), but the RNEA series had only very slightly lower conductivity.

**Table 3.3. Conductivity of bulkier copolyimides as a function of relative humidity, compared with Nafion and homopolymer\*.**

RH(%)	Conductivity (S/cm)							
	Nafion	Homopolymer	R([2B]PP)5 <sup>a</sup>	R([2B]PP)2.5 <sup>b</sup>	R([2N]P)5	R([2N]P)2.5	RN5	RN2.5
100	0.06	0.19 (0.07)	0.22 (0.05)	0.20 (0.01)	0.23	0.25	0.24 (0)	0.16 (0.05)
75	0.030	0.018 (0.003)	0.050 (0.01)	0.051 (0.01)	0.031	0.030	0.026 (0.006)	0.040 (0.004)
50	0.013	0.004 (-)	0.010 (0)	0.012 (0.006)	0.009	0.008	0.009 (0.001)	0.008 (0.001)
35	2.0E-3	1.5E-3 (7.2E-4)	4.4E-3 (0)	3.1E-3 (3.0E-4)	7.3E-3	2.6E-3	3.5E-3 (9.0E-4)	3.8E-3 (6.0E-4)
15	4.8E-5	3.1E-5 (2.1E-5)	1.4E-3 (7.5E-5)	9.0E-4 (8.7E-5)	3.7E-4	1.2E-3	5.1E-4 (1.1E-4)	5.2E-4 (1.0E-5)

\*: Averaged data; the standard errors are shown within brackets.

<sup>a</sup>: same sample, three times over 7days;

<sup>b</sup>: two samples, three times in all.

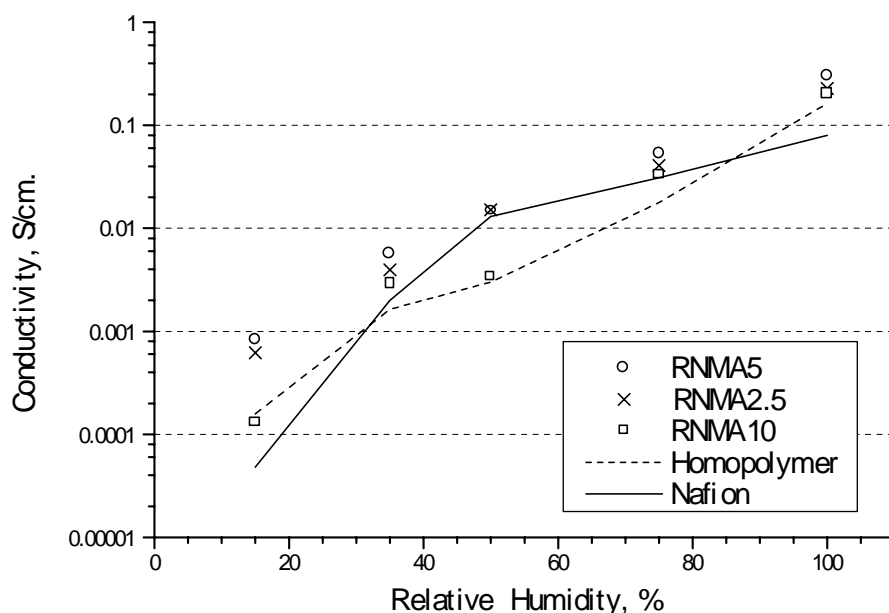


Figure 3A. Conductivity of RNMA copolymers vs. homopolymer and Nafion

#### WAXD analysis

**Table 3.4** presents the  $d$ -spacings data for the bulkier copolyimides. Since the homopolymer is used as the reference, we tested the reproducibility and thus the validity of WAXD measurements by making two x-ray scans on a new homopolymer fiber. The data for the intermolecular spacing of the homopolymer agree very well (6.03Å average with 0.07Å standard error). All the bulky co-monomers generated copolymers with larger interchain spacings ( $d_{HI}$ )

than the homopolymer within the experimental error. This correlates well with the conductivity data, shown in Table 3.3 and Fig. 3A; unfortunately there is still too much error to determine if the interchain distances for the copolymers correlate directly with their conductivities. We have shown that bulky co-monomers prevent the rigid rod chains from packing closely and thus help increase conductivity at low relative humidities.

**Table 3.4. Calculated  $d$ -spacings of bulkier polyimides.**

Polyimide	Equatorial diffractions		Meridional diffractions			
	$d_{H1}$ (Å)	$d_{H2}$ (Å)	$d_{V1}$ (Å)	$d_{V2}$ (Å)	$d_{V3}$ (Å)	$d_{V4}$ (Å)
Homopolymer (old)	6.03	3.81		8.03	5.42	
Homopolymer (new)	5.96	3.72	16.11	8.16	5.48	3.98
	6.10	3.69	17.08	7.98	5.39	3.92
R([2B]PP)5	6.28	3.65	16.12	8.11	5.47	
	6.08	3.72	16.12	8.07	5.45	
R([2B]PP)2.5	6.15	3.74	16.35	7.98	5.47	3.95
RN5	6.35	3.72	15.96	8.12	5.48	
RN2.5	6.22	3.74	15.84	7.99	5.44	3.93
R([2N]P)5	6.18	3.73	16.17	8.06	5.49	3.89
R([2N]P)2.5	6.25	3.73	16.17	7.99	5.46	4.06
RNMA5	6.21	3.81		7.95	5.50	

#### *Water Absorption*

**Table 3.5** shows much of the data collected to date. As expected, higher water absorption correlates with higher conductivity. An interesting point shown in this table is that the RNMA series absorbs 60 to 70% more water per sulfonic acid group from 75 to 35% relative humidity than does the homopolymer. They also have the highest water contents at 15% relative humidity, after RF5.

**Table 3.5 Influence of relative humidity on the water uptake, shown as moles of water per sulfonic acid group.**

Relative Humidity %	Moles of water per sulfonic acid group							
	RF5	RO5	R(3P)T5	R(4P)T5	RNMA5	RNMA 2.5	BP10 18/2	Homo-polymer
100	10.1	9.55	10.1	10.5	10.3	10.4	9.22	9.72
75	6.38	5.04	5.38	5.79	6.9	6.9	4.45	4.32
50	4.61	4.19	4.39	4.16	5.5	5.5	4.16	3.28
35	3.84	3.26	3.53	3.38	4.3	4.3	2.24	2.70
15	3.23	2.38	2.52	2.74	2.9	2.9	1.60	2.42

Angled

Bulky, Linear

Very Bulky, linear

Narrow, linear

#### *Water Resistance*

Most of the copolymers have been tested for water resistance. **Table 3.6**, repeats data given in the previous report but with new data added. All polymers containing bulky co-monomers, even in concentrations as low as 2.5 mole%, had good resistance to water.

**Table 3.6. Water resistance of polyimide membranes**

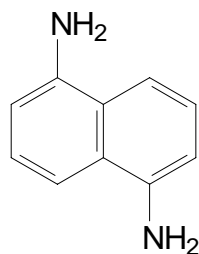
Polymer	Water at 50 °C (12 hr)	Water at 90 °C (12 hr)	Boiling water (48 hr)*
<b>Homopolymer</b>	Dissolved at RT	-	-
<b>RF5</b>	Dissolved after 2 hrs at 25°C	-	-
<b>RO5, RO10, RF10</b>	Dissolved**	-	-
<b>RF20, BF20(8/2)</b>	Stable	Disintegrated	-
BP10(18/2)	Stable	Stable	Stable
R(3P)T5, R(4P)T5	Stable	Stable	Stable
BF10(18/2), BF20(16/4)	Stable	Stable	Stable
PNHA2.5, 5 and 10	Stable	Stable	Stable
PNMA2.5, 5 and 10	Stable	Stable	Stable
PNEA2.5, 5 and 10	Stable	Stable	Stable

Immersion in boiling water was subsequently extended to three weeks. Most films started to tear by that time.

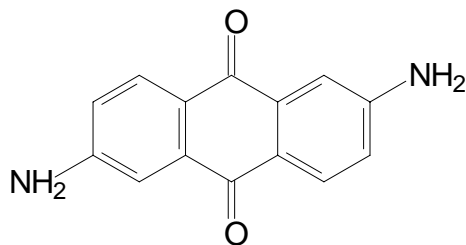
\*\* Films stable at RT.

### 3.2 Polyimide co-polymers with stepped backbones

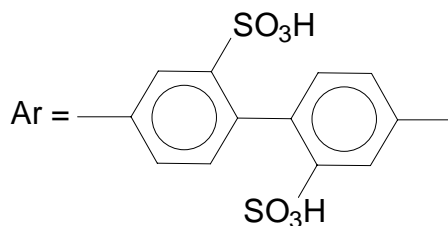
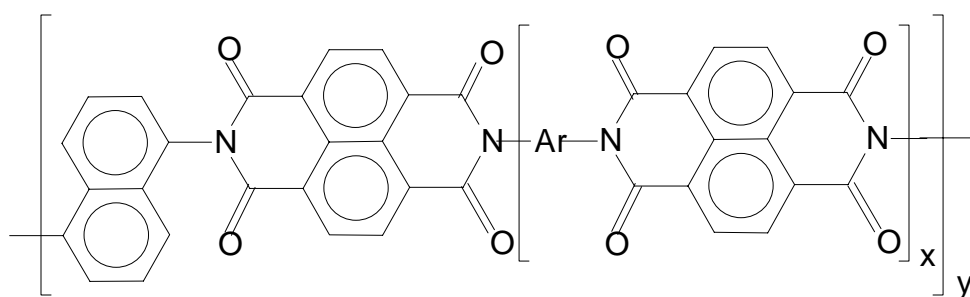
A series of copolyimides containing naphthyl or anthraquinonyl moieties in the backbone were synthesized from two new aromatic diamines (1,5-DAN and 2,6-DAA). These polymers will have much bigger voids in the structure than the homopolymer does without sacrificing polymer rigidity. In order to demonstrate the relationship between structure and properties of copolyimides, cascade-type copolyimides which have different chain lengths (x (predicted degree of polymerization between joints) = 4, 9 or 19) have been synthesized.



1,5-Diamononaphthalene (1,5-DAN)

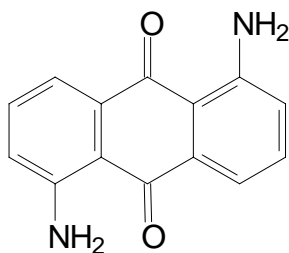


2,6-Diaminoanthraquinone (2,6-DAA)



Cascade-type copolyimide

Complete characterization of the polymers will be carried out in the next quarter. Also, 1,5-diaminoanthraquinone (1,5-DAA) will be used as a co-monomer. 1,5-DAA should provide bigger voids in the structure than 1,5-DAN or 2,6-DAA.



1,5-Diaminoanthraquinone (1,5-DAA)

Details of the monomer and polymer synthesis are given in Appendix A.

**Task 4. Novel polymer incorporation into micro fuel cell.**

A large batch (10 g) of the RF5 copolyimide was synthesized for use in membrane casting/printing studies. Printing films from a 5% solution in DMSO and using a 400 mesh screen produced very good edge definition. However, the polymer films were very thin,  $\approx 1\text{ }\mu\text{m}$ . Increasing the solution concentration to 8% produced significantly thicker films, from 20 to 100  $\mu\text{m}$ . The fuel cell results obtained with these films are reported under Task 2 above.

**Task 5. Palladium thick film deposition and characterization**

no new data to report

**2. DIFFICULTIES/PROBLEMS**

- Deposition of well-defined, pinhole free polymer layers of the appropriate thickness is still an issue.
- Demonstration of sufficiently high permeability anode fuel distributor in fuel cell structure has not been achieved.
- A further increase in the volumetric energy density of the Pd/H storage block is desired.



## Supplemental Information

### Synthesis of random copolyimides

The random copolyimides were prepared by one-step polymerization. The molecular ratio of monomers NTCDA:DAPS:2,6-DAA (or 1,5-DAN) was selected as 100:90:10. A typical polymerization procedure is as follows. DAPS (0.58 g, 1.68 mmol), 2,6-DAA (0.044 g, 0.19 mmol) and TEA (0.34 g, 3.37 mmol) in 21 mL of *m*-cresol were stirred at 100 °C under N<sub>2</sub> for 1 h. NTCDA (0.50 g, 1.86 mmol) and 5 drops of quinoline were added to the reaction mixture. It was refluxed at 200 °C for 16 h. After the solution cooled to ambient temperature, 10 mL of *m*-cresol was added to the solution for dilution. The viscous solution was poured slowly into the mixture of conc. HCl (100 mL) and MeOH (700 mL) with stirring. The precipitate was filtered and dried at 50 °C under vacuum for 24 h.

### Synthesis of cascade-type copolyimides

The molecular ratio of monomers NTCDA:DAPS:1,5-DAN (or 2,6-DAA) was selected as 100:95:5, 100:90:10 and 100:80:20. A typical example of polymerization for this series of polymers is as follows. NTCDA (0.50 g, 1.86 mmol) in 21 mL of *m*-cresol was stirred at 90 °C under N<sub>2</sub> for 1 h. DAPS (0.58 g, 1.68 mmol) and TEA (0.34 g, 3.37 mmol) were added to the reaction mixture. After it was stirred at 160 °C for 15 h, 1,5-DAN (0.03 g, 0.19 mmol) and 5 drops of quinoline were added to the solution. It was heated to reflux at 200 °C under N<sub>2</sub> for 20 h. After the solution was cooled to ambient temperature, 10 mL of *m*-cresol was added to the solution for dilution. The viscous solution was poured slowly into the mixture of conc. HCl (100 mL) and MeOH (700 mL) with stirring. The precipitate was filtered and dried at 50 °C under vacuum for 24 h.

## 1. RESEARCH STATUS

### Task 1. Micro Fuel Cell Power Unit/Microfabrication Development

#### *1.1 Demonstration and Testing of Fabrication Steps*

The basic sequence of fabrication steps is given in **Table 1.1**.

**Table 1.1** Fabrication Procedure – Sequence of deposition steps and materials used

<u>Layer Description</u>	<u>Material</u>
Insulation/Sealant	Commercial polymeric ink
anode current collector	Commercial gold ink
anode catalyst	Pt/C, Nafion
polymer electrolyte	Nafion/EG
cathode catalyst	Pt/C, Nafion
cathode current collector	Commercial gold ink

During the past quarter, fabrication efforts have focused on cells fabricated on microporous filter membranes. We have been unable to develop a printable ink that yields a conductive and highly porous layer on which to fabricate the rest of the fuel cell. As a result, we are now fabricating fuel cells starting with a microporous material as the substrate. When the microporous membranes are used, it is necessary to seal the membrane area around each fuel cell. For this purpose, an insulating sealant layer is printed prior to the fuel cell fabrication as detailed in Table 1.1. The requirements for the microporous membrane include thermal stability (we are working with inks cured at up to 110°C), solvent stability (the substrates will be contacted by the solvents in the inks) and an appropriate surface energy (the inks must wet the surface sufficiently to print evenly and adhere). Our trials with this concept have mainly used cellulose acetate and nylon membranes, as based on the manufacturer's literature, these membranes appeared to have the best combination of the necessary properties. Several other membranes have been considered and found to be inferior to the nylon membranes, as detailed in **Table 1.2**. The combination of pore size and surface energy of the microporous membranes is an important parameter, we would like the current collector and anode inks to wet the surface, but not penetrate deeply into the membrane pores to achieve maximum permeability. Naturally, a large pore volume is desired for maximum permeability, as is a thinner substrate. In regions outside the active area of the fuel cell, we would like the insulation/sealant ink to fully penetrate the substrate to achieve maximum impermeability in these areas. Based on our previous difficulties in developing/discovering acceptable catalyst and current collector inks, at this time we are only considering varying the substrate and/or insulation/sealant ink.

**Table 1.2** Microporous Membranes considered as Fuel Cell Substrates

Material	Pore Size	Comments
Cellulose Acetate	0.65, 1.2, 5 $\mu\text{m}$	solvent resistance questionable
Nylon	0.45, 1.2, 10 $\mu\text{m}$	acceptable
Polycarbonate	5 $\mu\text{m}$	insufficient mechanical strength
Gore-Tex®	0.02 $\mu\text{m}$	Gold ink poorly adherent
PVDF	0.1 $\mu\text{m}$	Gold ink poorly adherent
polyether sulfone (PES)	0.2 $\mu\text{m}$	poor solvent resistance
glass fiber	10 $\mu\text{m}$	rough surface leads to shorted cells
“FN” - Teflon/polypropylene	0.2 $\mu\text{m}$	low $\text{H}_2$ permeability

**Task 2. Performance and diagnostic testing of micro fuel cell power unit.**

Typical polarization curves for two cells fabricated on cellulose acetate membranes are shown in **Figure 2.1**. The cathodes were exposed to the laboratory air (75°F, 42%RH), the anodes were fed with hydrogen humidified at room temperature. Also shown in this figure is the polarization curve obtained under similar conditions for a ‘free-standing’ cell, a cell consisting of a Nafion 117 membrane on which the anode, cathode and current collectors were deposited using the same inks used in the microfuel cell fabrication. The microfabricated cells produce  $\approx 4 \text{ mW/cm}^2$  at 0.5V, the free-standing cell  $\approx 10 \text{ mW/cm}^2$ . The main difference between the two types of cells is the presence of the porous membrane substrate on which the microfabricated cells are constructed. The difference in the power output of the two cells is due to the mass transfer resistance resulting from the presence of the substrate, which limits the transport of hydrogen to the anode. It should be noted that the polarization curves shown in Figure 2.1 were acquired by sweeping the cell voltage at 2 mV/s from its open circuit value to zero volts. Even with this relatively slow sweep, the power output of the microfabricated cell is over-estimated; the true steady-state power output is closer to  $2 \text{ mW/cm}^2$ . The performance of the free-standing cell, which has less of a mass transfer limitation, is more accurately represented in the slow sweep data. When the 10  $\mu\text{m}$  pore nylon membranes are used as substrates, polarization curves similar to those shown in Figure 2.1 for the cellulose acetate substrates are obtained. The advantages of the nylon membranes are in fabrication yield and consistency of performance, as detailed below.

An example of the steady-state performance of a microfabricated cell is shown in **Figure 2.2**. In this case a cell fabricated on a nylon membrane was used, with humidified hydrogen and the laboratory air was at 48% RH. The cell voltage was held at 0.5V over the 20 hour period shown, and the current recorded. The average power produced over this period is  $1.75 \text{ mW/cm}^2$ . The variations seen in the current output are due to random variations in the air currents within the laboratory.

An example of consistency of fabrication achieved using the nylon membranes as substrates is shown in **Figure 2.3**. The power produced at 0.5 V for 18 cells fabricated in a single afternoon is shown. None of cells were shorted, or otherwise failed to produce electricity. The power levels produced range from 1.3 to  $2.5 \text{ mW/cm}^2$ , with an average of  $1.9 \pm 0.4$ . The hydrogen used

was humidified in anticipation of operating these cells on the borohydride based hydrogen generator described in Task 5. It should be noted that these cells were tested over the space of 5 days, during which there were uncontrolled variations in both the temperature (72 – 78 °F) and humidity (42-52% RH) in the laboratory.

In order to evaluate the effect of the humidity content in the air on the performance of these cells, four cells were selected for testing as a function of relative humidity. For these tests, the cells were placed inside a sealed container, with feedthroughs for the hydrogen supply and exhaust. Aqueous solutions of LiCl of varying concentration were used to control the humidity inside the chamber. Placing the cells inside the chamber also eliminated the effects of random fluctuations in the air currents in the laboratory. The results are shown in **Figures 2.4 and 2.5** in terms of the power produced at 0.5V and the internal resistance of the cells. The latter was determined using AC impedance spectroscopy in the frequency range of 5-20 kHz. From Figure 2.4 it can be seen that the power output varies from  $\approx 0.5 \text{ mW/cm}^2$  at 15-20%RH to  $3.5 \text{ mW/cm}^2$  at 90%RH. The variation between the four different samples is generally small, although it is significant around 50%RH, the conditions used to generate the data shown in Figure 2.3. From Figure 2.5, it can be seen that above 60%RH, there is little change in the internal resistance of these cells. However, between 50 and 40%RH, the resistance starts to increase significantly. Small differences in the humidity level at which the resistance noticeably increases are responsible for the spread in the power output observed around 50% RH. There is a distinct correlation between increased resistance and lower power output, as would be expected. The sensitivity of the power output to relative humidity in the 40-50%RH range could be responsible for much of the variation seen in Figure 2.3.

In Figure 2.5 it can also be seen that the resistances at the lowest humidity levels are roughly 15X greater than the resistance at the highest humidity. While this variation is still significant, as shown in Figure 2.4, it does point out the advantage of operating on humidified hydrogen as produced by the aqueous borohydride system. Without the humidity provided with the fuel, it would be expected that the internal resistance would vary by a factor of 100 over the same range, as the electrolyte conductivity varies from 1 to 100 mS/cm from 15-100% RH as detailed in previous reports on this project.

The pulse power capabilities of these cells have also been investigated. The pulse response of these cells is provided by discharging the capacitance of the cells. For these tests, the cells were initially at open circuit, typically 0.8V, and the pulse level increased until the cell voltage during the pulse fell below 0.5V. For fuel cells operating on humidified hydrogen and air at  $\approx 50\%$  RH, single 10 msec pulses of  $50 \text{ mW/cm}^2$  could be delivered from cells fabricated on nylon membranes. At higher humidity levels in the air, e.g. 80%RH, the pulse capability increases by a factor of 2, as the internal resistance decreases. Similarly, if the humidity level is decreased below 50%, such that the internal resistance increases as shown in Figure 2.5, the pulse power that can be delivered while maintaining a cell voltage above 0.5V drops as low as  $5 \text{ mW/cm}^2$ .

To test the ability of the microfabricated cells to produce repetitive pulses, a controlled current pulse train as used. As shown in **Figure 2.6**, the pulse train consisted of a 10 msec pulse, followed by a 90 msec baseline period, i.e., a 10% duty cycle. The current drawn during the baseline period was  $500 \mu\text{A/cm}^2$ . For a given pulse current, the cell was operated until the cell

voltage during the pulse fell below 0.5V. For a pulse current of 25 mA/cm<sup>2</sup>, this cut-off was not reached until 90 minutes had passed. For a 50 mA/cm<sup>2</sup> pulse, the cut-off was reached in 10 minutes. Although over 50,000 pulses were drawn in these tests, there were no permanent effects on the steady-state performance of this cell.

A ‘real-life’ example of a pulse train similar to those described in the preceding paragraph is shown in **Figure 2.7**. This figure shows the current and voltage response when two series connected cells were used to power a laboratory timer (in normal operation, this timer is powered by a AAA battery). The background current required to drive the timer display and clock is less than 100  $\mu$ A. However, whenever a button is pushed on the timer, such as to increase the time to be counted down, the timer produces an audible ‘chirp’. To produce this sound, a pulse train lasting 15.5 msec is drawn as detailed in the figure. The peak current drawn is  $\approx$  6mA, the cells used were 0.2 cm<sup>2</sup> in area, for a pulse current density of  $\approx$ 30 mA/cm<sup>2</sup>.

In the above example, two cells were series connected during the fabrication process. During the past quarter, stacks of two and three cells in series have been successfully fabricated. In general, the performance of the series connected cells has been slightly poorer than expected based on the performance of the individual cells in the stack. An example of this is shown in **Figure 2.8**, for a two cell stack. A polarization curve for each cell was measured, and those polarization curves were summed (the voltages were added for a given current draw) and compared to the polarization curve obtained from the cells in series. While there should be some differences between the two curves due to the added resistance of the inter-cell connection, this resistance is not large enough to account for the difference seen between the two curves. In the next quarter, we will continue these studies to pin down the factors behind this effect.

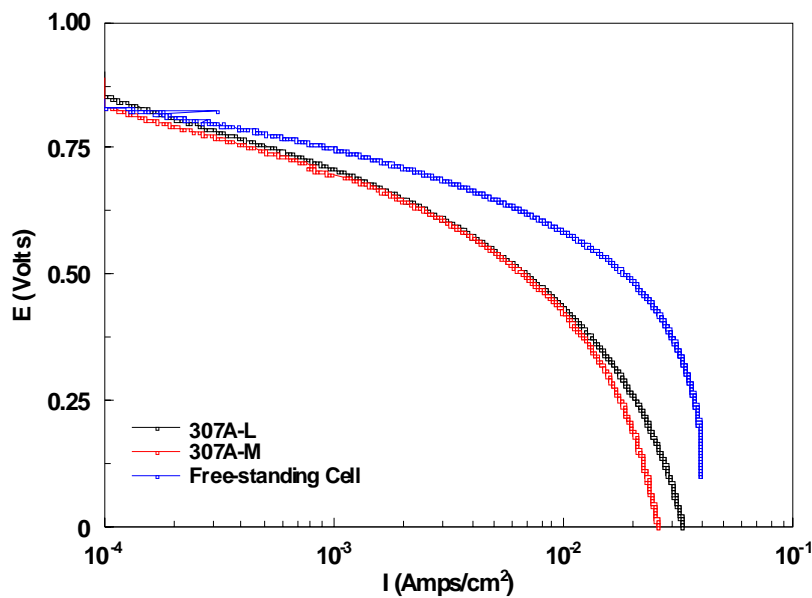


**Figure 2.1** Polarization curves obtained at 2 mV/s for two cells fabricated on cellulose acetate membranes, and for a free-standing cell fabricated on Nafion 117.

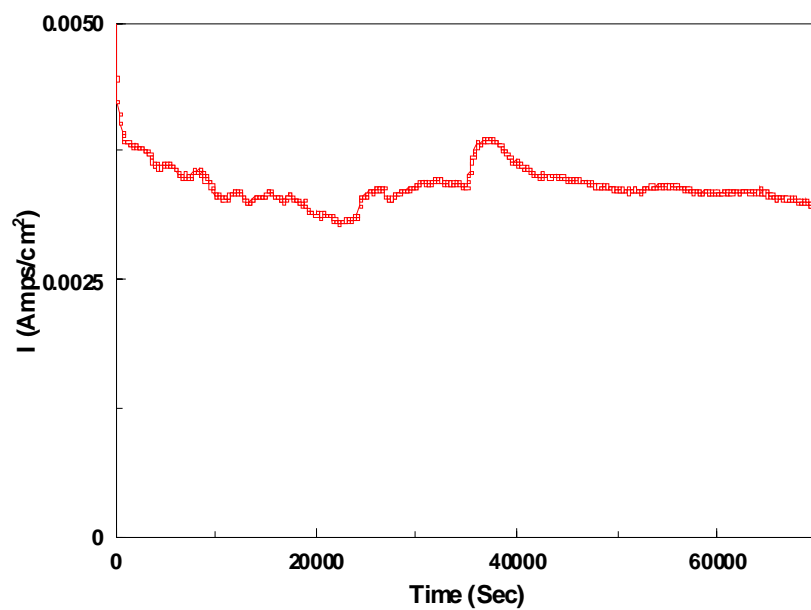


**Figure 2.2** Current output at 0.5V over 20 hours for a cell fabricated on nylon membrane. Humidified hydrogen and air at 48% RH.

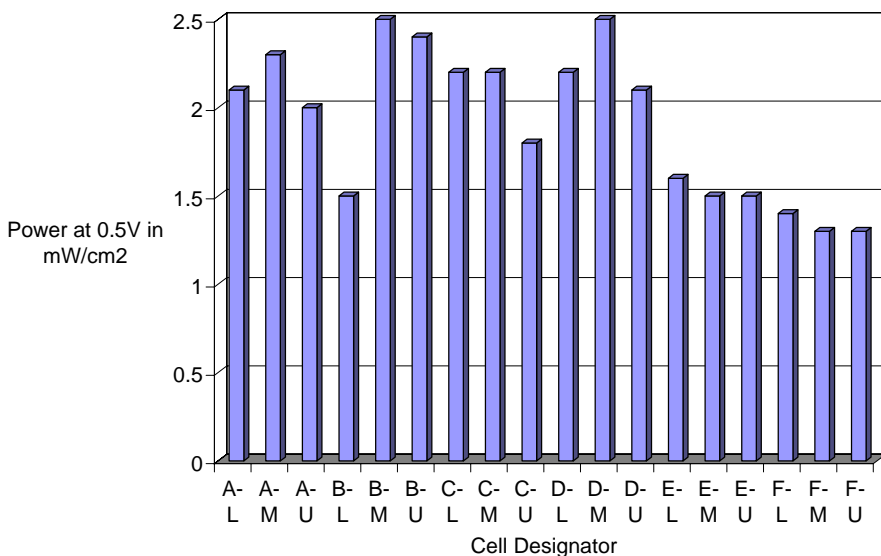


**Figure 2.3** Power output at 0.5V for 18 cells fabricated on nylon membrane.

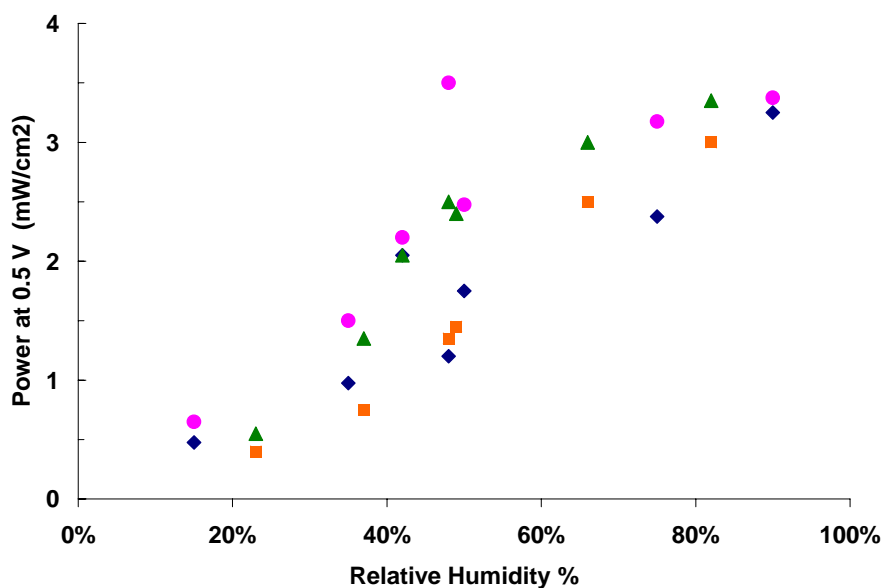


**Figure 2.4** Power output at 0.5V as a function of relative humidity in the air for four cells fabricated on nylon membrane. Hydrogen feed humidified at room temperature.

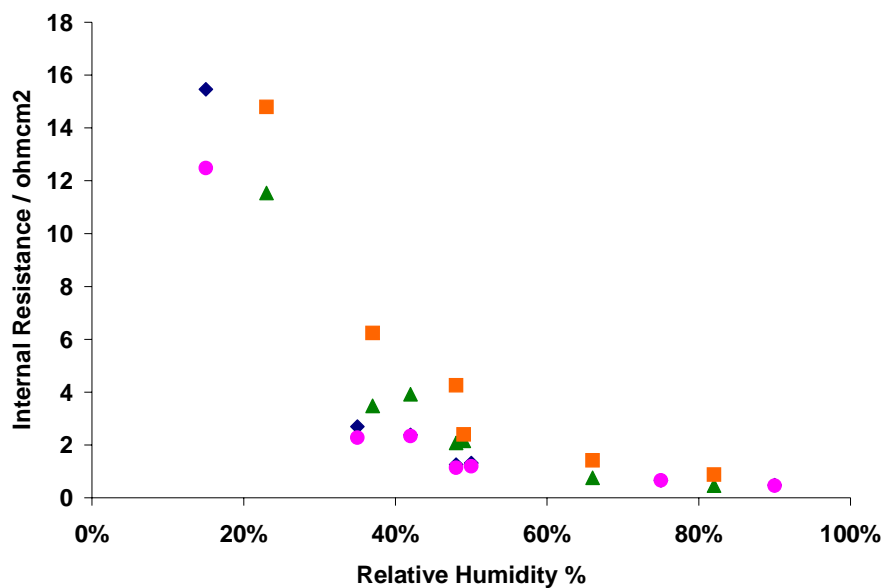


**Figure 2.5** Internal resistance as a function of relative humidity in the air for four cells fabricated on nylon membrane. Hydrogen feed humidified at room temperature.

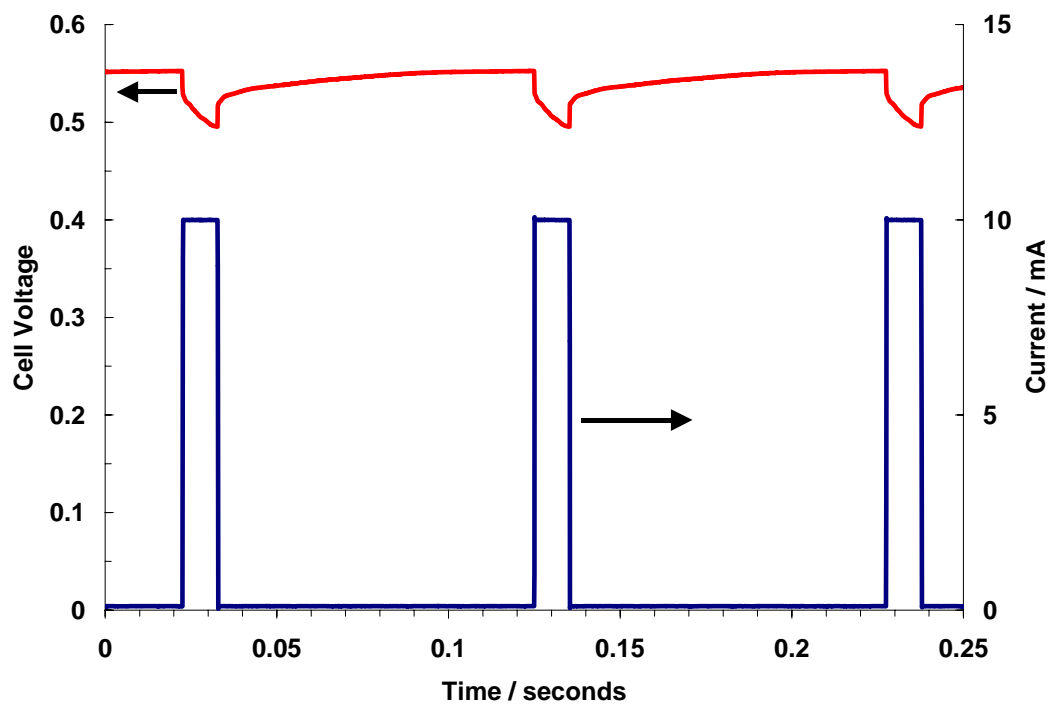


**Figure 2.6** Cell voltage during a repetitive pulse test. 10 mA pulses (50 mA/cm<sup>2</sup>), 10 msec wide on a 10% duty cycle. Baseline current 100  $\mu$ A.



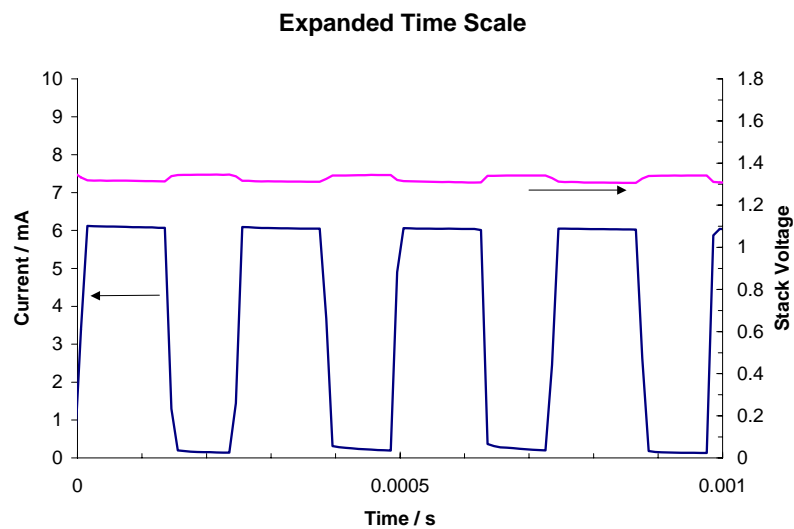
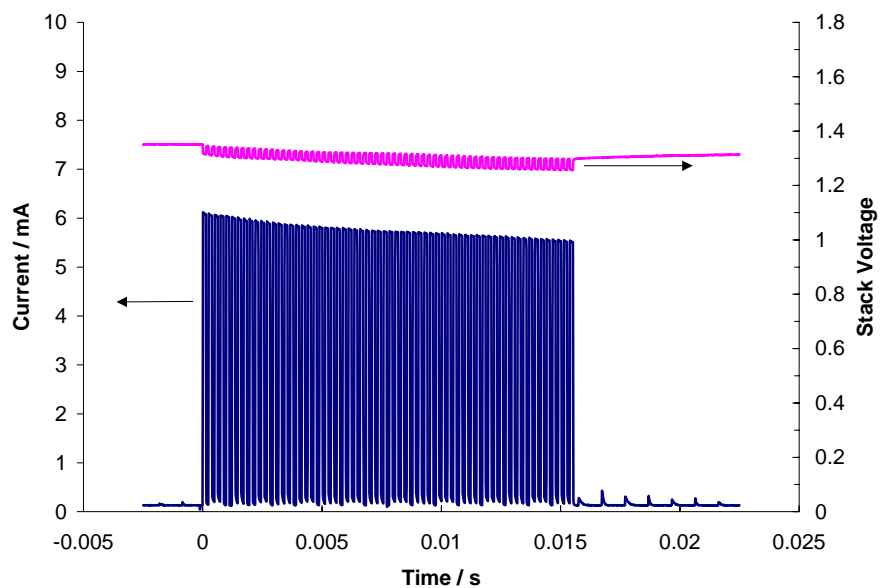


**Figure 2.7** Cell voltage and current drawn during an audible ‘chirp’ on laboratory timer. Two cells in series,  $0.2 \text{ cm}^2$  each. Hydrogen humidified at room temperature, air at 82%RH. Lower figure is the same data on an expanded time scale.

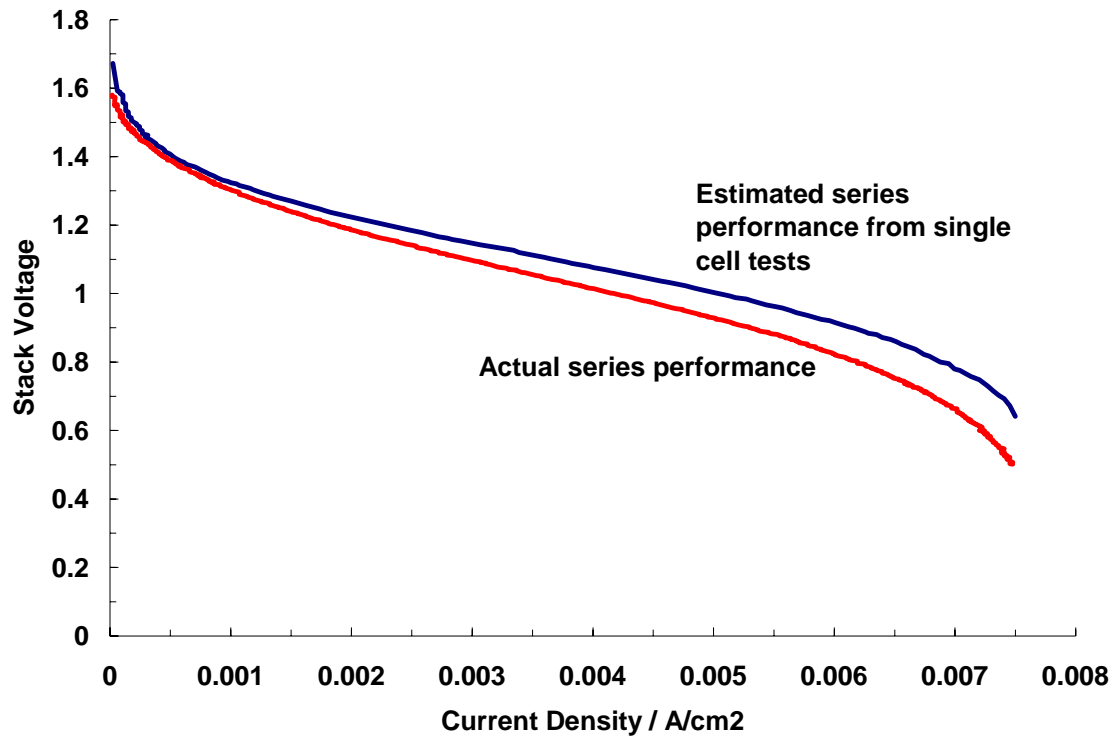


**Figure 2.8** Performance of two series connected cells as compared to the estimated series performance based on the performance of the individual cells.

### **Task 3.        Novel polymer synthesis and characterization**

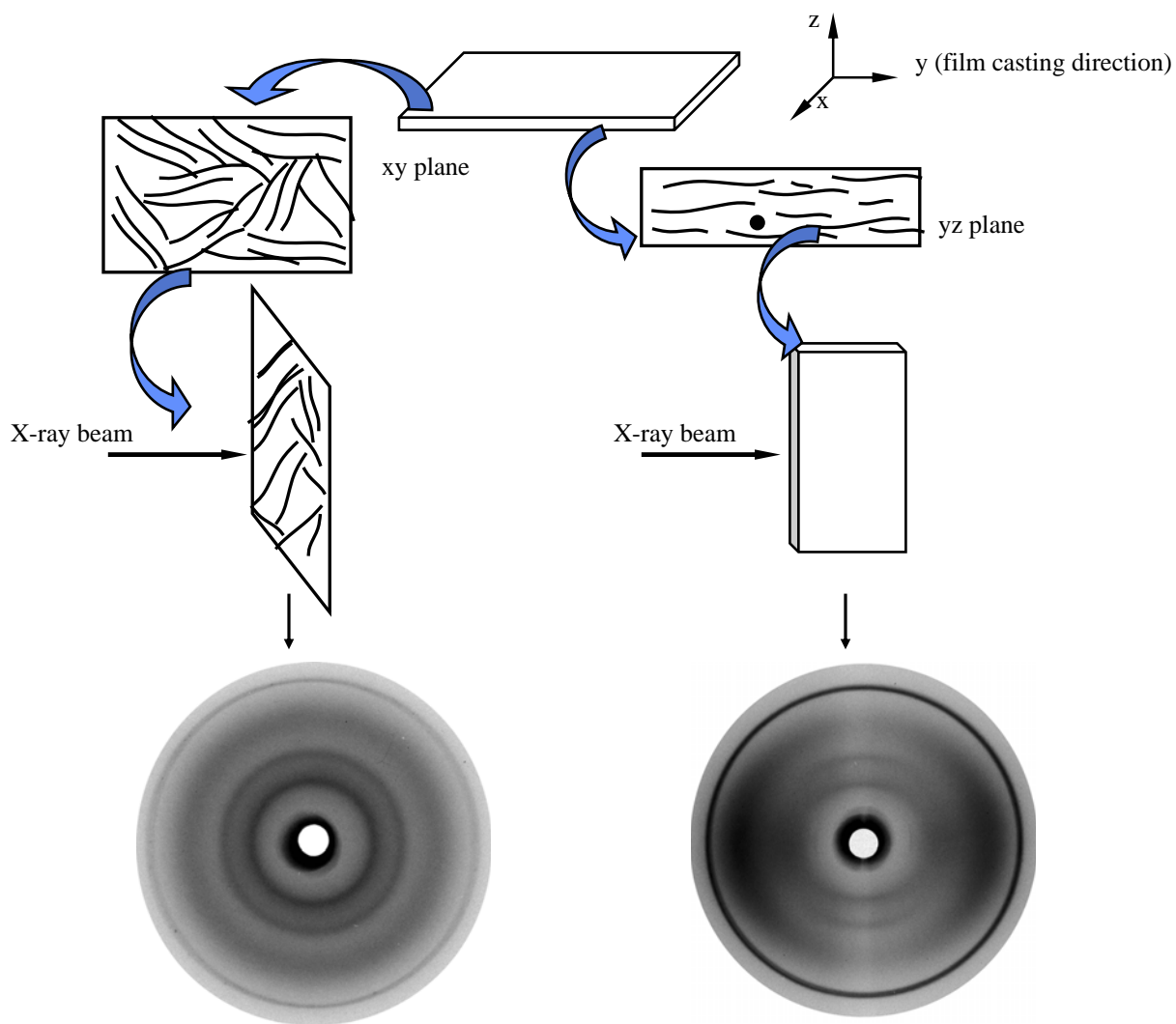
We are seeking novel proton conducting polymers that have reasonable proton conductivity at low humidity, good mechanical properties, low gas permeability, and dimensional stability. We have synthesized sulfonic acid containing co-polyimides that incorporated bulky diamines. The bulky groups are expected to push the polymer backbones apart and keep them apart along the whole chain length. This should create a nanoscale pore lined with sulfonic acid groups. Such pores should adsorb water very strongly even at relatively low humidity.

The problem with the homopolymer and the co-polymers containing small or angled comonomers is that they are water soluble. Random and block co-polymers either dissolve or fragment easily in water at elevated temperatures. We have synthesized sulfonic acid containing co-polyimides that incorporate a series of linear diamines with bulky side groups. These are more stable in water. We now have a series of co-polymers that absorb water well, and conduct at about the same level as the co-polymers previously discussed. They are all liquid crystal and their interchain distances are larger than that of the homopolymer. We continue to synthesize and characterize bulkier diamines seeking the optimal blend of the desired properties. While we have increased conductivity over previous polymers, there have been no dramatic increases. Similarly, while the stability of these polymers in water is better, they are still soluble at elevated temperatures. As a result, we are synthesizing analogous systems, which use a different principle to force the chains apart. New groups are being inserted into the polymers that create jogs or steps in the backbone while keeping the backbone segments co-linear. Depending on the size of these groups, the chains can be shifted by 1.4 to 50Å. The large spacers will dilute the carrier concentration, but may increase carrier mobility. Details of the latest synthesis efforts in this area can be found in Appendix A.

### 3.1. Packing of polyimide chains in membranes

The study of the packing of polyimide chains by X-ray diffraction method was continued in the past quarter; the XRD patterns of polymer films taken through the xy and yz planes were recorded as shown in Scheme 1. The xy plane XRD pattern showed liquid crystalline feature but large-scale isotropic packing, while the yz plane pattern showed side-by-side packing of the polymer chains similar to the fiber pattern. These results indicated that the rigid rod polymer chains tend to form liquid crystal domains that lie down and pack parallel to the film surface.

Therefore, the change in packing of the polyimide chains, which affects the unoccupied volume of the film, can be elucidated in the XRD results of oriented polyimide fibers. It further suggested that the interchain spacings of the copolymers obtained from the X-ray diffraction pattern of the polyimide fibers correlate with the bulkiness of the co-monomer used for copolymerization.



Scheme 1. XRD pattern of homopolymer films taken through the xy and yz planes

### 3.2. Orientation of polyimide films

Due to the need for increased water stability and mechanical strength, a study on orientating polyimide films was carried out this quarter. Polymer films cast from m-cresol in the triethylamine salt form were stretched using the following procedure. After the film was dried, it was washed with ethanol/H<sub>2</sub>SO<sub>4</sub> to convert the film to the acid form. Excess H<sub>2</sub>SO<sub>4</sub> was removed with several washings in pure ethanol. The film was taken out from ethanol and dried. A rectangular piece of film was cut parallel to the casting direction; the thickness and width were recorded. The film was mounted on a frame, and the length between the two gauges was recorded. The film was then immersed into ethanol so that it would swell and soften. The elongation process started after 1-2 minutes of immersion. During the stretching, it was observed that the width and thickness of the film decreased. The increase in length was recorded and elongation ratio was calculated.

DMTA tests of the mechanical properties of the stretched polyimide films showed that a film with 40% elongation has modulus of 16 GPa, about 3-4 times higher than that of the original film (3-4 GPa). The stability of the stretched films in water has not yet been determined. An apparatus to bi-axially stretch films is being designed.

### 3.3. Water stability of UV crosslinked polyimides

We are still seeking ways to produce polyimides with higher water stability and reasonably high proton conductivity for fuel cell tests. Previously, we have thermally crosslinked polyimide films and observed enhanced stability, however this procedure is not compatible with the current microfuel cell fabrication process. This quarter, a new task of UV cross-linking to modify the polyimides' structure was initiated. The general procedure used is as following: a diazide photoinitiator (4,4'-Diazidostilbene-2,2'-disulfonic acid disodium salt) was mixed thoroughly with salt form polyimides to make 5wt% (total weight) DMSO solution. Polyimide films were cast at 60°C following by vacuum drying at 80°C for 24h. During the process of solution preparation and film casting, the whole system was protected carefully from light. The film was then exposed to UV light for a given period. The films were then washed with ethanol/H<sub>2</sub>SO<sub>4</sub> several times and ethanol several times to convert the polymer to the acid form followed by drying thoroughly under vacuum.

Unfortunately, the cross-linking degree is limited even with very high photo initiator concentration (~1000 mol%) and long time exposure (2 h) at conventional UV intensity. The best films were stable for 2 hr in water at 90°C before dissolving, indicating insufficient cross-linking. The UV spectra of the polyimides and the diazide photoinitiator revealed that the polyimides themselves absorb UV stronger within all regions than the photoinitiator. Therefore, the photo cross-linking efficiency was poor. Currently, we are seeking new photoinitiators that absorb at higher wavelength to conduct further experiments.

### 3.4 Conductivity at higher temperatures

Conductivity experiments were carried out on homopolymer membrane and the angled copolyimide known as RF5. The samples were enclosed in polypropylene bottles above a LiCl

solution. Different concentrations of LiCl solution were used to obtain different relative humidities. The experiments are carried out on these two membranes at 5 different relative humidity (15, 35, 50, 75 and 90%) and at room temperature, 40, 60 and 80°C. The results obtained, for the homopolymer and the angled copolyimide, are summarized in **Tables 3.1 and 3.2**, respectively.

**Table 3.1:** Conductivity values for the Homopolymer film at different relative humidity and at different temperatures.

	Conductivity (S/cm) at room temperature	Conductivity (S/cm) at 40°C	Conductivity (S/cm) at 60°C	Conductivity (S/cm) at 80°C
RH=15%	$3.8 \cdot 10^{-4}$	$4.1 \cdot 10^{-4}$	$6.6 \cdot 10^{-4}$	$1.1 \cdot 10^{-3}$
RH=35%	$2.7 \cdot 10^{-3}$	$3.4 \cdot 10^{-3}$	$8.3 \cdot 10^{-3}$	$1.0 \cdot 10^{-2}$
RH=50%	$3.8 \cdot 10^{-3}$	$4.9 \cdot 10^{-3}$	$8.6 \cdot 10^{-2}$	$2.8 \cdot 10^{-2}$
RH=75%	$3.4 \cdot 10^{-2}$	$5.0 \cdot 10^{-2}$	Sample broken	Sample broken
RH=90%	0.16	0.2	0.13	Sample broken

**Table 2:** Conductivity values for the RF5 film at different relative humidity and at different temperatures.

	Conductivity (S/cm) at room temperature	Conductivity (S/cm) at 40°C	Conductivity (S/cm) at 60°C	Conductivity (S/cm) at 80°C
RH=15%	$3.2 \cdot 10^{-4}$	$5 \cdot 10^{-4}$	$1.1 \cdot 10^{-3}$	$1.4 \cdot 10^{-3}$
RH=35%	$4.49 \cdot 10^{-3}$	$5.2 \cdot 10^{-3}$	$7.5 \cdot 10^{-3}$	$1.2 \cdot 10^{-2}$
RH=50%	$8.4 \cdot 10^{-3}$	$1.1 \cdot 10^{-2}$	$1.7 \cdot 10^{-2}$	$3.3 \cdot 10^{-2}$
RH=75%	$3.2 \cdot 10^{-2}$	$4.3 \cdot 10^{-2}$	$7.1 \cdot 10^{-2}$	0.13
RH=90%	0.17	0.15	Sample broken	Sample broken

The results show an increase of the conductivity with the temperature at a given relative humidity except for 90% RH, where the results may be influenced by the beginning of the breakage of the films. It should be noted that based on previous results, neither of these films would be expected to have good stability under elevated temperature, elevated humidity conditions. The conductivity measured for the RF5 film at 15%RH and room temperature is significantly lower, by about 1/3rd, than expected. With the exception of this data point, the RF5 copolyimide has higher conductivity, particularly at lower relative humidities, than the homopolymer. This result indicates that the copolyimide's enhanced water uptake, previously observed at room temperature, is maintained at higher temperatures.

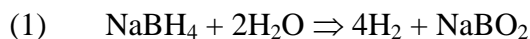
#### Task 4. Novel polymer incorporation into microfabricated fuel cell.

Two fabrication runs were attempted using a 7 wt% solution of the RF5 polymer (acid form) in DMSO. At this concentration the solution has an acceptable viscosity, however the thickness of the polymer layer resulting from a single coating of the solution is insufficient due to the low solution concentration. As a result, most of the cells were found to be electrically shorted after fabrication. Deposition of the electrolyte in multiple layers resulted in the build-up of stress

within the electrolyte layer which eventually caused delamination of the fuel cell from the substrate (10  $\mu\text{m}$  nylon membrane). An alternative solvent which would allow for higher solution concentrations, or an alternative means of depositing the polyimide electrolyte may be required.

### **Task 5. On-board Hydrogen Storage/Generation**

Previously, we had planned to use a thick film printed layer of high surface area palladium particles to provide a means of hydrogen storage. While no major difficulties were encountered developing this layer, there were two drawbacks; 1) the energy density was lower than expected due to a relative high volume fraction of binder needed to make a printable ink, and 2) the low equilibrium pressure for palladium hydride significantly impacted the power that could be produced, particularly in light of the lower than expected hydrogen permeability in the substrate. As a result, a decision was made in the last quarter to consider an alternative means of hydrogen storage that would retain the advantages of the palladium hydride: passive, ambient temperature operation. Hydrogen storage in the form of stabilized aqueous solutions of sodium borohydride ( $\text{NaBH}_4$ ) was chosen. When sufficient base is added to raise the solution pH to  $\approx 14$ , these solutions are stable at room temperature for months. However, when brought in contact with a suitable catalyst, they readily decompose according to reaction (1):



Sodium borohydride is readily soluble in water, and solutions of over 30 wt%  $\text{NaBH}_4$  can be made at room temperature. The solutions are not air-sensitive, are non-flammable, and the decomposition product is non-toxic. For a 30 wt% solution, stabilized with 10 wt%  $\text{NaOH}$ , the following theoretical energy densities can be calculated, 2337  $\text{mWh/cm}^3$  and 2091  $\text{mWh/g}$ . This is equivalent to a chemical or metal hydride storage of  $\approx 7$  wt%  $\text{H}_2$ . Palladium hydride, due to the density of palladium, is only a 0.8 wt% hydride material. While the energy density of these solutions is lower than that of hydrocarbons by a factor of 3-5, there is a distinct advantage in that the borohydride solutions can be decomposed into hydrogen at room temperature in a very simple process. Reforming hydrocarbons to hydrogen is considerably more difficult and requires elevated temperatures. The only requirement for the borohydride system is that the fuel be stored separately from the decomposition catalyst. The borohydride system also offers two distinct advantages for the passive microfabricated fuel cell under development in this program. The first advantage, as compared to the palladium hydride system, is that the hydrogen can be produced at atmospheric pressure, eliminating the power density limitations associated with the low equilibrium pressure of palladium hydride. The second advantage is that the hydrogen that is produced is saturated with water vapor, thus providing a continual source of water vapor to the fuel cell. This has a very distinct benefit in maintaining higher electrolyte conductivity, and thus higher power generation capability as shown under Task 2 above.

In **Figure 5.1**, the hydrogen generation rate from a 20 wt%  $\text{NaBH}_4$  solution stabilized with 10 wt%  $\text{NaOH}$  is shown for a carbon supported Pt catalyst. The catalyst used was in the form of a commercial fuel cell electrode material with a loading of 0.35  $\text{mg Pt /cm}^2$  of catalyst. Four separate samples of catalyst are compared, in each test approximately 1.5  $\text{cm}^2$  of catalyst was

contacted with  $0.5 \text{ cm}^3$  of solution. Within experimental error (the hydrogen production was crudely measured using an inverted, water-filled, volumetric cylinder and a stop-watch) the hydrogen generation rate in each trial is  $0.07 \text{ cm}^3 \text{ H}_2 \text{ (STP)/min cm}^2$ . The  $\approx 15 \text{ min}$  delay in reaching a steady-state rate of hydrogen generation is mainly related to the design of the hydrogen collection system. This result indicates that very little catalyst is required, for  $1 \text{ mg}$  of Pt, the hydrogen generation rate would be  $\approx 0.4 \text{ sccm}$ , an amount sufficient to operate a fuel cell at a current of  $62 \text{ mA}$ . For a  $10 \text{ mW}$  fuel cell as under consideration here, only  $0.33 \text{ mg}$  of Pt would be required to generate sufficient hydrogen, assuming a cell voltage of  $0.5 \text{ V}$ .

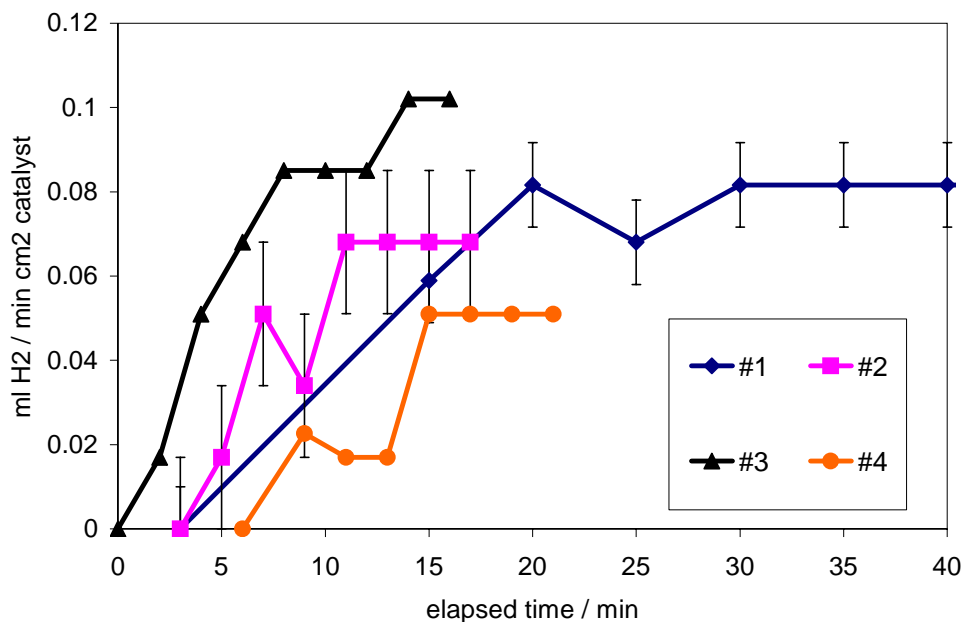


**Figure 5.1** Hydrogen generation rates from a solution of 20 wt%  $\text{NaBH}_4$  and 10 wt%  $\text{NaOH}$  at  $75^\circ\text{C}$ . Catalyst: Pt on XC-72 carbon – Etek Elat electrode,  $0.35 \text{ mg Pt/cm}^2$ . Fresh catalyst used for each trial. Error bars are shown on only two trials for clarity, the error bars on the other two trials (#1, #4) are similar to that of trial #2.

A simple design for a hydrogen generator for the microfuel cell is shown schematically in **Figure 5.2**. A small well contains the borohydride solution, which is injected into the well with a syringe when the fuel cell is activated. The decomposition catalyst is printed onto the bottom of the well. The well is capped with the microfuel cell, with the underside of the microfuel cell substrate exposed to the hydrogen that bubbles up from the catalyst at the bottom of the well. A small vent in the side of the well, above the solution level, allows air to be exhausted when the borohydride solution is injected, and maintains the hydrogen pressure at slightly above ambient.



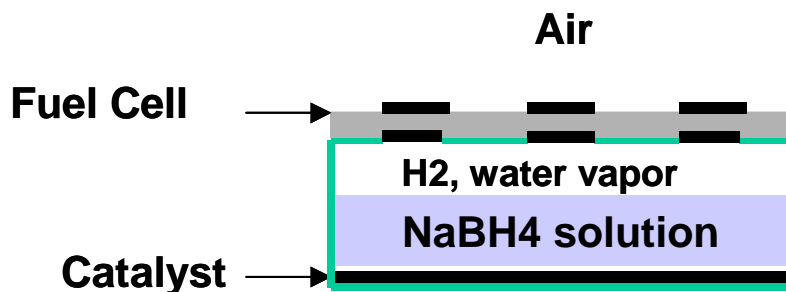


**Figure 5.2** Schematic drawing of borohydride generator coupled to a microfabricated fuel cell.

The amount of energy stored can be varied by simply varying the depth of the well. The obvious drawback of the system shown in Figure 5.2 is that it is orientation dependent, the fuel cell must be held in the orientation shown so that the borohydride solution contacts the decomposition catalyst and that only hydrogen and water vapor are vented. We are currently working on more advanced designs that would be orientation independent and would incorporate a check valve on the hydrogen vent while remaining completely passive and readily manufacturable.

In **Figure 5.3**, polarizations curves are shown for a microfabricated fuel cell operated on hydrogen from a cylinder, humidified by passing through a room temperature bubbler, and for the same cell mounted on a borohydride generator of the type shown in Figure 5.2. There are slight differences in the two polarization curves, however, the difference in the power produced is not significant.

The borohydride generator used to obtain the polarization curve shown in Figure 5.3 used a solution volume of  $0.6 \text{ cm}^3$ . The fuel cell was continually operated at 0.5V for over 90 hours on one charge of borohydride solution. Over this period, the current produced was monitored and integrated. The integrated current produced, 1,822 coulombs, was over 67% of the theoretical value for complete decomposition of  $0.6 \text{ cm}^3$  of the 20 wt%  $\text{NaBH}_4$  solution used. The fuel cell was still operating at the end of the 90 hr period, however, the power output had dropped to about 25% of the initial value. Considering that the generator is not sealed, but vents excess hydrogen through a small opening, the fuel utilization achieved in this experiment is very promising.

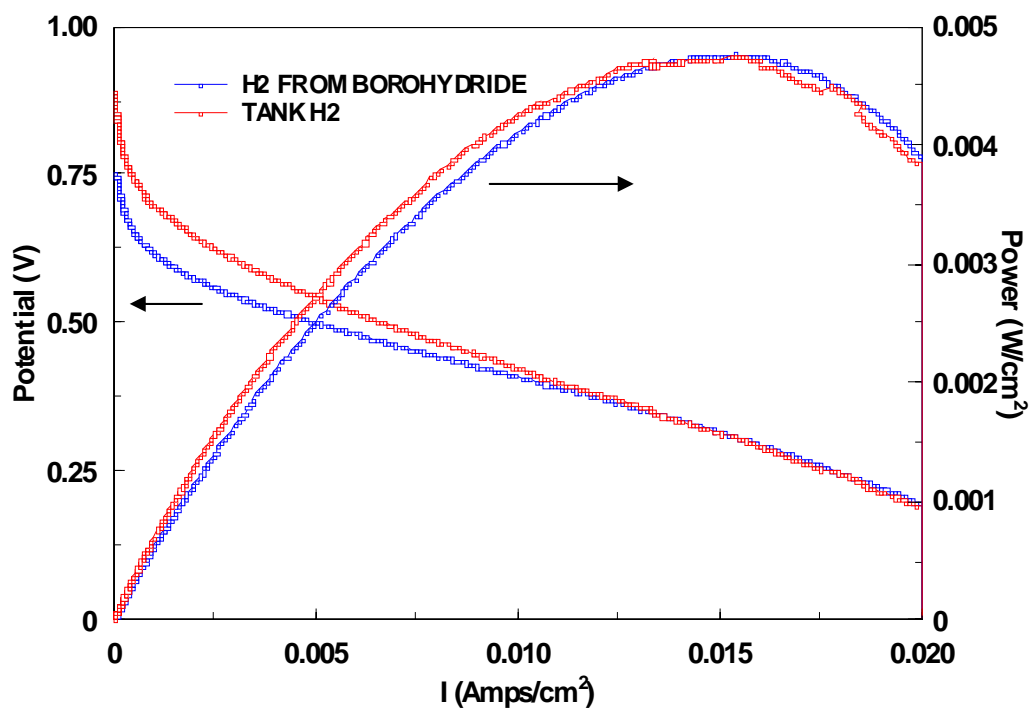


**Figure 5.3** Polarization curves for a microfabricated fuel cell (0.2 cm<sup>2</sup> area) operated on hydrogen from a cylinder, humidified at room temperature, and on hydrogen from an integrated borohydride generator. Fuel cell cathode is exposed to room air at 42% RH. IV curves obtained at a sweep rate of 2 mV/s, starting at open circuit.

## 2. DIFFICULTIES/PROBLEMS

- The power output of the fuel cell is still limited by the hydrogen permeation rate to the anode. A substrate with higher hydrogen permeability or an alternative substrate that can be etched away after fuel cell fabrication would result in a factor of 3 to 5 improvement in the power output at steady state.
- The trade-off between conductivity and water in-solubility of the polyimide co-polymers must be addressed. Earlier we had considered the conductivity target to be paramount. It now appears that some concessions will have to be made in order to achieve adequate stability. However, the definition of 'adequate stability' for the micro fuel cell (as opposed to conventional fuel cells) is still uncertain.
- Fabrication of fuel cells incorporating the novel polyimide electrolytes has met with limited success. The difficulties are related to depositing high quality layers of the electrolyte. It may be necessary to develop alternative solvents or deposition techniques in order for the polyimide electrolytes to be incorporated.
- The current design for the integrated micro fuel cell with hydrogen storage based on borohydride is orientation dependent. A more advanced design is required.

## September 2001 Progress Report

### 1. RESEARCH STATUS

#### Task 1. Micro Fuel Cell Power Unit/Microfabrication Development

Task complete.

#### Task 2. Performance and diagnostic testing of micro fuel cell power unit.

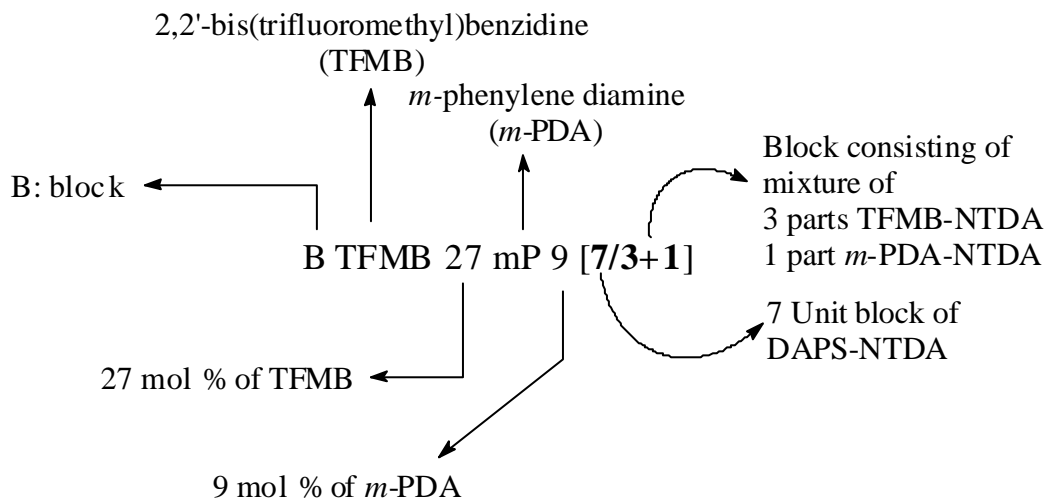
Task complete.

#### Task 3. Novel polymer synthesis and characterization

We are seeking novel proton conducting polymers that have reasonable proton conductivity at low humidity, good mechanical properties, low gas permeability, and dimensional stability. We have synthesized sulfonic acid containing co-polyimides that incorporated bulky diamines. The bulky groups are expected to push the polymer backbones apart and keep them apart along the whole chain length. This should create a nanoscale pore lined with sulfonic acid groups. Such pores should adsorb water very strongly even at relatively low humidity, and our work to date has substantially validated this hypothesis.

Until recently, we continued to synthesize and characterize bulkier diamines seeking the optimal blend of the desired properties. While we have increased conductivity over our earlier polymers, there have been no dramatic increases. In addition, these materials could not be successfully incorporated into microfabricated fuel cells due to difficulties associated with film casting. In general, the films have been too thin, were brittle, had internal stress after curing, were opaque (indicating voids or air bubbles within the film), and could be dissolved in hot water.

Recently, we have successfully synthesized polymers with both superior mechanical properties and that have greatly improved stability. Films incorporating the co-monomer meta-phenylene di-imide dianhydride (*m*-PDA) at the 10% level are mechanically far superior to any of our previous polyimides; these films are ductile, tough, and clear. Furthermore, these films have been cast in the acid form, which is a requirement for our fuel cell fabrication process. Films incorporating *m*-PDA, and a fluorinated co-monomer, bis(trifluoro methyl) benzidine (TFMB), are both mechanically tough, and stable in water, as the TFMB provides a degree of hydrophobicity to inhibit dissolution in water. The structures of these monomers and the synthesis route to the polymer are given in the Appendix. Initial results with TFMB films were reported in the progress report dated 1/12/2000. At that time, it was noted that TFMB contents greater than 30% were stable in water, but were poorly conductive. The combination of TFMB with *m*-PDA retains stability in water, and increases conductivity relative to films containing TFMB alone, as the *m*-PDA co-monomer acts as a displacing unit, creating nano-scale pores, as we have shown previously with other displacing co-monomers. Several copolyimides with different combinations of TFMB and *m*-PDA were synthesized during the past six months. The best of these is designated BTFMB27mP9[7/3+1] (B signifies a block copolymer and the numbers indicate molar fraction of the co-monomers out of 100, so this polymer has 27 mole% of TFMB and 9 mole% of *m*-PDA; 7 indicates 7 unit block of 4,4'-diamino-2,2'-biphenyldisulfonic acid (DAPS) and 1,4,5,8-naphthalenetetracarboxylic dianhydride (NTDA), and 3+1 indicates a block consisting of mixture of 3 parts of TFMB-NTDA and 1 part of *m*-PDA-NTDA) which had reasonable conductivity, and was very stable in water at 90 °C.



### Conductivity measurement

The conductivities of homopolymer, BTFMB27mP9[7/3+1] and its 5% TIBA and 20% Zn salts are shown in **Table 1**. The 5% TIBA salt of BTFMB27mP9[7/3+1] showed lower conductivities than the pure acid form. The 20% Zn salt of the copolyimide had much lower conductivity than the 5% TIBA salt. Conductivity data on other co-polymers containing TFMB and mPDA were reported previously (report for February, 2001).

**Table 1** Conductivities of the Polyimides at 25 °C as a Function of Relative Humidity.

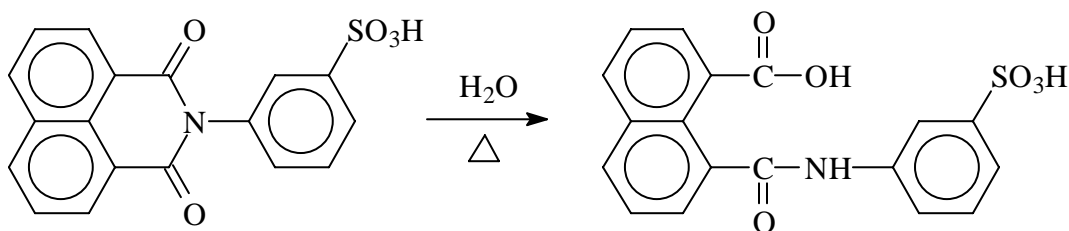
Relative Humidity (%)	Conductivity (S/cm)			
	Homopolymer	BTFMB27mP9 [7/3+1]	5% TIBA salt of BTFMB27mP9 [7/3+1]	20% Zn salt of BTFMB27mP9 [7/3+1]
100	0.23	0.11	0.089	0.033
75	0.038	0.019	0.015	1.0E-3
50	9.3E-3	3.2E-3	1.8E-3	9.7E-5
35	2.6E-3	1.3E-3	4.0E-4	1.7E-5
15	2.9E-4	1.8E-4	4.4E-5	too low to be determined

All films were cast in the acid form from DMSO.

### Hydrolytic Stability

Long-term stability of sulfonated polyimides is necessary if they are to be used in a fuel cell. Recently, Mercier, Pineri, Genies et al prepared model compounds, and investigated the effect of sulfonic acid on the hydrolytic scission (**Scheme 1**) of imide group of the compounds. The model compound was placed in water at 80 °C for 20 days, and the degraded structure was analyzed as a function of time using NMR. Even though the research was quite systematic for the model compound, studies on the sulfonated polymer were not described.

We observed that our sulfonic acid containing polyimides slowly degraded under ambient conditions. It was decided to systematically study the degradation under ambient conditions and also at elevated temperature in water. The results of this study are presented below.



**Scheme 1** Acid catalyzed hydrolysis of imide group.

### Viscosity measurements

Two batches each of homopolymer and BTFMB27mP9[7/3+1] fibers were kept under ambient laboratory conditions. Samples were taken every few months, and viscosities were measured. Solution viscosity is a relative measure of polymer molecular weight. For most linear polymers, the relation between the viscosity  $[\eta]$  and molecular weight can be expressed simply in the equation

$$[\eta] = K'M^a$$

where  $K'$  and  $a$  are constants and functions of the solvent as well as of the polymer type. So, molecular weight decrease by degradation can be analyzed by the viscosity measurement if  $a$  is  $\approx 1$ . For rigid rod polymers, it is usually between 1 and 1.5.

There is a relation between number of repeat units of a polymer ( $N$ ) and time ( $t$ ) for random chain scission. It is expressed as

$$(1/N_t) - (1/N_0) = kt$$

where  $N_0$  and  $N_t$  are the number of repeat units of the polymer at time zero and  $t$ , and  $k$  is a rate constant for the chain scission. For our sulfonic acid containing polyimides, we do not have any absolute value for the  $N$ . Therefore, we used  $[\eta]$  which is proportional to  $N$ .

The plots of  $(1/[\eta]_t - 1/[\eta]_0)$  vs. time (days) for these polymers are presented in **Figures 1** and **2**. Slopes and standard deviations from the plots are listed in **Table 2**. The slopes correlate with the degradation rate of the polymers. A steeper slope means a higher rate of degradation.

The degradation rates of the homopolymer and BTFMB27mP9[7/3+1] are similar, even though the copolyimide had only 64% of the sulfonic acid groups of the homopolymer. As shown previously, the BTFMB27mP9[7/3+1] polymer has more water molecules per sulfonic acid group than the homopolymer. The extra water in the copolyimide could accelerate the degradation. This might be the reason that the homopolymer and BTFMB27mP9[7/3+1] have similar rates of degradation.

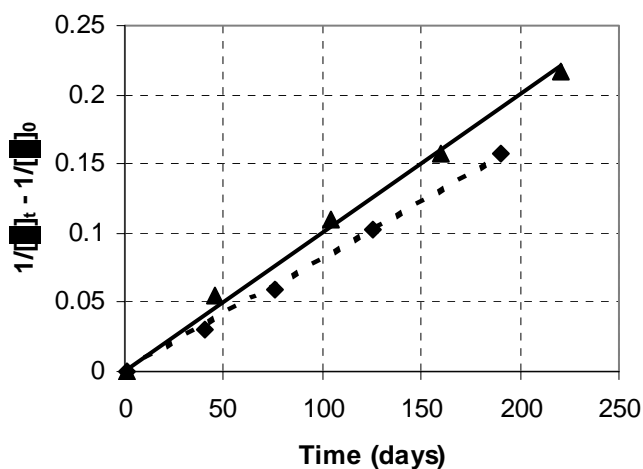


**Figure 1**  $(1/[\eta]_t - 1/[\eta]_0)$  vs. time for homopolymer (solid line: batch iv0; dotted line: batch iv8).

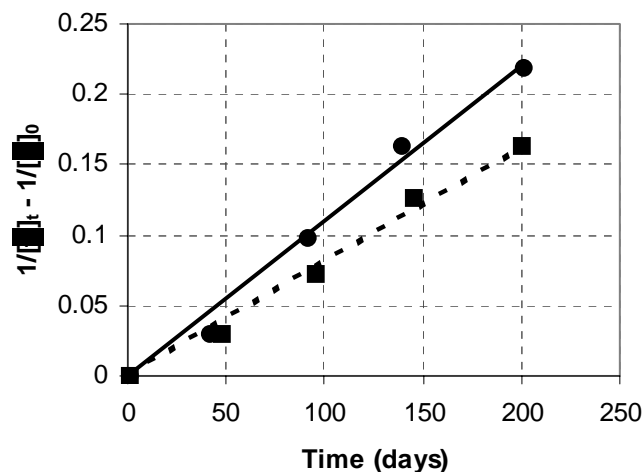


**Figure 2**  $(1/[\eta]_t - 1/[\eta]_0)$  vs. time for BTFMB27mP9[7/3+1] (solid line: batch iv15; dotted line: batch iv9).

**Table 2** Slope and Standard Deviation of Plots of  $(1/[\eta]_t - 1/[\eta]_0)$  vs. Time for Polyimides.

Polyimides	$[\eta]_0$ dL/g	$[\eta]_{(\text{days})}$ dL/g	Slope (/day)	Standard deviation
Homopolymer (batch iv0)	7.1	2.8 (220 days)	9.7E-4	3E-5
Homopolymer (batch iv8)	9.3	3.8 (190 days)	8.4E-4	2E-5
BTFMB27mP9[7/3+1] (batch iv15)	4.4	2.3 (200 days)	11.4E-4	7E-5
BTFMB27mP9[7/3+1] (batch iv9)	6.3	3.1 (200 days)	8.5E-4	4E-5

The results shown in Table 2 are consistent with our observations that after >6 months, the polymers are brittle and difficult to handle. It is not clear if this imbrittlement will cause failure of an operating fuel cell, however, cells cannot be fabricated with aged polymer.

#### *FT-IR analysis*

FT-IR spectra of fresh and one year old homopolymer were compared. The spectrum of the one year old homopolymer shows a small peak at  $1785\text{ cm}^{-1}$  that does not appear in the spectrum of the fresh homopolymer. We believe that the peak corresponds to carbonyls of anhydride end groups of degraded polyimide. There are several reasons for proposing that the peak at  $1785\text{ cm}^{-1}$  is for the anhydride end groups. The C=O stretching band for anhydride groups of 1,4,5,8-naphthalenetetracarboxylic dianhydride appears at  $1780\text{ cm}^{-1}$ , and C=O stretching band for -CO<sub>2</sub>H groups of 1,4,5,8-naphthalenetetracarboxylic acid appears at  $1727\text{ cm}^{-1}$ . Also, Biswas et al synthesized polyamic acid from 1,4,5,8-naphthalenetetracarboxylic dianhydride and



diaminocarbazole and analyzed it using FT-IR. The C=O stretching band for  $\text{-CO}_2\text{H}$  in the polyamic acid appears at  $1720\text{ cm}^{-1}$ . According to our viscosity measurements, there was severe degradation; the viscosity of homopolymer dropped from 9.3 to 3.8 dL/g in 190 days. The viscosity drop implies chain cleavage, rather than just hydrolysis to the amic acid. There is no evidence for the appearance of  $\text{-CO}_2\text{H}$  peak ( $1720$  to  $1727\text{ cm}^{-1}$ ), which would indicate hydrolysis to the amic acid or the diacid. The only observable new peak is at  $1785\text{ cm}^{-1}$ , indicating formation of the anhydride. This is reasonable since 6-membered rings are very stable and the acid environment insures that ring formation is rapid.

The tri-isobutylamine (TIBA) salt of BTFMB27mP9[7/3+1] was prepared to find out if lowering the acidity would slow down the hydrolytic scission of the imide group. BTFMB27mP9[7/3+1] and its 5% TIBA salt were placed separately in  $90\text{ }^\circ\text{C}$  deionized water for 25 days. They were analyzed using FT-IR and both show a small peak at  $1786\text{ cm}^{-1}$ .

Similarly, the 20% Zn salt of BTFMB27mP9[7/3+1] was synthesized and compared with BTFMB27mP9[7/3+1]. They were placed separately in  $90\text{ }^\circ\text{C}$  deionized water and monitored using FT-IR. The FT-IR spectra of BTFMB27mP9[7/3+1] were obtained after 20 and 40 days, and compared with its fresh FT-IR spectrum. The peak at  $1582\text{ cm}^{-1}$ , which is assigned to the aromatic C-C stretch, was used as a reference, and the spectra were normalized with respect to it. The carbonyl peaks could then be compared. As shown in **Figure 3**, the peak at  $1786\text{ cm}^{-1}$  increased with time. The imide peaks at  $1714$  and  $1676\text{ cm}^{-1}$  decreased with time, confirming its hydrolysis. The 20% Zn salt showed a similar pattern of degradation.

The FT-IR results are consistent with the viscosity measurements shown above. Even when the acidic nature of the system is lowered by addition of alternate cations (which greatly reduces conductivity), the rate of chain scission is not significantly altered. At this time, we do not know if this will lead to fuel cell failure, since the electrolyte is always supported by the substrate and other components in the microfabricated fuel cell. However, it is clear from experience that fuel cell fabrication cannot be performed with aged polymer, and it is likely that alternative materials will be needed. One class of alternate materials, which will be immune to hydrolysis and that maintains our concepts of rigid rod polymers separated by bulky groups to provide nano-scale pores, will be pursued under a new program funded under BAA 01-09, as part of a joint effort with Georgia Institute of Technology.

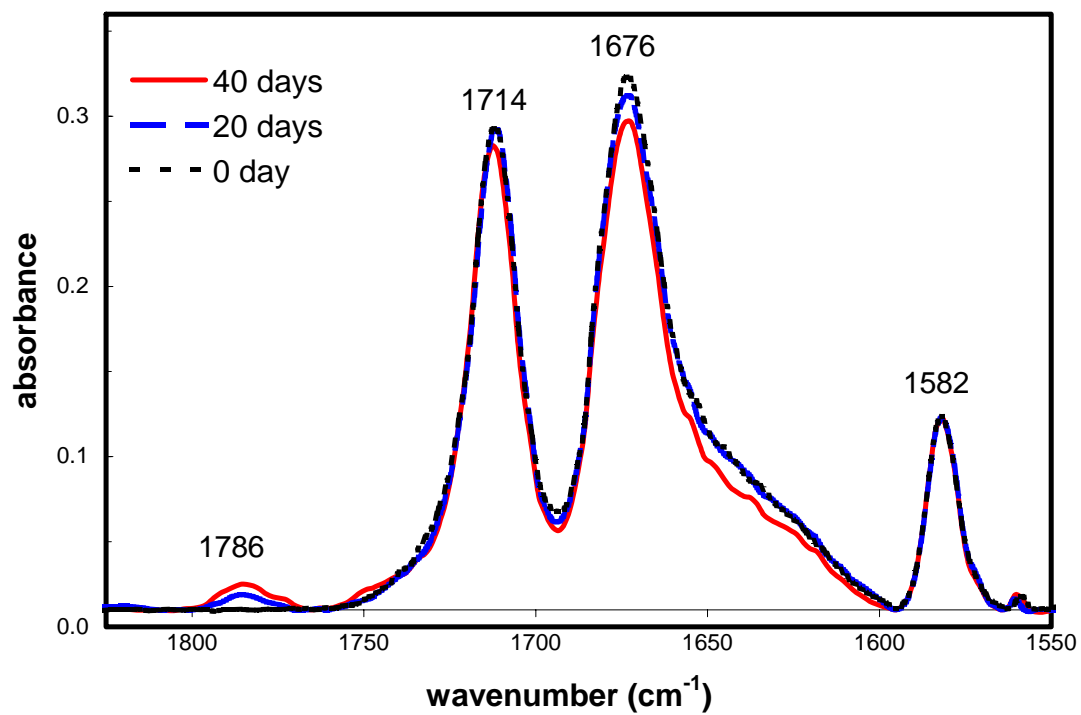


**Figure 3** FT-IR spectra of BTFMB27mP9 after 0, 20 and 40 days in 90 °C water.

#### Task 4. Novel polymer incorporation into microfabricated fuel cell.

Previous attempts at incorporation of a polyimide based electrolyte using the RF5 and BTFMB27mP9[7/3+1] polymers were not successful. Most of the cells were electrically shorted after fabrication, suggesting that the electrolyte layer was too thin. Deposition of the electrolyte in multiple layers resulted in the build-up of stress within the electrolyte layer that eventually caused delamination of the fuel cell from the substrate.

During the past six months, we have focused on the role of the cathode catalyst ink in the fabrication. It was determined that the solvent that was previously used in this ink was capable of dissolving the previously deposited layer of polyimide electrolyte. While it is desirable for the cathode ink to partially dissolve the electrolyte in order to obtain a structure with low interfacial resistance and that will not delaminate, the catalyst ink had to be reformulated. A new ink formulation was developed that uses a solvent that swells, but does not dissolve the polyimide electrolytes. The results presented here were obtained with the reformulated cathode ink. Two separate batches of cells have been fabricated (14 cells in the 1<sup>st</sup> batch, 12 cells in the 2<sup>nd</sup>) without any failures.

Typical polarization curves for these cells are shown in Figure 4 below.

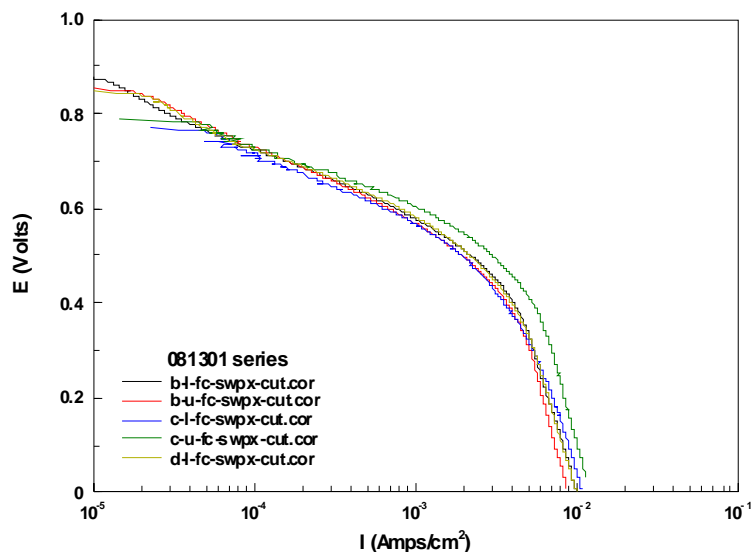


**Figure 4.** Polarization curves for five separate cells fabricated with polyimide electrolyte and reformulated cathode ink. Anode feed: hydrogen, 2 sccm. Cathode: air breathing, 42%RH. Cell area: 0.25 cm<sup>2</sup>. Polarization curve recorded at 2 mV/s.

The power output of these cells is similar to, but slightly lower than that obtained previously using Nafion as an electrolyte. The primary factor limiting the performance is the supply of hydrogen reaching the anode, which is limited to  $\approx 10 \text{ mA/cm}^2$  by the substrate. The reason for the lower power output obtained with the polyimide electrolyte as compared to Nafion (when

higher power was expected) can be seen in **Figure 5**, in which impedance spectra are shown for these cells. The high frequency resistance of these cells, which is typically the sum of the electrolyte resistance and the resistance of the current collectors, is 10-30  $\Omega$ . From the known conductivities of the current collectors and the electrolyte, this value should be 2-3  $\Omega$  (25  $\mu\text{m}$  thick electrolyte layer with a conductivity of 5 mS/cm at 40%RH). One likely explanation for the large high frequency resistance is that the re-formulated cathode ink does not make a low resistance interface with the polyimide electrolyte. During the time remaining on this area, an investigation of this and other possible causes for the unexpectedly high internal resistance of these cells will be investigated.

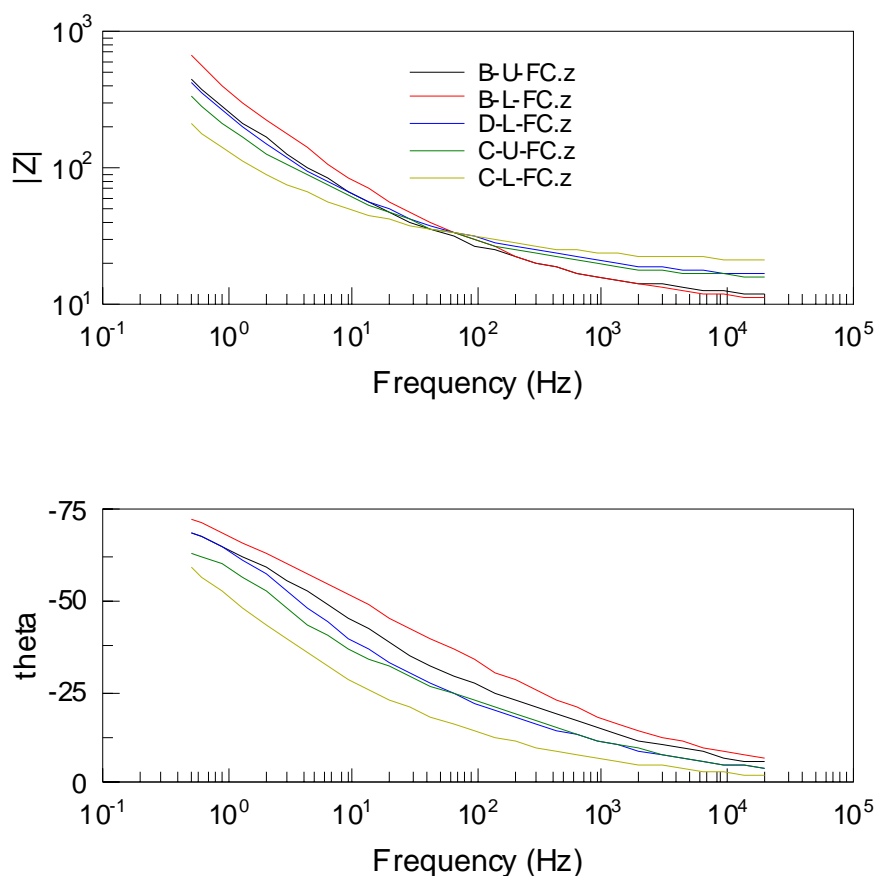


**Figure 5.** Impedance results obtained from microfabricated cells incorporating polyimide electrolyte and reformulated cathode ink. Bode format. Impedance acquired at open circuit potential with hydrogen and air, 10 mV AC perturbation.

## **Task 5. On-board Hydrogen Storage/Generation**

During the past six months, an undergraduate student in the Department of Materials Science has completed a senior project in this area. As a senior project, this effort is not being funded with DARPA funds, but the work is directly related to this program. During this project, the palladium ink previously developed for printing of a palladium hydride storage layer was re-evaluated. In addition, a promising alternative hydride material,  $\text{La}_{(1-x)}\text{Al}_x\text{Ni}_5$  was identified. Preliminary investigations with this material have begun in anticipation of the contract extension to begin with FY02.

### **2. DIFFICULTIES/PROBLEMS**

- The power output of the fuel cell is still limited by the hydrogen permeation rate to the anode. A substrate with higher hydrogen permeability or an alternative substrate that can be etched away after fuel cell fabrication would result in a factor of 3 to 5 improvement in the power output at steady state. These issues will be addressed in the extension to this program starting in FY02.
- The trade-off between conductivity and water in-solubility of the polyimide co-polymers is still an issue. Considerably progress has been achieved with the incorporation of the fluorinated TFMB and m-PDA comonomers as described above. However, even this route has not yielded ideal results and we are now aware of the hydrolysis issue with these materials. An alternative polymer electrolyte which retains the concepts of an aromatic, rigid rod polymer with built-in nano-scale pores will be pursued under our new program in collaboration with Georgia Institute of Technology ("An Integrated Micro Fuel Cell/Si CMOS/Sensor Technology", principal investigator Dr. Paul Kohl, funded under BAA 01-09).

## August 2002 Progress Report

### 1. RESEARCH STATUS

#### **Task 1: Fabrication Enhancements for Improved Reactant Accessibility**

##### Technical Approach

This task will examine water soluble sacrificial materials to be used during the fabrication process. At the appropriate point in the fabrication process, the sacrificial material will be extracted in order to open the structure. This is necessary to enhance hydrogen accessibility to the anode to achieve higher power densities. We believe it should be possible to increase the power density levels from 2 mW/cm<sup>2</sup> to levels of > 10 mW/cm<sup>2</sup>. This should increase the range of DoD applications for this technology.

Water-soluble materials have been chosen for this effort due to the nature of the materials used in the microfabricated fuel cell. Each of the components in the device - anode and cathode current collectors, anode and cathode catalyst layers and the polymer electrolyte, are polymers or incorporate polymeric binders. All of the various polymers used have limited thermal stability, and/or can be readily etched/dissolved by strong solvents. As a result, we are attempting to develop a system using water as a benign solvent. Unfortunately, even exposure to liquid water may damage the device, as non-cross-linked polymer electrolytes readily swell in liquid water. As a result, caution must be exercised and a careful procedure developed.

##### Status

An example of the results obtained with one class of water-soluble sacrificial material is shown in Figure 1-1. After a relatively short exposure to water, as seen in the upper figure, the sacrificial matter, which appears pink in the figure, is still in place. After a longer exposure, the sacrificial material has been almost completely removed as desired, revealing the underlying anode current collector (gold color). However, a crack can be seen in the current collector. At this time it is uncertain if these cracks will cause a failure of the device.

##### Future Work - Fabrication Enhancements

Evaluation of fuel cells fabricated with the first sacrificial materials will begin shortly. These trials will determine if we can successfully complete fuel cell fabrication with these materials, and determine if the power density is enhanced as expected.

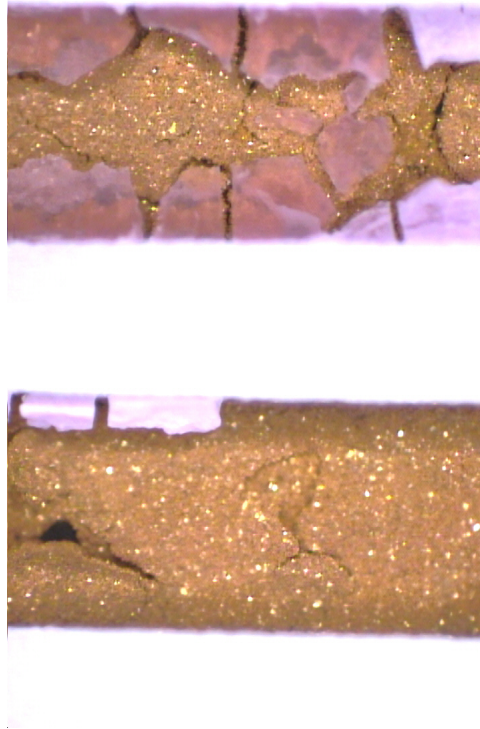


**Figure 1-1** Two stages in the removal of sacrificial material from microfabricated fuel cell. Substrate is alumina. Sacrificial material appears pink, gold material below is the anode current collector. Upper view - short exposure time, bottom view, longer exposure time.

## **Task 2: Metal Hydride Fuel Storage**

### **Technical Approach**

Hydride hydrogen storage certainly has many advantages including being a solid state material with no operational dependency on orientation. In addition, high volumetric energy densities can be achieved with these materials. A major goal of this proposed task was to produce a metal hydride material that is tailored to this fuel cell application, with an equilibrium pressure near atmospheric pressure at room temperature, and that can be applied in a thick film fabrication process. CWRU proposes to limit the scope of this task to the  $\text{LaAl}_x\text{Ni}_{5-x}$  hydride family, as it has desirable properties that the microfabricated fuel cell requires. This material is also commercially available. We expect that a successful completion of this task will lead to integrated devices with energy densities on the order of  $500 \text{ mWh/cm}^3$  for a 50 mWh storage capacity.

### **Status**

$\text{LaAl}_{0.3}\text{Ni}_{4.7}$  hydride material with an additional surface modification has been formulated into a thick film printable ink with very low binder content. A second member of the AB5 family of hydrides,  $\text{CaNi}_5$ , has also been evaluated. For both hydrides, the binder content was on the order of 1 wt%. In our previous hydride inks based on palladium, the binder content was 10-15 wt%, which yielded a far lower energy density material.

An automated Sievert's apparatus was constructed and put into operation during this period. This apparatus allows for hydrogen sorption/desorption testing of up to six samples simultaneously. Various hydride powders and inks have been subjected to repetitive sorption/desorption testing consisting of 10 minute exposure to  $\approx 1000$  torr  $\text{H}_2$  (sorption step) followed by 10 min exposure to vacuum (desorption, pressure = 10 millitorr). Typical results from this apparatus are shown in Figure 2-1; sorption curves at various points during the first 1000 cycles are shown for the  $\text{LaAl}_{0.3}\text{Ni}_{4.7}$  hydride material. SEM micrographs after 1000 cycles showed no change in particle size, and no change in the adhesion of the ink to the substrate. These tests have been extended to over 2000 cycles without any significant change in the total amount of hydrogen stored, or in the rate at which hydrogen is adsorbed or desorbed. Over the same period, the ink based on the  $\text{CaNi}_5$  hydride has lost  $\approx 15\%$  of its original hydrogen storage capacity. Tests detailed in the previous report showed that desorption rates equivalent to  $200 \text{ mA/cm}^2$  could be easily obtained from either hydride material. This rate is roughly 10X what is required for the microfabricated fuel cell.

### **Future Work - Hydride Storage**

The performance of the hydride inks has been very promising, and the next step will be to include them in the fabrication of complete micro fuel cells. Then we will begin our evaluation of microfuel cell performance, and overall energy and power densities can be determined for the new system.



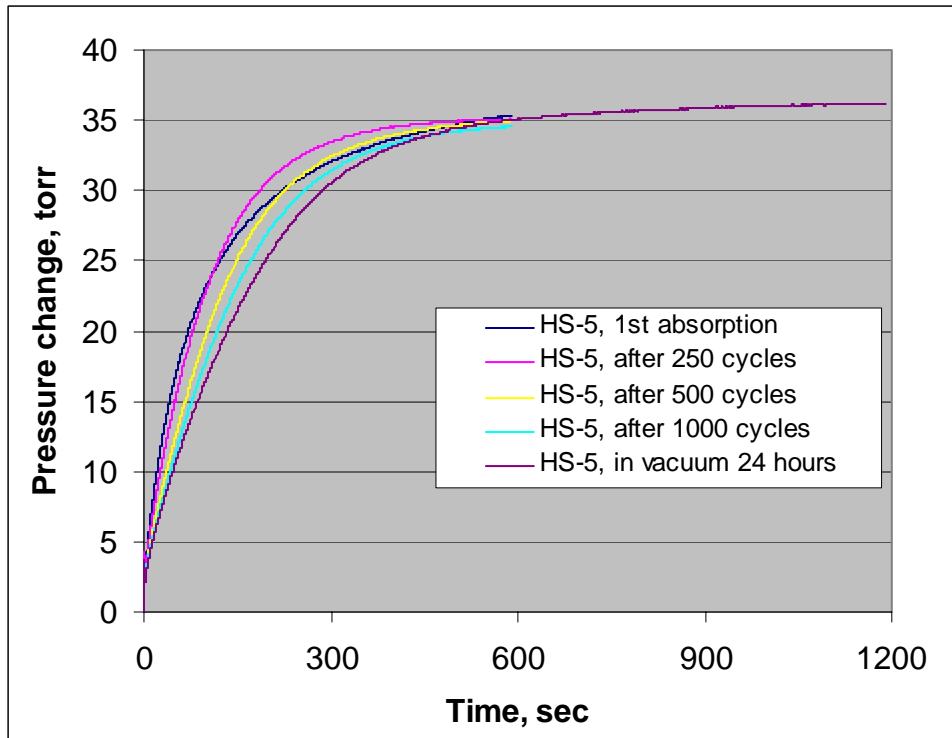


**Figure 2-1:** Sorption curves for modified  $\text{LaAl}_{0.3}\text{Ni}_{4.7}$  over 1000 sorption/desorption cycles.

### **Task 3: Electrolyte Deposition Enhancement**

#### **Technical Approach**

In the fabrication of prototype micro fuel cells to date, the polymer electrolyte has typically been applied manually. Thick film printing of the electrolyte layer has been shown, but the results were not ideal. In this task, CWRU will investigate alternative methods and techniques that will perform this fabrication step in a more automatic and consistent manner, such as with micro-pen or ink jet deposition. The goal is to demonstrate prototype fuel cells that are reproducible and easily manufactured.

#### **Status**

A commercial jet-printing device has been selected and is on order from the Aysmtek division of Nordson Inc. We are confident that this machine will greatly increase our capabilities in this area. The purchase of this unit reflects a substantial investment ( $\approx \$80,000$ ) in this program by the Dean of the School of Engineering at CWRU. At the same time, we have made considerable progress in depositing Nafion electrolyte films using thick film deposition. The solvent system for the Nafion electrolyte has been modified, and the films deposited using the modified system are greatly improved.

A comparison of line-scan profiles for thick film printed Nafion films is shown in Figure 3-1. The profiles were obtained using a laser profilometer. In this figure, it can be seen

that the film deposited from the improved solvent system is much thicker ( $\approx 90\text{ }\mu\text{m}$  thick) and has sharp, steep edges. The profile for the film deposited by our old method is much thinner, and has highly sloped edges. Overhead views of the two types of films are shown in Figures 3-2a and 3-2b. The enhanced definition obtained with the improved solvent system is clearly seen.

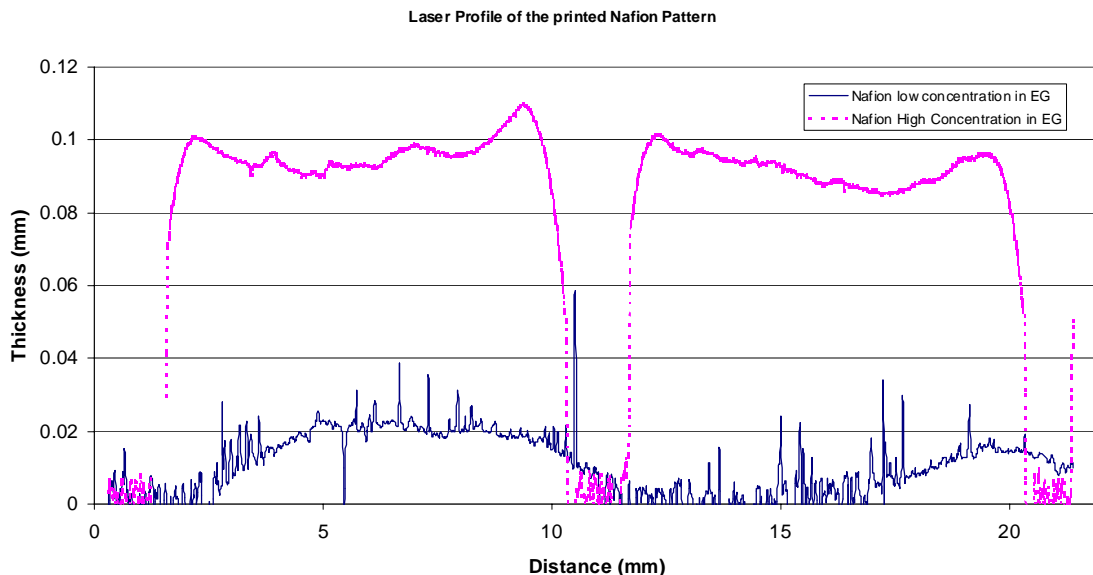


**Figure 3-1.** Line-scan profiles of thick film printed Nafion films. Pink curve - film printed from improved solvent system. Blue curve: film printed with previous solvent system.

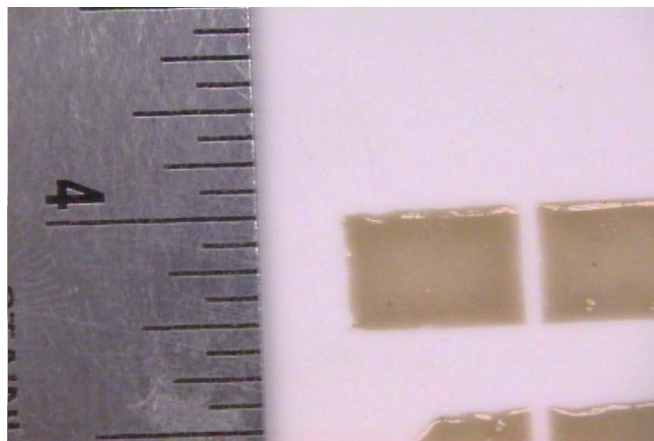


**Figure 3-2A** Nafion films printed from improved solvent system

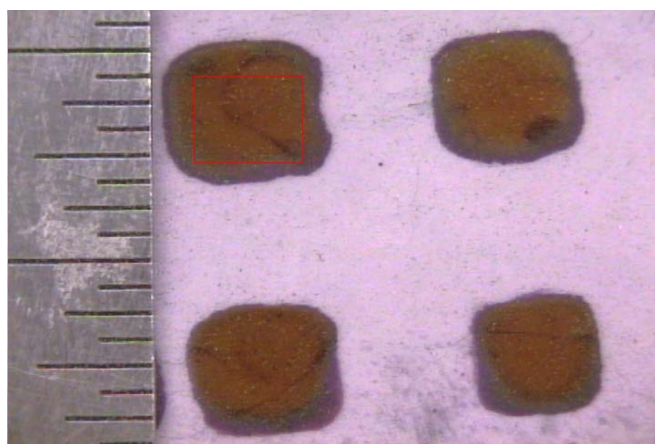


**Figure 3-2B** Nafion films printed from previous solvent system. Red line depicts desired deposit area.

## March 2003 Progress Report

### 1. RESEARCH STATUS

#### **Task 1: Fabrication Enhancements for Improved Reactant Accessibility**

##### Technical Approach

This task will examine water soluble sacrificial materials to be used during the fabrication process. At the appropriate point in the fabrication process, the sacrificial material will be extracted in order to open the structure. This is necessary to enhance hydrogen accessibility to the anode to achieve higher power densities. We believe it should be possible to increase the power density levels from 2 mW/cm<sup>2</sup> to levels of > 10 mW/cm<sup>2</sup>. This should increase the range of DoD applications for this technology.

Water-soluble materials have been chosen for this effort due to the nature of the materials used in the microfabricated fuel cell. Each of the components in the device - anode and cathode current collectors, anode and cathode catalyst layers and the polymer electrolyte, are polymers or incorporate polymeric binders. All of the various polymers used have limited thermal stability, and/or can be readily etched/dissolved by strong solvents. As a result, we are attempting to develop a system using water as a benign solvent. Unfortunately, even exposure to liquid water may damage the device, as non-cross-linked polymer electrolytes readily swell in liquid water. As a result, caution must be exercised and a careful procedure developed.

##### Status

The sacrificial materials and processes have been significantly improved, completing the last of the year one milestones. An example is shown in Figures 1.1 a, b and c. In Figure 1.1a, a laser machined alumina substrate is shown after the sacrificial material is deposited to fill the laser-machined openings in the substrate. Only one cell (diameter = 0.5 cm) on the wafer is shown. In Figure 1.1b, the same substrate is shown after the anode current collector is deposited by thick film printing over the filled substrate. The current collector ink wets and prints properly over both the alumina and the sacrificial material. The outline of the opening in the substrate can faintly be seen, the planarity of the surface is not ideal, but is acceptable. In Figure 1.1c, the backside of wafer is shown, after the sacrificial material is removed. Unlike the previous process shown in the last report, the sacrificial material is almost completely removed, without damage to the current collector.

##### Future Work - Fabrication Enhancements

Fabrication of complete devices using the improved sacrificial process is underway. These cells will be tested to determine if the anticipated improvement in power output is realized.



**Figure 1.1a** 0.5 cm diameter through hole in alumina, after deposition of sacrificial material.

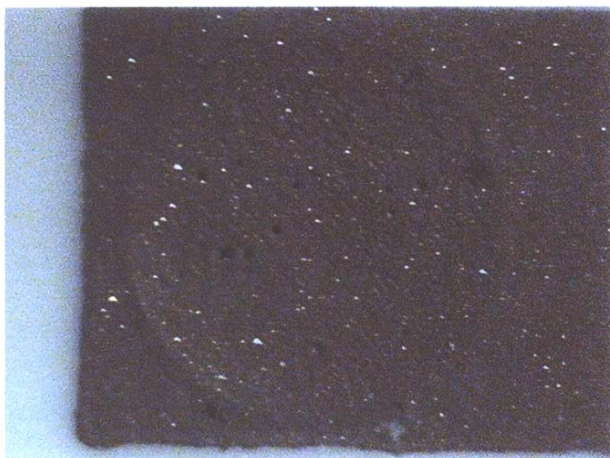


**Figure 1.1b** After printing of anode current collector.



**Figure 1.1c** Viewed from back, after removal of the sacrificial material.

## **Task 2: Metal Hydride Fuel Storage**

### **Technical Approach**

Hydride hydrogen storage certainly has many advantages including being a solid state material with no operational dependency on orientation. In addition, high volumetric energy densities can be achieved with these materials. A major goal of this proposed task was to produce a metal hydride material that is tailored to this fuel cell application, with an equilibrium pressure near atmospheric pressure at room temperature, and that can be applied in a thick film fabrication process. CWRU proposes to limit the scope of this task to the  $\text{LaAl}_x\text{Ni}_{5-x}$  hydride family, as it has desirable properties that the microfabricated fuel cell requires. This material is also commercially available. We expect that a successful completion of this task will lead to integrated devices with energy densities on the order of  $500 \text{ mWh/cm}^3$  for a 50 mWh storage capacity.

### **Status**

The first generation of improved hydride materials were based on a modified  $\text{LaAl}_x\text{Ni}_{5-x}$  hydride, and made into a thick film printable ink using a water soluble binder. During the past 6 months, we have continued to test these materials. In addition, a second-generation ink, using the same hydride material, but incorporating a non-water-soluble binder has been developed. The first generation inks have now been cycled over 5000 times without loss in hydrogen storage capacity, or a change in the hydrogen sorption/desorption rate. In addition, these inks remained adherent to the substrate (alumina) throughout the cycle tests and have been found to retain their activity even after exposure to ambient humidity air for 55 weeks. Despite these successes, the second generation ink has been developed to expand the fabrication possibilities and to further improve the performance of the hydride storage in the humid fuel cell environment. This effort has also been successful, a non-water-soluble binder has been found that retains the desirable properties of the first generation system; very low binder content ( $<1 \text{ wt\%}$ ) for high energy density storage, rapid sorption/desorption rates for hydrogen, and the ink can be prepared, printed and cured in ambient air without loss of hydrogen storage activity. This ink is now undergoing long term cycle testing in both dry and humid hydrogen.

### **Future Work - Hydride Storage**

The remaining work on this task is to incorporate the hydrogen storage modules with microfabricated fuel cells and to determine the performance and energy density of the combined device. These devices will be fabricated after the processes improvements from Tasks 1 and 3 are completely integrated into the fuel cell production.

### **Task 3: Electrolyte Deposition Enhancement**

#### **Technical Approach**

In the fabrication of prototype micro fuel cells to date, the polymer electrolyte has typically been applied manually. Thick film printing of the electrolyte layer has been shown, but the results were not ideal. In this task, CWRU will investigate alternative methods and techniques that will perform this fabrication step in a more automatic and consistent manner, such as with micro-pen or ink jet deposition. The goal is to demonstrate prototype fuel cells that are reproducible and easily manufactured.

#### **Status**

In the previous report, results were shown for an improved method of depositing Nafion polymer electrolyte using the thick film printer. Since then, we have focused on the production of complete fuel cells using the thick film process for depositing Nafion. Complete cells have now been successfully fabricated incorporating thick film printed electrolyte layers. The complete fabrication sequence is shown in Figure 3.1a-d.

#### **Future Work - Electrolyte Deposition**

We will continue to investigate deposition of polymer electrolyte films using our Asymtek microdispensing tool as an alternative to the thick film process. The goal will be to improve upon the uniformity of the deposited films, which for the thick film process is acceptable but not ideal. In addition, using the microdispensing tool should give much greater control over the thickness of the electrolyte layer. Prototype fuel cells fabricated with both tools will be tested.

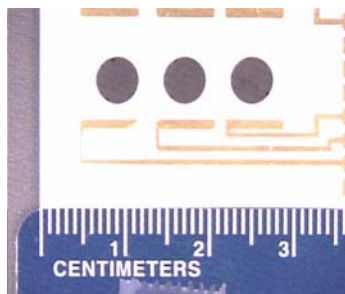


**Figure 3.1a** Alumina substrate with hydride fuel storage - three cells.

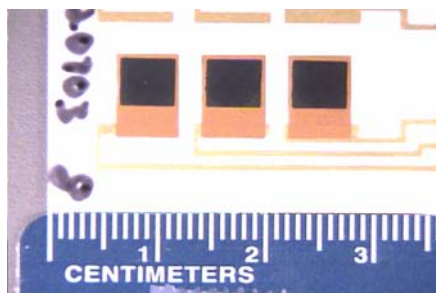


**Figure 3.1b** After deposition of anode current collector and anode catalyst.

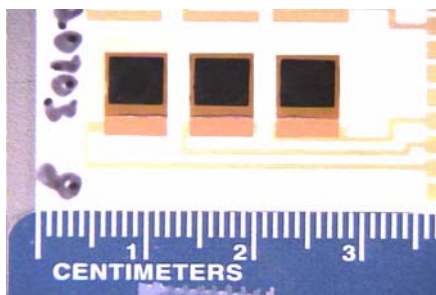


**Figure 3.1c** After deposition of polymer electrolyte layer.

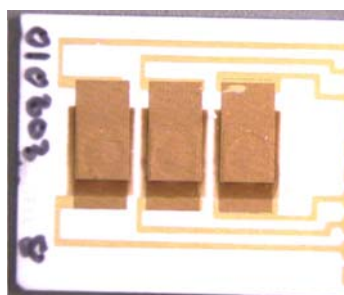


**Figure 3.1d** After deposition of cathode catalyst and cathode current collector.

#### **Task 4: Search for Insertion Opportunities and Development Partners**

##### Approach

In this task, CWRU will specifically look for opportunities throughout the DoD where devices can benefit from integrating a microfabricated fuel cell or used as power delivery devices in a stand-alone configuration. CWRU expects that this task will involve a design component with perhaps some modeling based on laboratory data acquired from prototypes. We will also work to establish relationships with commercial manufacturers and venture capital firms interested in this technology.

##### Status

We have continued to meet with companies and venture capital firms interested in the commercialization possibilities arising from this program. During the past six months, we have had substantial discussions with six separate firms.



## 1. RESEARCH STATUS

### **Task 1: Fabrication Enhancements for Improved Reactant Accessibility**

#### Technical Approach

This task will examine water-soluble sacrificial materials to be used during the fabrication process. At the appropriate point in the fabrication process, the sacrificial material will be extracted in order to open the structure. This is necessary to enhance hydrogen accessibility to the anode to achieve higher power densities. We believe it should be possible to increase the power density levels from 2 mW/cm<sup>2</sup> to levels of > 10 mW/cm<sup>2</sup>. This should increase the range of DoD applications for this technology.

Water-soluble materials have been chosen for this effort due to the nature of the materials used in the microfabricated fuel cell. Each of the components in the device - anode and cathode current collectors, anode and cathode catalyst layers and the polymer electrolyte, are polymers or incorporate polymeric binders. All of the various polymers used have limited thermal stability, and/or can be readily etched/dissolved by organic solvents. As a result, we are attempting to develop a system using water as a benign solvent. Unfortunately, even exposure to liquid water may damage the device, as non-cross-linked polymer electrolytes readily swell in liquid water. As a result, caution must be exercised and a careful procedure developed.

#### Status

In the previous semi-annual report, we had reported the development of a sacrificial process that allowed for fabrication of complete fuel cells, and for which the sacrificial material could be completely removed in the final step. Unfortunately, device yields using this process were low due to swelling of the polymer electrolyte layer. Excessive swelling consistently resulted in device failures due to delamination from the substrate. As a result, we have temporarily changed our approach, and have gone back to fabricating the fuel cell on top of a film of the metal hydride ink developed in Task 2 below. When this approach was tried previously, the results were poor due to low hydrogen permeability through the hydride material. However, the newer generations of the hydride ink are considerably more permeable to hydrogen. With only one significant change, (the temperature ramp during the curing process for the anode ink has to be slower to prevent anode delamination) we are able to fabricate complete fuel cells with the hydride ink in the substrate as shown in Figure 3.1a.

The effectiveness of this approach can be seen in the polarization curves shown in **Figure 1.1**. The curve labeled 'Nylon' represents the base case - a cell fabricated on a porous nylon membrane from the first phase of this project. Printing the fuel cell on the porous membrane results in a loss of porosity, limiting the rate at which hydrogen can pass through the substrate to reach the anode. The result is the limiting current of 14 mA/cm<sup>2</sup> that is seen in the polarization curve. With a limiting current this low, achieving a power density of 10 mW/cm<sup>2</sup> (e.g., 0.5V @ 20 mA/cm<sup>2</sup>) is not possible. An example of our recent results obtained by fabricating the fuel cell on top of the metal hydride layer is shown by the curve labeled 'Single MFC'. In this case, the limiting current, if there is one, is greater than 30 mA/cm<sup>2</sup>. In **Figure 1.2**, both the raw and iR corrected curves for the cell fabricated on the hydride ink are shown. The raw data (the true power output of the cell) has a maximum power density of

5 mW/cm<sup>2</sup>. This result is 2.5X the power output obtained with the base case cell, but is still below our goal of 10 mW/cm<sup>2</sup>. From the iR corrected curve, it can be seen that even if the internal ohmic resistance of the cell could be eliminated, the performance would not reach the goal. This indicates that the catalytic activity of the anode and cathode need to be improved in order to reach the target power density. One simple approach to increase the catalytic activity is to increase the platinum loading in each electrode. For the cell used here, the platinum loadings were estimated to be 0.1 - 0.15 mg/cm<sup>2</sup>. It should be possible to increase the loading by 2 to 5X without difficulty.

#### Future Work - Fabrication Enhancements

- By using a supported platinum catalyst with a higher platinum content than the 20 wt% catalyst previously used, cells with a higher platinum loading will be fabricated to determine if this will increase the catalytic activity sufficiently to achieve the power density target of 10 mW/cm<sup>2</sup>.

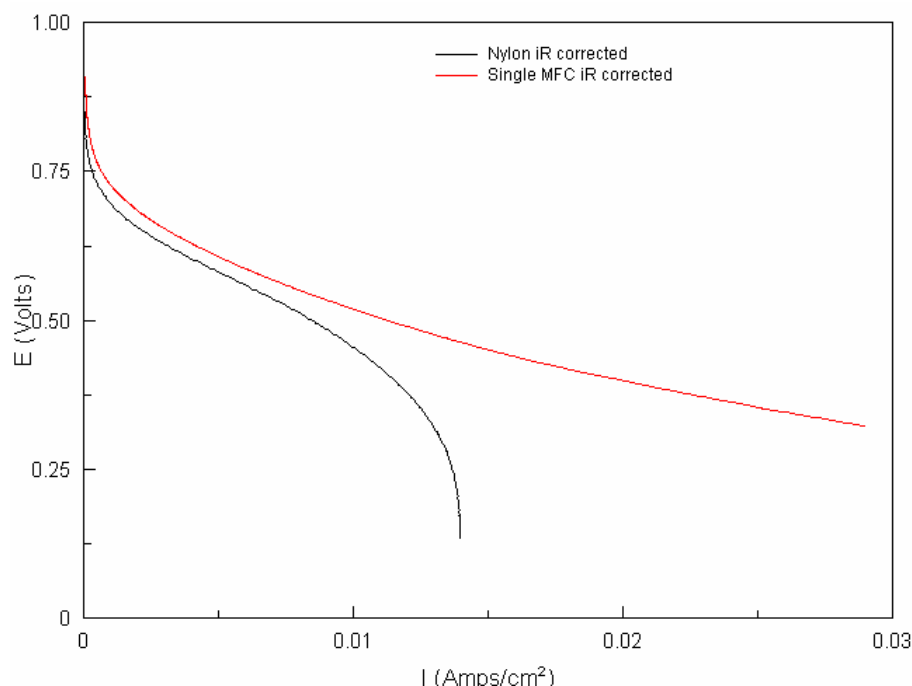


**Figure 1.1** Fuel cell polarization curves. Curve labeled ‘Nylon’ is for a cell fabricated on a porous Nylon substrate (June 2000). Curve labeled ‘Single MFC’ is for a cell fabricated on an alumina substrate filled with metal hydride ink (July 2003). Both curves are iR corrected to more clearly show the effects of reactant supply limitations. Both curves obtained with air at 50%RH and hydrogen.

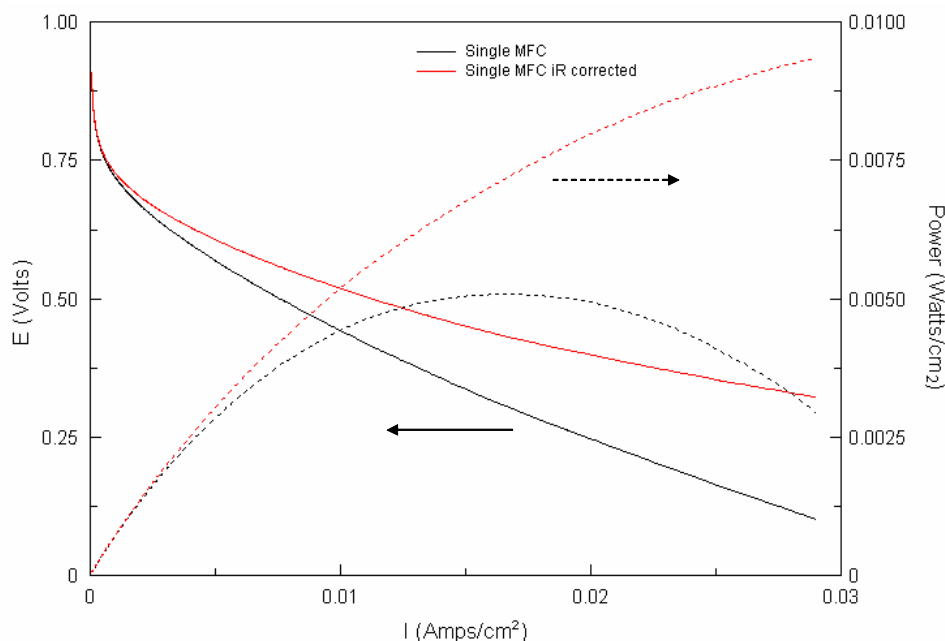


**Figure 1.2** Raw and iR corrected polarization curves for microfuel cell fabricated on alumina filled with metal hydride. Room temperature, reactant gases: 50%RH air and  $H_2$ .

## **Task 2: Metal Hydride Fuel Storage**

### **Technical Approach**

Hydride hydrogen storage has several advantages including being a solid material with no operational dependency on orientation. In addition, high volumetric energy densities can be achieved with these materials. A major goal of this proposed task was to produce a metal hydride material that is tailored to this fuel cell application, with an equilibrium pressure near atmospheric pressure at room temperature, and that can be applied in a thick film fabrication process. A second important goal is that the hydride material remains active after exposure to air or water vapor. Typically, metal hydrides passivate rapidly on exposure to air or water vapor so that they will not adsorb hydrogen unless exposed to high hydrogen pressures. As the fabrication process requires exposure to air, and high hydrogen pressures would destroy the device, this passivation must be prevented. The scope of this task was limited to the  $\text{LaAl}_x\text{Ni}_{5-x}$  hydride family, as it has desirable properties that the microfabricated fuel cell requires. This material is also commercially available. We expect that a successful completion of this task will lead to integrated devices with energy densities on the order of  $500 \text{ mWh/cm}^3$  for a 50 mWh storage capacity.

### **Status**

The first generation of improved hydride materials were based on a modified  $\text{LaAl}_x\text{Ni}_{5-x}$  hydride, and made into thick film printable ink using a water-soluble binder. During the past 6 months, we have continued to test these materials. In addition, several second-generation inks, using the same hydride material, but incorporating a non-water-soluble binder have been developed. The first generation inks have now been cycled over 5000 times without loss in hydrogen storage capacity, or a change in the hydrogen sorption/desorption rate. In addition, these inks remained adherent to the substrate (alumina) throughout the cycle tests and have been found to retain their activity even after exposure to ambient humidity air for 55 weeks. Despite these successes, the second-generation inks have been developed to expand the fabrication possibilities and to further improve the performance of the hydride storage in the humid fuel cell environment. This effort has also been successful, a non-water-soluble binder has been found that retains the desirable properties of the first generation system; very low binder content ( $<1 \text{ wt}\%$ ) for high energy density storage, rapid sorption/desorption rates for hydrogen, and the ink can be prepared, printed and cured in ambient air without loss of hydrogen storage activity. This ink is now undergoing long term cycle testing in both dry and humid hydrogen. In repeated testing using a Sievert's apparatus to quantify the amount of hydrogen that could be stored, capacities of  $1200\text{-}1800 \text{ mAh/cm}^3$  of ink were obtained with the second-generation ink based on the modified  $\text{LaAl}_x\text{Ni}_{5-x}$  hydride. Our calculations show that capacities in the upper end of this range should be sufficient to meet our goal of an energy density of  $500 \text{ mWh/cm}^3$  for a device consisting of a fuel cell integrated with a hydride storage block of 50 mWh capacity.

One of the advantages of using hydride in the substrate in place of a sacrificial layer is that it provides a closely coupled source of hydrogen. The amount of hydrogen that can be stored for the design shown in Figure 3.1a can be calculated from the mass of hydride ink used in the substrate. This calculation shows that the equivalent of 14.5 mAh can be stored as hydrogen in one circular well ( $0.2 \text{ cm}^2$  area by  $600 \text{ }\mu\text{m}$  thick). If the backside of the well is sealed, the hydride can be electrochemically charged with hydrogen. The fuel cell is placed in a hydrogen environment, and has a positive potential applied to it. Under these conditions, the upper electrode oxidizes hydrogen to protons which travel across the electrolyte layer to the inner electrode, where the protons are reduced to

re-create hydrogen. The hydrogen generated at the inner electrode passes through the current collector and is taken up by the hydride material. For this step, a constant voltage of 0.3 V is applied. The current is recorded as a function of time, and this result is integrated to estimate the amount of hydrogen stored. The efficiency of the process was determined by operating the device as a fuel cell. The fuel cell was connected to a load and held at a constant voltage (in this case 0.5 V) until the output current fell to zero, indicating that the stored hydrogen had been completely consumed. The ratio of the integrated output current to the integrated current during charging gives the efficiency of the charging process. Ideally, the efficiency should be close to 100% and the amount of charge stored should be 14.5 mAh. However, to date we have only achieved efficiencies on the order of 33%, and the usable amount of charge stored is only  $\approx 2.5$  mAh. From these results we suspect that the process used to seal the back of the hydride well is not sufficiently leak tight, and that hydrogen is being lost through the back of the device to the outside air.

It should be noted that our goal for this project was a device with a 50 mWh (100 mAh at 0.5V) capacity. To achieve this goal, a larger volume of hydride is required. Our plan has been to deposit a large volume of hydride on a second substrate, which would be bonded to the back of the substrate on which the fuel cell stack is fabricated. These large area hydride wells have been fabricated with up to 200 mAh capacity.

#### Future Work - Hydride Storage

- Investigate improved methods of bonding alumina substrates together to prevent loss of stored hydrogen.
- Incorporate the larger hydrogen storage modules with microfabricated fuel cells and determine the performance and energy density of the combined device.

### **Task 3: Electrolyte Deposition Enhancement**

#### **Technical Approach**

In the fabrication of prototype micro fuel cells to date, the polymer electrolyte has typically been applied manually. Thick film printing of the electrolyte layer has been shown, but the results were not ideal. In this task, CWRU will investigate alternative methods and techniques that will perform this fabrication step in a more automatic and consistent manner, such as with micro-pen or ink jet deposition. The goal is to demonstrate prototype fuel cells that are reproducible and easily manufactured.

#### **Status**

In the previous report, results were shown for an improved method of depositing Nafion polymer electrolyte using the thick film printer. Since then, we have focused on the production of complete fuel cells using the thick film process for depositing Nafion. Complete cells have now been successfully fabricated incorporating thick film printed electrolyte layers. The complete fabrication sequence is shown in **Figure 3.1a-d**. **Figure 3.1e** shows three complete cells connected in series to produce a 1.5V device. **Table 3A** summarizes the fabrication steps. Table 3B summarizes the curing procedure for each step.

#### **Future Work - Electrolyte Deposition**

None planned at this time.

**Table 3A** Summary of Thick Film Deposition Steps for Micro Fuel Cell Fabrication

Layer	Mask Type	Mask Properties	Thickness (μm)
Anode Current Collector	Screen	280	15-20
Anode	Stencil	1 mil	10-15
Electrolyte	Stencil	4 mil	35-40
Cathode	Stencil	1 mil	10-15
Cathode Current Collector	Screen	280	15-20

**Table 3B** Summary of Curing Procedures

Layer	Cure Temperature °C	Cure Time minutes
Anode Current Collector	110	10
Anode Catalyst	40	10
	70	15
	110	15
Electrolyte	110	25
Cathode Catalyst	110	10
Cathode Current Collector	110	10

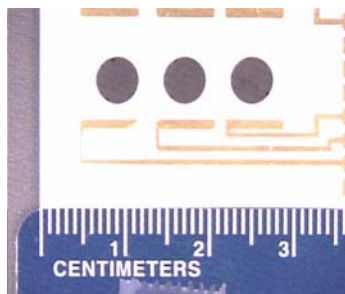


**Figure 3.1a** Alumina substrate with hydride fuel storage - three cells.

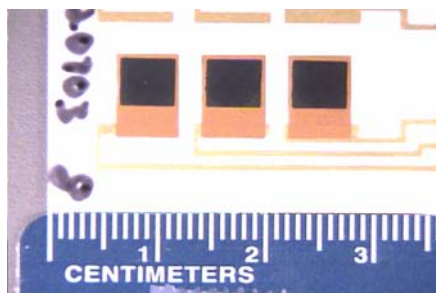


**Figure 3.1b** After deposition of anode current collector and anode catalyst.

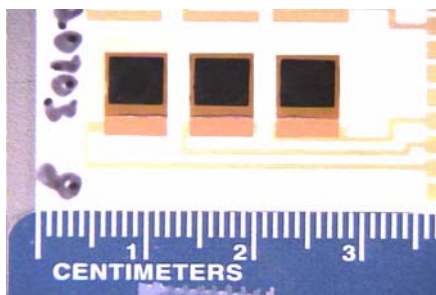


**Figure 3.1c** After deposition of polymer electrolyte layer.

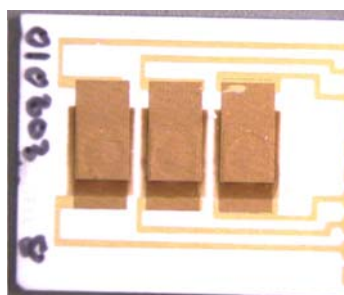


**Figure 3.1d** After deposition of cathode catalyst and cathode current collector. Three single cells.

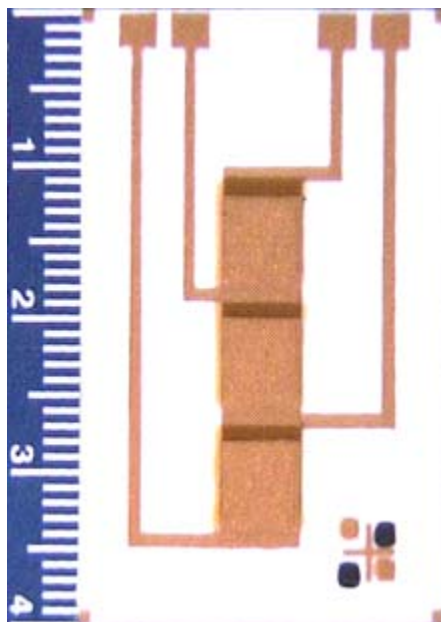


**Figure 3.1e** Complete stack - three cells in series. The positive terminal of the stack is the leftmost of the four gold tabs at the top of the photo. The negative terminal of the stack is the 3<sup>rd</sup> tab from the left. The other two tabs allow the potential of each cell to be monitored.



#### **Task 4: Search for Insertion Opportunities and Development Partners**

##### Approach

In this task, CWRU will specifically look for opportunities throughout the DoD where devices can benefit from integrating a microfabricated fuel cell or used as power delivery devices in a stand-alone configuration. CWRU expects that this task will involve a design component with perhaps some modeling based on laboratory data acquired from prototypes. We will also work to establish relationships with commercial manufacturers and venture capital firms interested in this technology.

##### Status

We have continued to meet with companies and venture capital firms interested in the commercialization possibilities arising from this program. We are in the process of preparing a proposal in conjunction with Old Colorado Communications Inc., a developer of wireless communications and data logging solutions, to develop wireless sensors for ecological monitoring.

## 1. RESEARCH STATUS

### **Task 1: Fabrication Enhancements for Improved Reactant Accessibility**

#### Technical Approach

This task will examine water-soluble sacrificial materials to be used during the fabrication process. At the appropriate point in the fabrication process, the sacrificial material will be extracted in order to open the structure. This is necessary to enhance hydrogen accessibility to the anode to achieve higher power densities. We believe it should be possible to increase the power density levels from 2 mW/cm<sup>2</sup> to levels of > 10 mW/cm<sup>2</sup>. This should increase the range of DoD applications for this technology.

Water-soluble materials have been chosen for this effort due to the nature of the materials used in the microfabricated fuel cell. Each of the components in the device - anode and cathode current collectors, anode and cathode catalyst layers and the polymer electrolyte, are polymers or incorporate polymeric binders. All of the various polymers used have limited thermal stability, and/or can be readily etched/dissolved by organic solvents. As a result, we are attempting to develop a system using water as a benign solvent. Unfortunately, even exposure to liquid water may damage the device, as non-cross-linked polymer electrolytes readily swell in liquid water. As a result, caution must be exercised and a careful procedure developed.

#### Status

Previously, we had reported the development of a sacrificial process that allowed for fabrication of complete fuel cells, and for which the sacrificial material could be completely removed in the final step. Unfortunately, device yields using this process were low due to swelling of the polymer electrolyte layer. Excessive swelling consistently resulted in device failures due to delamination from the substrate. As a result, we have changed our approach, and have gone back to fabricating the fuel cell on top of a film of the metal hydride ink developed in Task 2 below. When this approach was tried previously, the results were poor due to low hydrogen permeability through the hydride material. However, the newer generations of the hydride ink are considerably more permeable to hydrogen. With only one significant change, (the temperature ramp during the curing process for the anode ink has to be slower to prevent anode delamination) we are able to fabricate complete fuel cells with the hydride ink in the substrate. In the previous report, we reported power densities up to 5 mW/cm<sup>2</sup> at 50%RH from devices fabricated in this manner. In the past 6 months we have refined our fabrication technique and improved the power output as detailed below.

Typical results obtained in the last 6 months are detailed in **Figures 1.1 - 1.3** below. In Figure 1.1 a comparison is shown between the I-V curves for the earlier generation of cells (from July 2000) and the most recent results. The comparison shows that the maximum power output has increased from 2 mW/cm<sup>2</sup> to  $\approx 7$  mW/cm<sup>2</sup> (dry hydrogen / air at 50%RH, room temperature). The highest power density realized under these conditions was 7.5 mW/cm<sup>2</sup>. The earlier cells were limited by hydrogen access to the anode, which resulted in a limiting current density of  $\approx 15$  mA/cm<sup>2</sup>. Fabricating the cells on top of the metal hydride material allows sufficient hydrogen accessibility that the cells are now limited by other factors - oxygen access to the cathode and the electrolyte resistance.

In Figure 1.2, the effect of the electrolyte resistance is demonstrated by lowering the relative humidity, as can be seen in the comparison of the I-V curves obtained with air at 50 and 20% RH. At 20% RH, the electrolyte is much less conductive, the I-V curve is much steeper and the power output is much lower (about 1 mW/cm<sup>2</sup>).

In Figure 1.3, a comparison is shown between the standard cell shown in the previous figures, and a cell in which the electrolyte layer and the cathode current collector layer were both made  $\approx 50\%$  thinner. The results shown in Figure 1.3 are essentially as expected. The thinner electrolyte layer greatly reduces the internal resistance, yielding a flatter I-V curve. The thinner cathode current collector allows easy oxygen access to the cathode, and the limiting current of  $\approx 30$  mA/cm<sup>2</sup> seen in the standard cell is not seen. With these changes, the maximum power output is roughly doubled to 15 mW/cm<sup>2</sup> (0.3V @ 50 mA/cm<sup>2</sup>). However, the thin electrolyte layer allows considerably greater hydrogen permeation, substantially reducing the open circuit potential. The hydrogen lost by permeation across the electrolyte to the cathode is  $\approx 10$ -15 mA/cm<sup>2</sup>. In other words, even when operating at the maximum power point,  $\approx 25\%$  of the hydrogen is lost and is not used to make electricity. In addition, our fabrication yields with the thin electrolyte layer are very low. Recent efforts to develop improved electrolyte deposition procedures are detailed under Task 3 below. However, due to the poor fabrication yield, and the excessive hydrogen permeation, we do not consider the thin electrolyte cell to be a viable device.

#### Future Work - Fabrication Enhancements

- By using a supported platinum catalyst with a higher platinum content than the 20 wt% catalyst previously used, cells with a higher platinum loading will be fabricated to determine if this will increase the catalytic activity sufficiently to achieve the power density target of 10 mW/cm<sup>2</sup>.

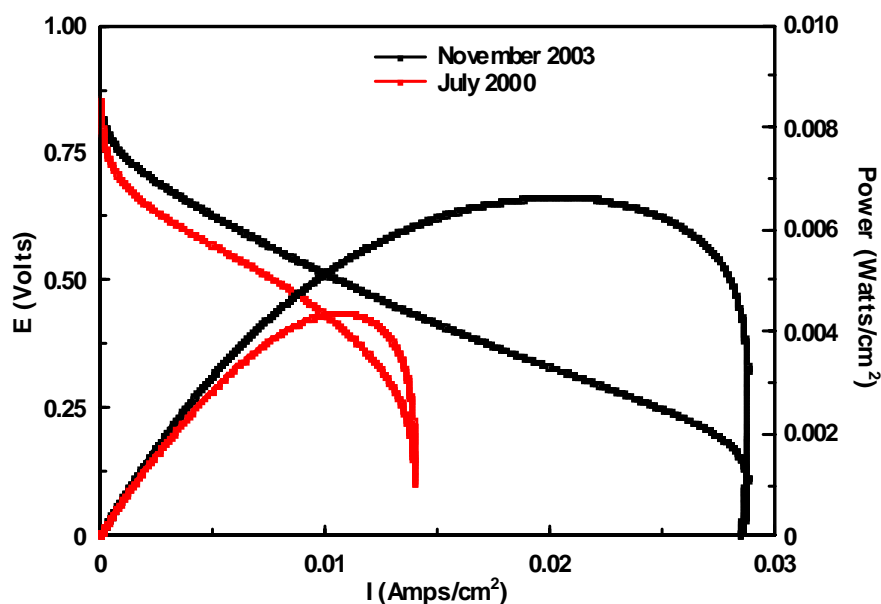


**Figure 1.1** Polarization curves for typical microfabricated fuel cells from July 2000 and recent cells. Anode feed: hydrogen, Cathode: air at 50%RH. Room temperature.

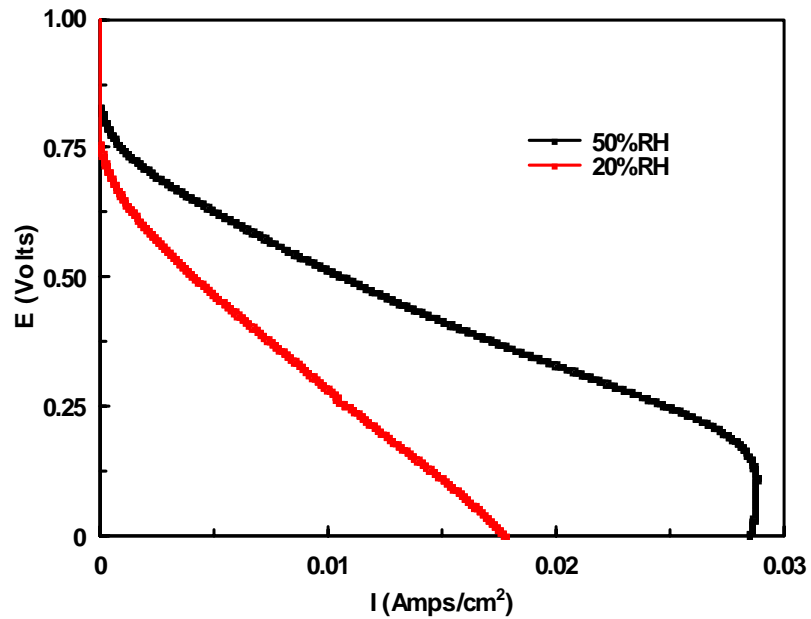


**Figure 1.2** Polarization curves obtained with air at 50 and 20%RH. Anode feed: dry hydrogen. Room temperature.

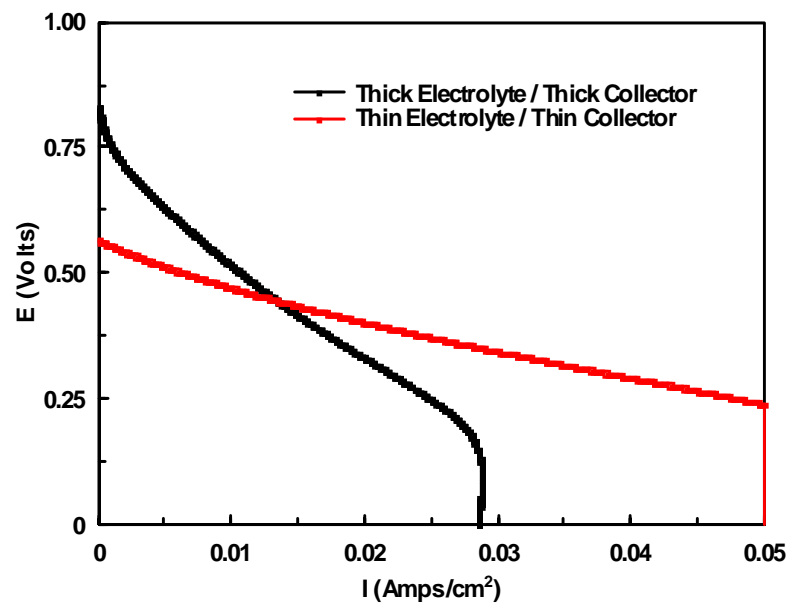


**Figure 1.3** Comparison of polarization curves for standard cell (labeled ‘thick electrolyte/thick collector’) and cell with  $\approx 50\%$  thinner electrolyte layer and cathode current collector (‘thin electrolyte/thin collector’). Air at 50%RH, dry hydrogen, room temperature.

## **Task 2: Metal Hydride Fuel Storage**

### **Technical Approach**

The use of metal hydrides for hydrogen storage has several advantages including orientation independent operation. In addition, high volumetric energy densities can be achieved with these materials. A major goal of this proposed task was to produce a metal hydride material that is tailored to this fuel cell application, with an equilibrium pressure near atmospheric pressure at room temperature, and that can be applied in a thick film fabrication process. A second important goal is that the hydride material remains active after exposure to air or water vapor. Typically, metal hydrides passivate rapidly on exposure to air or water vapor so that they will not adsorb hydrogen unless exposed to high hydrogen pressures. As the fabrication process requires exposure to air, and high hydrogen pressures would destroy the device, this passivation must be prevented. The scope of this task was limited to the  $\text{LaAl}_x\text{Ni}_{5-x}$  hydride family, as it has desirable properties that the microfabricated fuel cell requires. This material is also commercially available. We expect that a successful completion of this task will lead to integrated devices with energy densities on the order of  $500 \text{ mWh/cm}^3$  for a 50 mWh storage capacity.

### **Status**

The first generation of improved hydride materials were based on a modified  $\text{LaAl}_x\text{Ni}_{5-x}$  hydride, and made into thick film printable ink using a water-soluble binder. In addition, several second-generation inks, using the same hydride material, but incorporating a non-water-soluble binder have been developed. During the past 6 months, we have continued to test these materials. The first generation inks have now been cycled over 5000 times without loss in hydrogen storage capacity, or a change in the hydrogen sorption/desorption rate. In addition, these inks remained adherent to the substrate (alumina) throughout the cycle tests and have been found to retain their activity even after exposure to ambient humidity air for 55 weeks. The second-generation inks have been developed to expand the fabrication possibilities and to further improve the performance of the hydride storage in the humid fuel cell environment. This effort has also been successful, a non-water-soluble binder has been found that retains the desirable properties of the first generation system; very low binder content ( $<1 \text{ wt}\%$ ) for high energy density storage, rapid sorption/desorption rates for hydrogen, and the ink can be prepared, printed and cured in ambient air without loss of hydrogen storage activity. This ink is now undergoing long term cycle testing in both dry and humid hydrogen.

The long term cycle testing consists of a 10 minute exposure to dry or humid hydrogen, followed by a 10 min desorption cycle in vacuum using a Sievert’s apparatus. For the humid hydrogen tests, the hydrogen was humidified to 75%RH at room temperature before being introduced into the sorption chamber. The test has now exceeded 4000 cycles with the humidified hydrogen, the hydride material is still active and both the total amount of hydrogen stored and the rates of hydrogen uptake and release are essentially unchanged.

In repeated testing to quantify the amount of hydrogen that could be stored, capacities of  $1200\text{-}1800 \text{ mAh/cm}^3$  of ink were obtained with the second-generation ink based on the modified

LaAl<sub>x</sub>Ni<sub>5-x</sub> hydride. Our calculations show that capacities in the upper end of this range should be sufficient to meet our goal of an energy density of 500 mWh/cm<sup>3</sup> for a device consisting of a fuel cell integrated with a hydride storage block of 50 mWh capacity.

#### Future Work - Hydride Storage

- Investigate improved methods of bonding alumina substrates together to prevent loss of stored hydrogen.
- Incorporate the larger hydrogen storage modules with microfabricated fuel cells and determine the performance and energy density of the combined device.

### **Task 3: Electrolyte Deposition Enhancement**

#### Technical Approach

In the fabrication of prototype micro fuel cells early in this program, the polymer electrolyte was applied manually. Thick film printing of the electrolyte layer has been developed, but the results were not ideal. In this task, CWRU will investigate alternative methods and techniques that will perform this fabrication step in a more automatic and consistent manner, such as with micro-pen or ink jet deposition. The goal is to demonstrate prototype fuel cells that are reproducible and easily manufactured.

#### Status

A major cause of fuel cell failure during production is the shorting of the anode catalyst layer to the cathode layer catalyst. The electrolyte layer between the two catalysts is supposed to prevent them from making low resistance electrical contact (see **Figure 3.1** for structure of the fuel cell). Previously the electrolyte layer has been thick film printed through a 4-mil thick stainless steel stencil. The incidence of shorting was unacceptable with this deposition method. It was found that printing a second layer of electrolyte on top of the first layer through the same stencil greatly reduced the number of shorts. However, a thick electrolyte layer does not lead to desirable fuel cell properties.

Several ideas have been suggested to why the electrolyte layer fails to keep the two catalyst layers separated. One idea is that the electrolyte gets bubbles in it when it is printed through the stencil. Another was that because the hydride layer that is under the anode catalyst layer is not perfectly flat; the depression in the center of the hydride causes the electrolyte layer to be thin around the edges of the cell. Thus, when the cathode catalyst is printed on top of the electrolyte, it dissolves the thin coating of electrolyte at the edges. Since the catalyst layer ink and the electrolyte solution contain the same solvent, the catalyst layer will tend to interact with the electrolyte layer. One further suggestion was that the anode current collector, a layer of gold thick film ink, was interacting with both the anode catalyst and the electrolyte and causing them to short.

In order to avoid the possibility of bubbles in the electrolyte, the deposition method of the electrolyte was changed. The thick film printer uses a squeegee to force the electrolyte through the stencil onto the fuel cell substrate. The Asymtek printer jets material onto a substrate as microliter sized droplets using a positive displacement pump. It was anticipated that by jetting the electrolyte fluid bubble formation would be avoided.

This theory was first tested by printing the electrolyte material onto alumina substrates that had gold lines thick film printed on them (see **Figure 3.2**). It was thought that the electrolyte would be deposited onto the alumina over the gold fingers and the electrolyte would flow slightly to level itself. Two different variations of the electrolyte, made with Nafion and ethylene glycol, were printed. One was 13 wt% electrolyte and the other 23.9 wt.% electrolyte. The 23.9 % electrolyte was more viscous than the 13 wt.%. It was assumed the higher percentage electrolyte would result in a thicker electrolyte layer after drying and better edge definition.

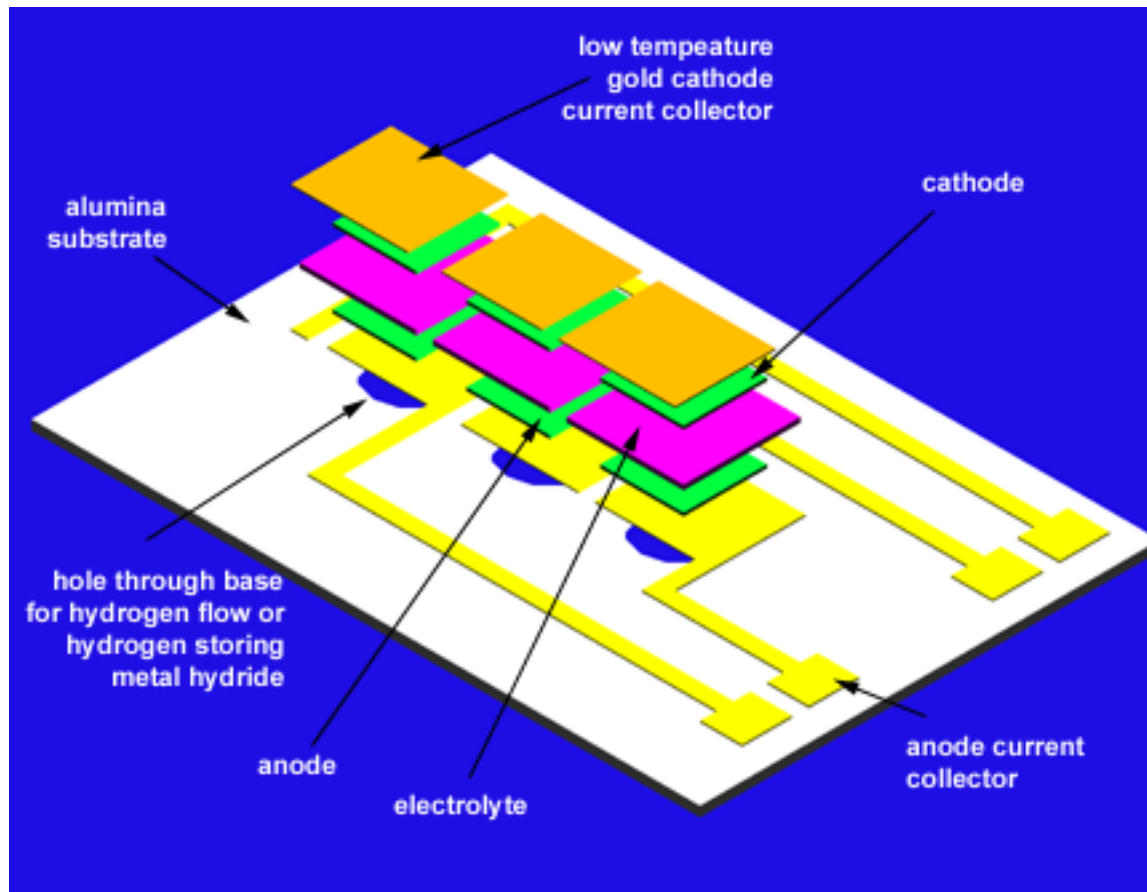


**Figure 3.1** Exploded view of microfuel cell construction.

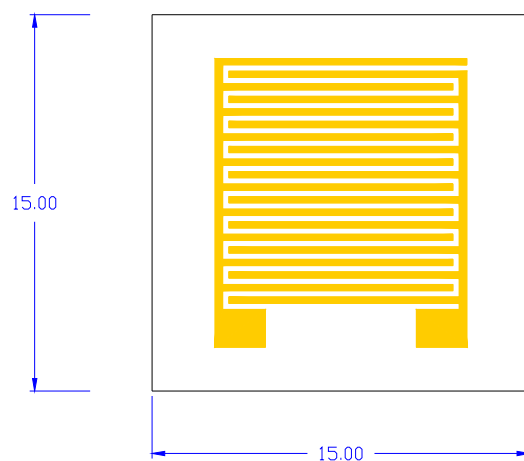


**Figure 3.2** Test substrate for electrolyte printing - interdigitated gold lines on alumina. Gold lines are 10 μm thick, 500 μm wide.

The results of the Asymtek printing of the electrolyte were not entirely as expected. The higher weight percentage electrolyte did produce a thicker coating ( $\approx 40\text{ }\mu\text{m}$  vs  $\approx 30\text{ }\mu\text{m}$ ), and with less pronounced edge effects (compare scans A1-3 and B1-3 in **Figure 3.3** below). However, instead of a smooth, even coating, the top of the layer reflected the gold line pattern on the substrate (See **Figure 3.3**). The gold lines themselves are on the order of 10 microns thick. The electrolyte does not level itself but reflects the underlying surface it is deposited on. This suggests that when it is printed on an actual fuel cell that any small variations in height cannot be compensated for by the electrolyte resulting in thinner and thicker areas over the fuel cell surface.

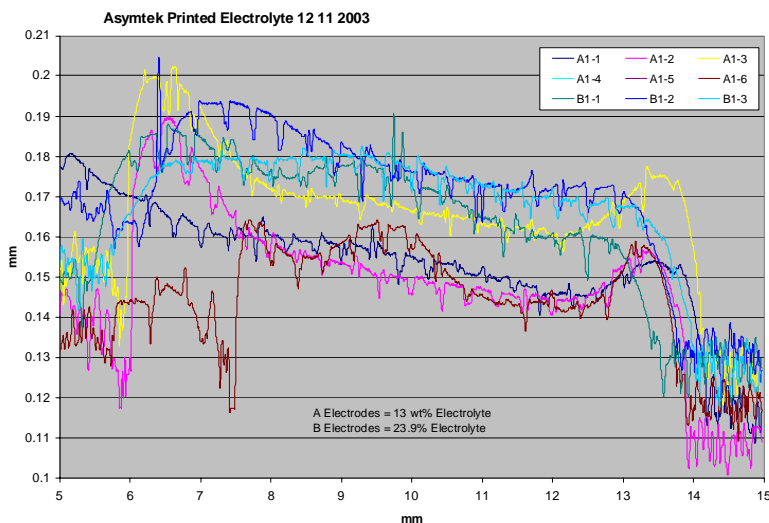


**Figure 3.3** Profilometry results of Nafion printed using Asymtek micro dispenser. “A” scans printed with 13 wt% Nafion solution. “B” scans printed with 24 wt% solution.

Although the electrolyte did not level as desired, the layer itself was continuous and had no bubbles in it. It was not possible to make electrical contact to the gold lines through the electrolyte. The electrolyte layer was thought to be thick enough, on the order of 20 to 40  $\mu\text{m}$ , to produce workable fuel cells.

Fuel cells were produced by following the thick film process until the point where the electrolyte was to be deposited. The electrolyte was then deposited using the Asymtek printer and the settings used in the above trials. The same two concentrations of electrolyte were used, 13 wt% and 23.9 wt.% electrolyte. Both concentrations of electrolyte did not flow well on the anode catalyst layer. The electrolyte tended to be uneven across the surface of the catalyst. All the fuel cells resulting from this method were shorted except the ones that either had two layers of electrolyte deposited on them or a very thick coating of electrolyte.

It was then decided to try another method of determining why the electrolyte layer failed and how to correct it. To get rid of the variable of the bottom layer of the catalyst being uneven due to the hydride, the catalyst ink was printed on top of a smooth alumina substrate that had been coated in gold (see **Figure 3.4**). Three rows of three cells of the catalyst were printed. The catalyst was printed through a 4-mil stencil. Three substrates were made in total. After the catalyst was cured at 110 C, one of the set of 3 cells had its height measured by a laser profilometer. Despite the fact that the underlying gold layer and substrate were very flat, the catalyst layer is not flat. It has slightly raised edges and distinct side bands that should not be present (see **Figure 3.5**). This is, most likely, an artifact of the thick film printing of the catalyst through a stencil.

All three rows of cells then had electrolyte deposited on them using the Asymtek printer. Both concentrations of electrolyte were used, 13 wt% and 23.9 wt.% electrolyte, as well as 8 different sets of printing parameters (ET-1 - ET-8). Neither concentration of electrolyte flowed on the catalyst layer. The electrolyte tended to be uneven across the surface of the catalyst. The electrolyte was cured and its height measured by the laser profilometer. Next, two of the rows had another layer of catalyst deposited by thick film printing through a 4 mil stencil. The height of the cells was again measured using the profilometer. Finally, a layer of Ercon gold was printed through a 4-mil stencil (see **Figure 3.6** for side view of layers). The third row of cells in each group had the



top catalyst layer omitted and the Ercon gold was printed directly on the electrolyte to see if the gold ink caused a breakdown of the electrolyte layer.

A digital multimeter was used to measure the resistance from the bottom gold layer to the Ercon gold layer. Whether a particular cell was shorted or not is given in **Table 3A**. Cells ET-1, ET-2 and ET-3 were made using a 23.9 wt.% electrolyte and ET-4 through ET-8 were made using the 13 wt% electrolyte.

One fact that emerged from these tests is that the Ercon gold does not negatively impact the electrolyte. Except for one combination of electrolyte and printing conditions, the Ercon gold does not degrade the electrolyte or penetrate through to the catalyst below. Therefore, the shorting problem of the fuel cells is unlikely to be due to the current collector of the fuel cell.

There are no bubbles produced when the Asymtek deposits the electrolyte layer on the catalyst. Therefore, the presence of open areas in the cured electrolyte due to bubble formation is unlikely to be the cause of the shorting between the catalyst layers.

The question of whether the unevenness of the hydride layer that is under the anode catalyst layer causes the electrolyte layer to be thin around the edges of the cell leading to the cell shorting is difficult to definitively answer. From these experiments, it appears that the electrolyte does not spread as evenly or smoothly on the catalyst as it does on bare alumina or gold covered alumina. So it is possible much of the shorting is caused by the layers having open areas in them due to uneven deposition.

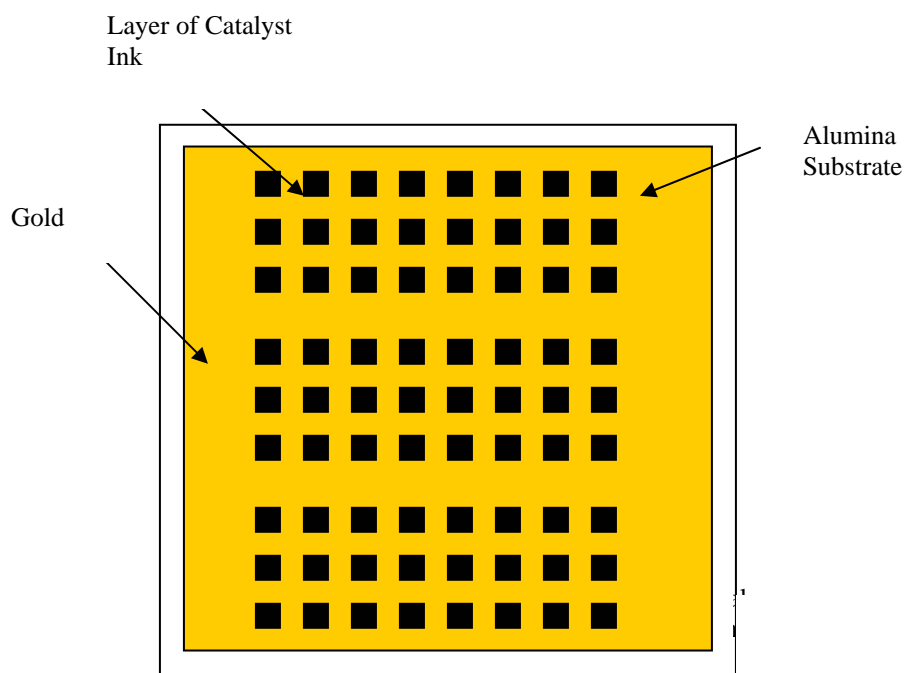
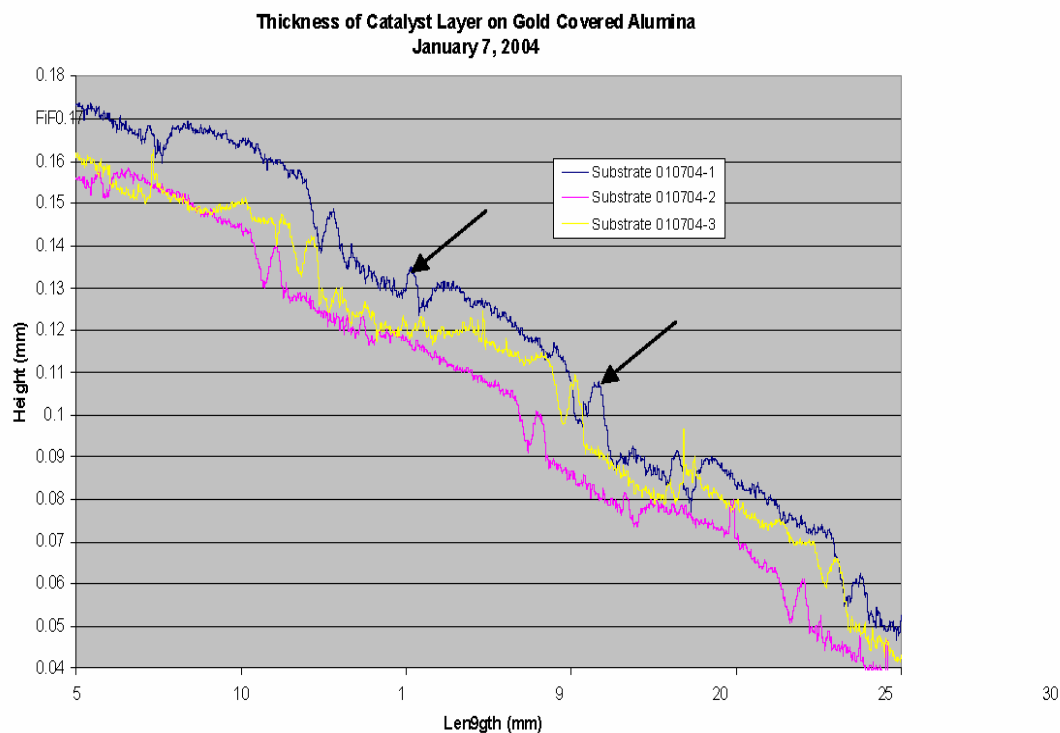
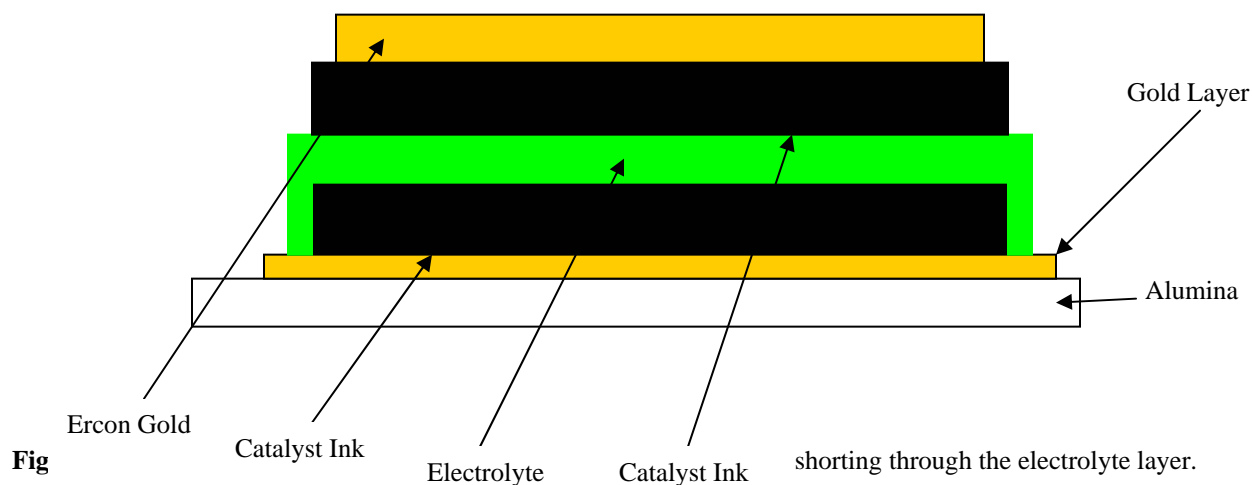


Figure 3.4 Smooth test substrate with catalyst ink for electrolyte printing trials. Catalyst regions are 5 x 5 mm.



**Figure 3.5** Profilometer results from printing of catalyst ink on smooth gold on alumina. Arrows indicate undesired sidebands at the perimeter of each deposit.



Looking further at the results at besides one combination, ET-8, of electrolyte/Asymtek parameters that nearly always resulted in shorting, there was no clear pattern as to what electrolyte/Asymtek parameters would always produce a good cell. Combination ET-3 always resulted in non-shortened cells but the other seven combinations had both good and bad cells produced.

One very interesting result was the uneven surface of the final cells. **Figure 3.7** shows the profile of each combination for the center row of cells. The electrolyte layer does not level off the surface of the cell. This effect seems to be greater when comparing the cells made with the 13 wt% and 23.9 wt.% electrolyte. The 13 wt% electrolyte tends to flow better and make flatter cells.

**Figure 3.8** shows the profilometry results for the three cells of trial ET-1 after each deposition step: printing of the inner catalyst layer, printing the electrolyte the profile, and after the top catalyst layer has been printed. The top catalyst layer does not flow very well on the electrolyte and it does not level off. The raised height along the edges after printing the electrolyte is still very noticeable after printing the top catalyst layer. Clearly, the unevenness in height from one layer is carried over to the next layer. For every parameter set used, there is a very noticeable dip near the center in many of the cell profiles.

Excluding process ET-8 which experienced printing problems and excluding Row 2/Cell 3 results which also had printing problems due to misalignment, the 13 wt% electrolyte layers had a 15% incidence of electrical shorting while the 23.9 wt.% printed cells were about a 7% incidence of shorting. However, the more concentrated solution leads to very thick and very un-even electrolyte layers.

#### Future Work

Another test substrate with the 13 wt% electrolyte printed on catalyst ink will be made. One, two or three layers of the electrolyte will be deposited to see what final thickness and incidence of shorting there is. The flatter the cells can be made the less chance of shorting due to thin patches there should be. Since the actual fuel cells start out being non-flat, unlike the test cells, it is important that all layers on top of the hydride self-level.

**Table 3A** Summary of Electrical Tests with various electrolyte printing parameters  
X indicates electrical short.

Row 1	Parameters Used							
	ET-1	ET-5	ET-4	ET-2	ET-6	ET-8	ET-3	ET-7
Cell 1						X		
Cell 2			X			X		
Cell 3		X				X		X
Row 2								
	ET-7	ET-2	ET-8	ET-3	ET-6	ET-1	ET-4	ET-5
Cell 1								

Cell 2		X						
Cell 3			X		X	X	X	X
Row 3								
	ET-8	ET-3	ET-7	ET-2	ET-5	ET-4	ET-1	ET-6
Cell 1	X							
Cell 2	X				X			
Cell 3	X	X	X	X	X	X	X	X

Notes: Row 2, Cell 3 electrolyte layer misaligned

Row 3, Cell 3 electrolyte layer misaligned

each ET-# designates a different set of printing parameters for the electrolyte layer. Cells ET-1, ET-2 and ET-3 were made using a 23.9 wt.% electrolyte solution and ET-4 through ET-8 were made using the 13 wt% electrolyte solution.

Cells in rows 1 and 2 had catalyst and gold printed on top of the electrolyte layer - see Figure 3.6

Cells in row 3 had only gold printed on top of the electrolyte layer.

## 1. RESEARCH STATUS

### Task 1: Fabrication Enhancements for Improved Reactant Accessibility

#### Technical Approach

This task will examine water-soluble sacrificial materials to be used during the fabrication process. At the appropriate point in the fabrication process, the sacrificial material will be extracted in order to open the structure. This is necessary to enhance hydrogen accessibility to the anode to achieve higher power densities. We believe it should be possible to increase the power density levels from  $2 \text{ mW/cm}^2$  to levels of  $> 10 \text{ mW/cm}^2$ . This should increase the range of DoD applications for this technology.

#### Status

No new results to report. Typical results obtained in the last 12 months show that the maximum power output has been increased to  $\approx 7 \text{ mW/cm}^2$  using dry hydrogen and air at 50%RH, at room temperature as shown in Figure 1.1. The highest power density realized under these conditions was  $7.5 \text{ mW/cm}^2$ . The earlier cells were limited by hydrogen access to the anode, which resulted in a limiting current density of  $\approx 15 \text{ mA/cm}^2$ . Fabricating the cells directly on top of the metal hydride material allows sufficient hydrogen accessibility that the cells are now limited by other factors - oxygen access to the cathode and the electrolyte resistance.

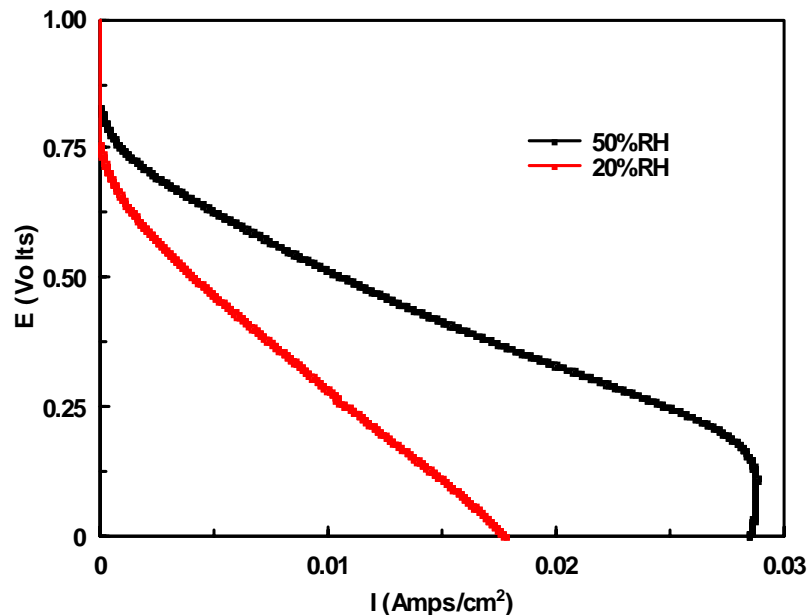


**Figure 1.1** Polarization curves obtained with air at 50 and 20%RH. Anode feed: dry hydrogen. Room temperature.

## **Task 2: Metal Hydride Fuel Storage**

### **Technical Approach**

The use of metal hydrides for hydrogen storage has several advantages including orientation independent operation. In addition, high volumetric energy densities can be achieved with these materials. A major goal of this proposed task was to produce a metal hydride material that is tailored to this fuel cell application, with an equilibrium pressure near atmospheric pressure at room temperature, and that can be applied in a thick film fabrication process. A second important goal is that the hydride material remains active after exposure to air or water vapor. Typically, metal hydrides passivate rapidly on exposure to air or water vapor so that they will not adsorb hydrogen unless exposed to high hydrogen pressures. As the fabrication process requires exposure to air, and high hydrogen pressures would destroy the device, this passivation must be prevented. The scope of this task was limited to the  $\text{LaAl}_x\text{Ni}_{5-x}$  hydride family, as it has desirable properties that the microfabricated fuel cell requires. This material is also commercially available. We expect that a successful completion of this task will lead to integrated devices with energy densities on the order of  $500 \text{ mWh/cm}^3$  for a 50 mWh storage capacity.

### **Status**

The first generation of improved hydride materials were based on a modified  $\text{LaAl}_x\text{Ni}_{5-x}$  hydride, and made into thick film printable ink using a water-soluble binder. In addition, several second-generation inks, using the same hydride material, but incorporating a non-water-soluble binder have been developed. During the past 12 months, we have continued to test these materials. The first generation inks have now been cycled over 5000 times without loss in hydrogen storage capacity, or a change in the hydrogen sorption/desorption rate. In addition, these inks remained adherent to the substrate (alumina) throughout the cycle tests and have been found to retain their activity even after exposure to ambient humidity air for 55 weeks. The second-generation inks have been developed to expand the fabrication possibilities and to further improve the performance of the hydride storage in the humid fuel cell environment. This effort has also been successful, a non-water-soluble binder has been found that retains the desirable properties of the first generation system; very low binder content (<1 wt%) for high energy density storage, rapid sorption/desorption rates for hydrogen, and the ink can be prepared, printed and cured in ambient air without loss of hydrogen storage activity.

## **Task 3: Electrolyte Deposition Enhancement**

### **Technical Approach**

In the fabrication of prototype micro fuel cells early in this program, the polymer electrolyte was applied manually. Thick film printing of the electrolyte layer has been developed, but the results were not ideal. In this task, CWRU will investigate alternative methods and techniques that will perform this fabrication step in a more automatic and consistent manner, such as with micro-pen or ink jet deposition. The goal is to demonstrate prototype fuel cells that are reproducible and easily manufactured.

### Status

A major cause of fuel cell failure during production is the shorting of the anode catalyst layer to the cathode layer catalyst. The electrolyte layer between the two catalysts is supposed to prevent them from making low resistance electrical contact (see **Figure 3.1** for structure of the fuel cell).

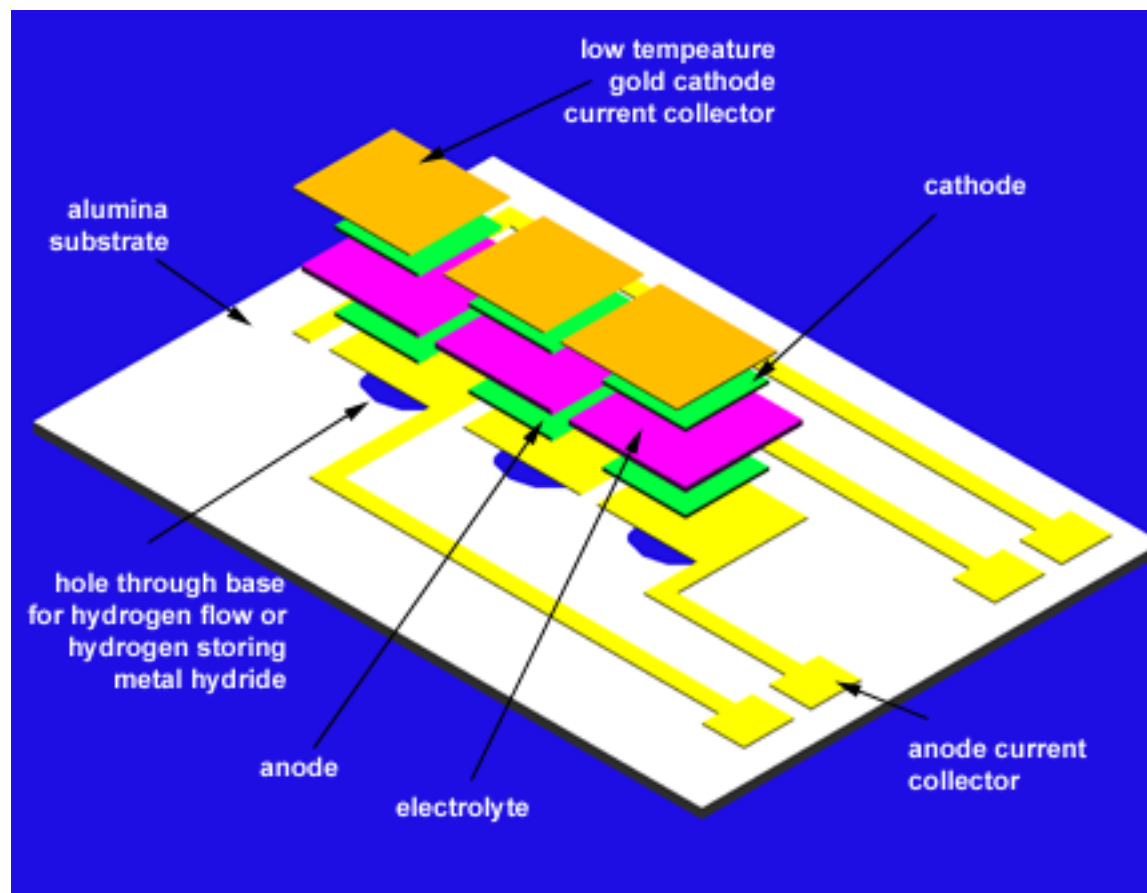
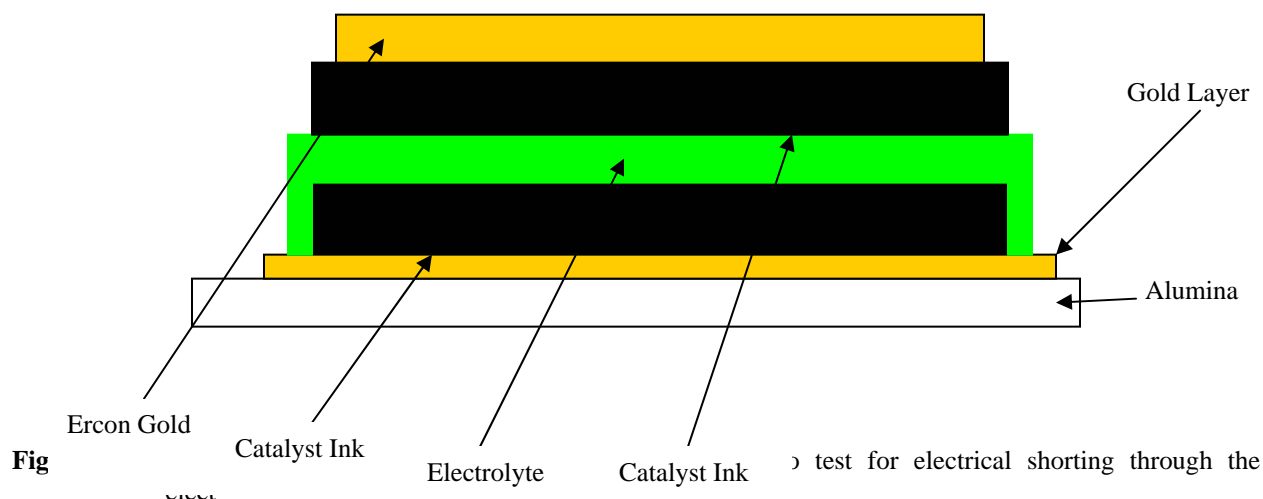


**Figure 3.1** Exploded view of microfuel cell construction.

In the last six months we have continued to look at modifying the electrolyte deposition procedure to minimize the number of shorted cells and thus improve our yields. In addition to fuel cell structures as shown in Figure 3.1, we have fabricated double-layer capacitor structures as shown in Figure 3.2. The capacitor structures are identical to the fuel cells, with the exception that the substrate for the capacitors is solid alumina, as opposed to the fuel cells which are printed on top of the metal hydride material deposited within holes in the alumina. The hydride provides hydrogen storage as well as providing a pathway for hydrogen to reach the anode. The capacitor structures do not require reactants, and are therefore fabricated on solid substrates.



The capacitor structures showed very high fabrication yields, over 90%. The test results shown in Table 3A from the capacitor structures were also promising, showing acceptable reproducibility. Under the conditions tested, and given the intended thicknesses of the electrodes and the electrolyte layer, we anticipated device capacitances of 10 mC and a high frequency resistance of 3 ohms. The average values as listed in Table 3A were 6.4 mC and 3.4 ohm.

**Table 3A** – Test results from microfabricated double layer capacitors. Results are from four separate devices, two cells in each device.

Cell	Est. C (mC)	RHF (ohm)
A1 L	8.80	3.30
A1 M	7.50	2.75
A2 L	5.60	3.50
A2 M	5.70	3.75
A3 L	6.80	3.15
A3 M	5.80	3.80
B1 L	5.20	3.50
B1 M	5.60	3.30
<i>Averaged Values</i>	<i>6.4 ± 1.2</i>	<i>3.4 ± 0.3</i>

All devices tested under argon (75%RH) at room temperature.

RHF – high frequency resistance determined by AC Impedance at 20,000 Hz.

Estimated Capacitance – determined from double layer charging current using a 100 mV/s potential sweep.

Cell area = 0.25 cm<sup>2</sup>

The high fabrication yields and good performance of the capacitor structures have confirmed that our fabrication issue with the microfabricated fuel cells is primarily related to their substrate. Deposited the hydride material into the through holes in the alumina results in a substrate that is to some extent rough and un-even. In addition, while the adhesion of the gold current collector layer to the alumina is good, its adhesion to the hydride material is considerably weaker. These factors result in much lower fabrication yields – the roughness/un-evenness of the substrate is magnified as each subsequent layer is deposited, and failures due to delamination are also more likely.



## **Task 4: Search for Insertion Opportunities and Development Partners**

### Approach

In this task, CWRU will specifically look for opportunities throughout the DoD where devices can benefit from integrating a microfabricated fuel cell or used as power delivery devices in a stand-alone configuration. CWRU expects that this task will involve a design component with perhaps some modeling based on laboratory data acquired from prototypes. We will also work to establish relationships with commercial manufacturers and venture capital firms interested in this technology.

### Status

In the past six months we have reached a collaboration agreement with The Ashlawn Group, LLC, of Alexandria, VA to develop this technology to provide power for 'smart' munitions. Ashlawn has considerable experience working in the munitions area for the US Army. The agreement covers development of printed fuel cell technology for munitions using CWRU technology developed under this effort. Our goal is to replace the thermal batteries currently used in 'smart' munitions. Ashlawn will develop the hydrogen storage and packaging for the microfabricated fuel cell consistent with requirements for munitions, i.e., 10 year shelf life, in

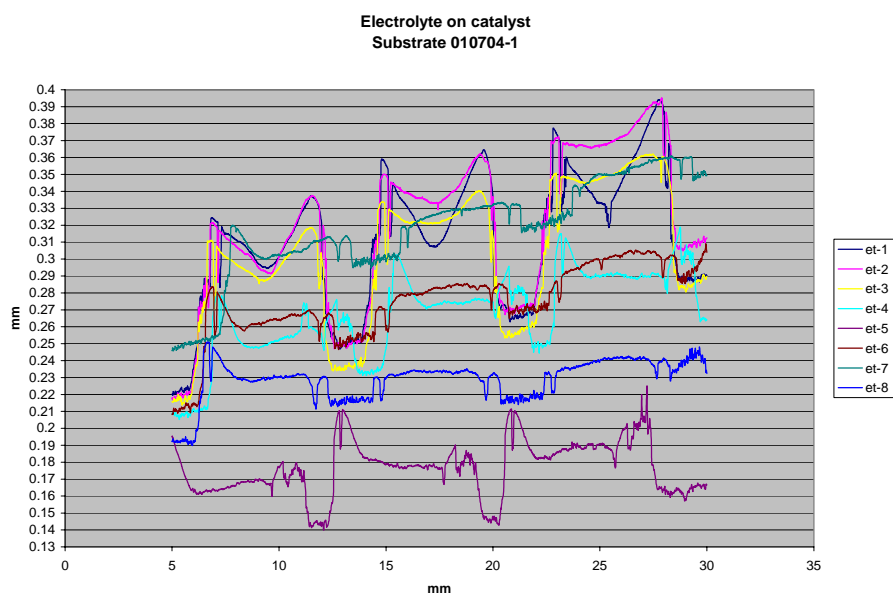


**Figure 3.7** Profilometry results for electrolyte layers deposited from 13 and 24 wt% Nafion solutions onto catalyst layers deposited on smooth gold on alumina substrates.

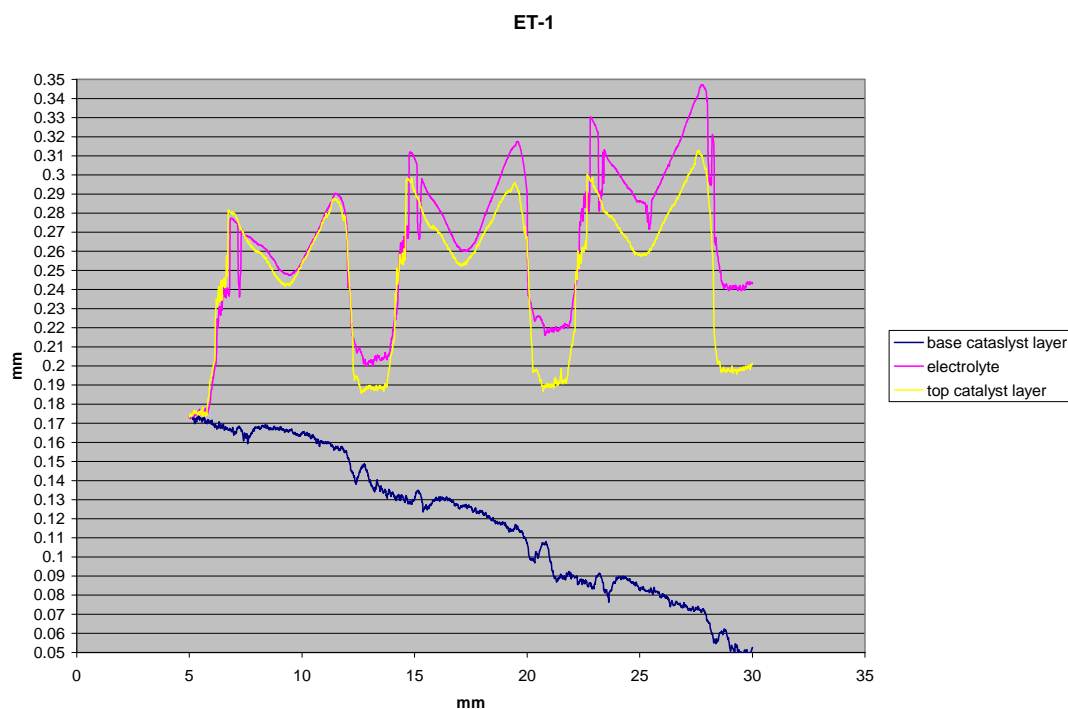


**Figure 3.8** Summary of profilometry results for process ET-1. After printed of first catalyst layer, after printing electrolyte, and after printing of the upper catalyst layer.

#### **Task 4: Search for Insertion Opportunities and Development Partners**

##### Approach

In this task, CWRU will specifically look for opportunities throughout the DoD where devices can benefit from integrating a microfabricated fuel cell or used as power delivery devices in a stand-alone configuration. CWRU expects that this task will involve a design component with perhaps some modeling based on laboratory data acquired from prototypes. We will also work to establish relationships with commercial manufacturers and venture capital firms interested in this technology.

##### Status

We have continued to meet with companies and venture capital firms interested in the commercialization possibilities arising from this program.

## APPENDIX B

### SUMMARY OF PROJECT TASKS AND MILESTONES

Tasks and Milestones for 7/97 to 6/00:

- Optimize carbon flowfield/gas distribution ports and anode catalyst (3/98)  
Status: Complete. The need for thick film printed carbon flow fields and for gas distribution ports in the substrate was eliminated by switching to microporous membrane substrates, eliminating several processing steps (4/00). An acceptable anode catalyst ink was developed (12/98).
- Synthesize and characterize novel polymer electrolyte (12/98)  
Status: Complete. A large family (over 30) of candidate electrolytes was synthesized.
- Complete fabrication development and testing of micro fuel cell power unit (6/99)  
Status: Complete. The first operational fuel cells were tested in 3/99.
- Complete development and characterization of hydrogen storage system (6/99)  
Status: Complete. Hydrogen storage systems based on metal hydride (palladium) and sodium borohydride were demonstrated.
- Incorporate novel polymer electrolyte into power unit (10/99)  
Status: Incomplete. Although the novel polymers developed were more conductive than Nafion, their hydrogen permeability and mechanical properties were poor, such that they could not be successfully incorporated into micro fuel cells.
- Demonstrate integrated fuel storage with power unit (6/00)  
Status: Complete. Integrated fuel cells with hydrogen generation from stabilized aqueous solutions of sodium borohydride were fabricated and tested (7/00).

Specific Highlights for the period 7/97-6/00 include:

- It was demonstrated that Nafion films deposited from concentrated solution in ethylene glycol achieved a proton conductivity of over 1 mS/cm at 15%RH and room temperature. This method produces the highest conductivity seen in Nafion under these conditions.
- Validation of the bulky co-monomer hypothesis in polyimides was demonstrated. Incorporation of bulky co-monomers led to polymer films that had exceptional water retention and conductivity at low relative humidities.
- Microfabricated fuel cells were integrated with a self-contained hydrogen supply. The hydrogen was stored in the form of a stabilized aqueous solution of sodium borohydride. Hydrogen was generated from the borohydride solution at room temperature using a Pt catalyst.
- Pulse power levels of over 50 mW/cm<sup>2</sup> were demonstrated for 10 msec pulses for microfabricated cells operating on H<sub>2</sub> and air (50% RH). Extended operation (90 minutes) was demonstrated for repetitive 10 msec pulses with a 10% duty cycle.
- Demonstrated fabrication of series connected cells on a single substrate using patterned current collector and electrolyte layers.

A No-cost Extension for the Period (Jan. - Sept. 2001) was applied for and granted. The tasks and milestones for this period included:

- Task 1. A series of polyimide co-polymers will be synthesized with the general formula:  
NTCDI<sub>(1-x)</sub> MPDIDA<sub>x</sub> DAPS<sub>(1-y)</sub> TFMB<sub>y</sub>, where 0<x<0.1 and 0<y<0.3. Characterization for conductivity, film casting and physical stability will be carried out in parallel with the synthesis effort.

STATUS: Completed. Hydrogen and oxygen permeability studies were not performed as they were replaced by the studies on hydrolytic stability.

Task 2. The polymer with the best blend of properties will be selected and synthesized in 10 g quantities for fuel cell fabrication.

STATUS: Completed. The BTFMB27mP9[7/3+1] polymer was selected and a 25g batch of this material were received for fuel cell fabrication on 8/10/01.

Task 3. Microfabricated fuel cells will be fabricated incorporating the selected polymer.

STATUS: Complete, but poor hydrolytic stability of the polyimide co-polymers resulted in fuel cell failure.

Specific Highlights for the period 1/01 – 8/01 include:

- By modifying the composition of the cathode catalyst, functional fuel cells were fabricated using the polyimide electrolyte for the first time.

A three-year extension of the project was applied for and granted. The specific goals for this additional work included:

- Increase power density at 50%RH to  $>10 \text{ mW/cm}^2$ .
- Increase energy density using metal hydride storage to  $>500 \text{ mWh/cm}^3$  for an integrated device with 50 mWh capacity.
- Improve fabrication so that stacks of at least six cells in series can be fabricated completely by automated methods.
- Identify insertion opportunities

Tasks and Milestones for 10/01 TO 9/04:

Task 1: Fabrication Enhancements for Improved Reactant Accessibility

1a) Develop sacrificial material/process suitable for non cross-linked electrolytes.

STATUS: COMPLETE

1b) Expand micro fuel cell fabrication to incorporate sacrificial material/process and demonstrate improved power density.

STATUS: COMPLETE, An improved power density has been shown with an alternate process using metal hydride in place of the sacrificial layer.

Task 2: Metal Hydride Fuel Storage

2a) Define baseline performance of  $\text{AB}_5$  based system; energy density, maximum charge/discharge rates, effects of cycling

STATUS: COMPLETE

2b) Demonstrate  $\text{AB}_5$  based hydrogen storage system integrated with microfabricated fuel cell with superior energy density.

STATUS: COMPLETE, energy density of hydride ink:  $1200 - 1800 \text{ mAh/cm}^3$ . Electrochemical charging of hydride incorporated with microfuel demonstrated.

Task 3: Electrolyte Deposition Enhancement

3a) Develop improved procedure for thick film printing of Nafion electrolyte films.

STATUS: COMPLETE

3b) Specify requirements for, identify, and purchase a commercial automated dispensing system capable of depositing polymer electrolytes from solution.

STATUS: COMPLETE

3c) Incorporate improved electrolyte deposition procedure into microfuel cell fabrication process and demonstrate automated production of multi-cell devices.

STATUS: COMPLETE. Fabrication of three cell series stacks demonstrated using both the thick film and microdroplet dispensing tools.

Task 4: Search for Insertion Opportunities

In this task, CWRU will specifically look for opportunities throughout the DoD where devices can benefit from integrating a microfabricated fuel cell or used as power delivery devices in a stand alone configuration.

STATUS: COMPLETE. A collaboration agreement to develop this technology for applications in 'smart' munitions has been reached with The Ashlawn Group, LLC.

Specific highlights for the period 10/01 to 9/04 include:

- An agreement of collaboration with The Ashlawn Group, LLC, of Alexandria, VA to develop this technology to provide power for 'smart' munitions. Ashlawn has considerable experience working in the munitions area for the US Army. The agreement covers development of printed fuel cell technology for munitions using CWRU technology developed under this effort. Our goal is to replace the thermal batteries currently used in 'smart' munitions. Ashlawn will develop the hydrogen storage and packaging for the microfabricated fuel cell consistent with requirements for munitions, i.e., 10 year shelf life, instantaneous activation, and able to withstand high G accelerations.
- $\text{LaAl}_{0.3}\text{Ni}_{4.7}$  hydride material with an additional surface modification was formulated into a thick film printable ink with very low binder content. Long term testing of our modified metal hydride materials for hydrogen storage confirms that the modification process yields active materials even when exposed to humid hydrogen over thousands of sorption/desorption cycles. The energy density of the hydride as a printable ink was 1200 - 1800 mAh/cm<sup>3</sup>.
- A modified solvent system for the Nafion polymer electrolyte has been developed that greatly improves the quality of thick film printed electrolyte films. Films with considerably sharper edges/side walls can now be deposited. This should greatly increase the device density on a substrate.
- The power density of the microfabricated fuel cells was increased to 7 mW/cm<sup>2</sup> at 50% RH and 0.5V

## Appendix C: Microfabricated fuel cells

J.S. Wainright<sup>a,c</sup>, R.F. Savinell<sup>a,c,\*</sup>, C.C. Liu<sup>a,d</sup>, M. Litt<sup>b,c</sup>

<sup>a</sup> Department of Chemical Engineering, Case Western Reserve University, Cleveland OH 44106-7217, USA

<sup>b</sup> Department of Macromolecular Science, Case Western Reserve University, Cleveland OH 44106-7217, USA

<sup>c</sup> Yeager Center for Electrochemical Sciences, Case Western Reserve University, Cleveland OH 44106-7217, USA

<sup>d</sup> Electronics Design Center, Case Western Reserve University, Cleveland OH 44106-7217, USA

Received 28 January 2003; received in revised form 11 April 2003; accepted 13 April 2003

---

### Abstract

This paper reports design, materials, and testing of microfabricated fuel cells that can be applied for small power generation. Multiple co-planar fuel cells in series have been built onto ceramic substrates (as well as silicon and polymer, but not reported here) using thick-film fabrication techniques. Testing of these fuel cells gave power densities in the milliwatt (per square centimeter) range for continuous power and tens of milliwatts under pulsing conditions, and have indicated performance limiters and opportunities for higher power densities. These fuel cells are intended to operate on ambient-supplied air, and thus the polymer electrolytes must be capable of operating under a range of humidity conditions. The target conductivity for these low power devices is  $> 1 \text{ mS cm}^{-1}$  at 15% RH. Although novel polymer electrolytes are being pursued at CWRU for this application, we report here Nafion<sup>®</sup> films cast from alternate solvents that have adequate conductivity for this application. Several on-board fuel storage approaches are being pursued. We have demonstrated high fuel utilization by a fuel cell operating with on-board source of hydrogen from aqueous sodium borohydride, as well from solid metal hydride systems.

© 2003 Elsevier Ltd. All rights reserved.

**Keywords:** PEM; Nafion<sup>®</sup>; Micropower; Hydrogen storage; Hydride

---

### 1. Introduction

Efficient small-scale power generation is critical to realizing the full benefit of many portable electronic devices. Wireless electronic devices, e.g. micro sensors and micro electromechanical or microfluidic systems, require electrical power for operation and data transmission. The availability of on-board power with appropriate sized power and energy capabilities, coupled with wireless data transmission, will open numerous possibilities for self-sustaining devices for remote or difficult to access locations. The power and energy needs for small portable devices may vary considerably depending on their design and function. Small microfabricated fuel cells open the door for energy delivery devices with independent sizing of power and energy capacity, while having the capability to

supply short pulses of peak power without significant adverse effect on energy utilization. Finally, such fuel cells have the potential for energy densities significantly greater than present and predicted battery technology.

Small fuel cells with various degrees of microfabrication have been reported in the literature. Thin film techniques were used to create flowfields [1–3], some with current collectors and catalyst layers [4–8] on a silicon substrate that were attached to a free-standing Nafion<sup>®</sup> film. Morse et al. [9] did not use a free-standing film, but instead spin-cast a membrane on the micro-fabricated support components. Individual fuel cell sizes were from 2 to 10 mm on a side, and down to 15  $\mu\text{m}$  on a side. Temperatures above room temperature during testing were maintained by an oven and fuel (hydrogen or methanol) was supplied from an external source.

This paper presents concepts and results arising from a program to develop a small and completely micro-fabricated polymer-based fuel cell with on-board hydrogen storage. The approach is to co-fabricate a sensor or sensor suite with sufficient analog/digital circuitry for

signal conditioning/processing, wireless communications capability (low-power RF) and a power source on a single wafer. The anticipated power requirements are for extended periods of very low (sub-milliwatt) power draws to power the sensor, with random or periodic pulses of 10–100 of milliwatts required for signal processing or data transmission. Potential operational lifetimes are from hours to days (surveillance at a particular location) to years (machinery monitoring). Development of a microfabricated power source is an enabling technology for the autonomous sensor concept. It is envisioned that this device would operate in a passive mode, without active control of temperature, humidity, reactant pressure or flow rate. This greatly simplifies the construction and operation of the fuel cell. The power density achievable in passive operation will naturally be less than that obtained in conventional fuel cells. However, the applications envisioned do not require high power densities.

## 2. Design principles and fabrication issues

The CWRU microfabricated fuel cell is being developed by using the following guiding principles:

- completely passive device-no fans, pumps, compressors to move reactants
- ambient temperature operation-no cooling or heating
- hydrogen fueled at near atmospheric pressure
- no external humidification-operation at ambient relative humidity
- fabrication process compatible with silicon-based microelectronics

The basic design of the fuel cell consists of a planar array of edge collected cells, such that all of the cathodes are exposed to the ambient air, while beneath all of the anodes is a common fuel manifold. Each of the components of the cells; current collectors, gas diffusion layers, catalyst layers, and electrolyte, is deposited in turn using thick film printing techniques. The hydrogen storage/generation capability is similarly fabricated in a second substrate, and bonding the two substrates together creates the final device. A schematic of the final device is shown in Fig. 1 and a photograph is shown in Fig. 2. This fabrication process is considerably different from the conventional PEM fuel cell stack construction in which individual components (electrolyte membranes, gas diffusion layers, bipolar plates, gaskets, endplates, etc) are separately manufactured, and then assembled into the stack. The following two sections will focus on the particular fabrication issues that have been addressed for the current collectors and the polymer electrolyte.

### 2.1. Current collectors/gas diffusion layers

In order to minimize the number of fabrication steps, the gas diffusion layer (GDL) in the microfabricated fuel cell is also used as the current collector. Typical gas diffusion layers for conventional PEM fuel cells such as carbon cloth or carbon paper have a thickness on the order of 300  $\mu\text{m}$ , porosities on the order of 80%, and conductivities on the order of 50–100  $\text{S cm}^{-1}$ . The relatively low conductivity is sufficient given that they are used in conjunction with ribbed flow fields with feature sizes on the order of 1 mm. However, for an edge-collected device, the conductivity required is considerably greater. In addition, with the thick film process, a thickness of 10–50  $\mu\text{m}$  is more realistic, while 300  $\mu\text{m}$  is very difficult to achieve.

The voltage drop along the current collector is given by

$$\Delta\phi_{\text{ir}} = (L^2/2)(i_{\text{avg}}/t\sigma)$$

where  $L$  is the length of the electrode perpendicular from the current-collector edge,  $i_{\text{avg}}$  is the average current density normal to the surface and assumed to be uniform,  $t$  is the thickness of the current collector and  $\sigma$  is the conductivity of the current collector.

Assuming that a maximum voltage drop of 10 mV over a 1-cm long current collector is desired for a fuel cell current density of 50  $\text{mA cm}^{-2}$ , a 25  $\mu\text{m}$  thick film needs to have a conductivity of 1000  $\text{S cm}^{-1}$ . Since the current collector must also be highly porous in order to act as a gas diffusion layer, it is clear that carbon-based materials are not ideally suitable for this component. Instead, metallic conductors are preferred. Our experience with attempting to thick film print current collector/GDLs based on metallic conductors has been that the difficulty lies in achieving sufficient porosity. In Fig. 3, fuel cell polarization curves are shown for two cells, one having a 30  $\mu\text{m}$  thick printed current collector/GDL, the other with a 50  $\mu\text{m}$  thick film of the same porous material. In both cases there is an appreciable loss due to diffusion of the reactants through the current collector/GDL layer, and the loss is considerably greater with the thicker film.

Additional gas permeation resistance can be expected through the substrate that supports the current collector. In practice, the inks are not printed directly onto the substrate because the pores are too large, and the ink from printing the current collector will fill the pores, thus increasing the gas permeation resistance substantially. For the fuel cells tested here, a thin porous nylon film (MAGNA nylon, pore diameter of .45  $\mu\text{m}$ , Osmonics Inc.) was secured onto a substrate and then non-porous insulating boundaries and current collectors were printed. The other fuel cell layers were then sequentially printed. The completed fuel cell with nylon



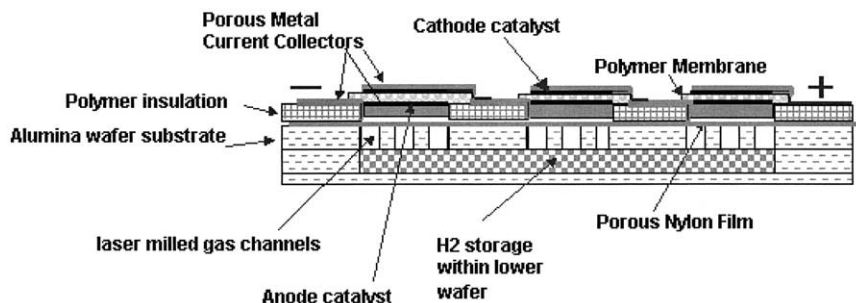


Fig. 1. Schematic cross-sectional view of microfabricated fuel cell with fuel storage. Three series connected cells are shown. Drawing not to scale.

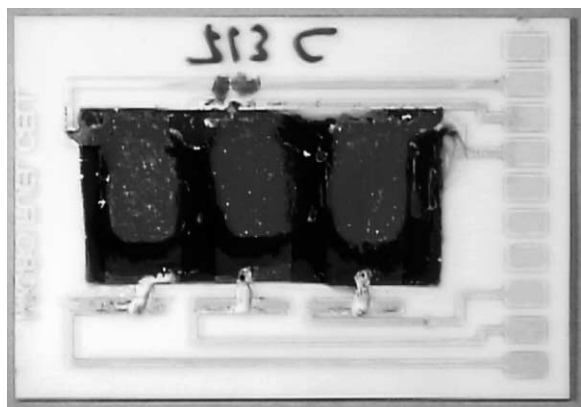


Fig. 2. A photograph of a three cells fabricated onto an alumina wafer with printed current leads that allow cells to be connected in parallel or in series.

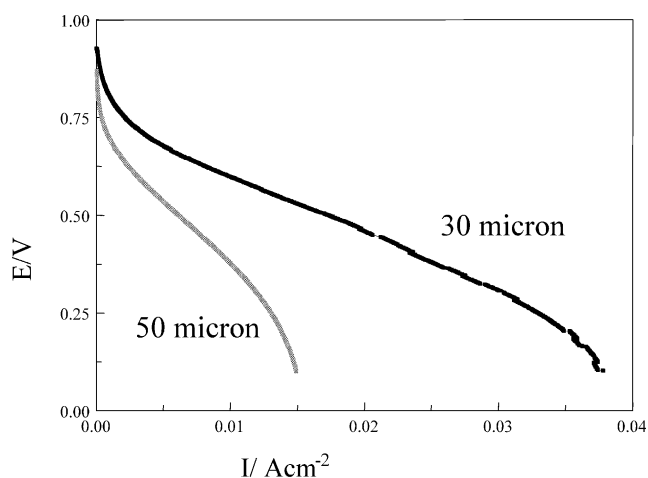


Fig. 3. Air breathing fuel cell polarization curves for two different thickness of a printed gold current collector/gas diffusion layer.

backing was then attached to a ceramic wafer with slots for gas access to the anode. The hydrogen gas then passed through the slots and the porous nylon film to reach the anode surface for oxidation. The observed limiting currents with this cell design were 10–30 mA cm<sup>-2</sup> with one atmosphere hydrogen gas feed.

## 2.2. Electrolyte issues

There are a number of electrolyte issues that must be considered. Like other macro PEM fuel cells, the electrolyte must be proton conducting, have a favorable environment for electrode reaction kinetics, and must permit gas access to the polymer-catalyst interface so reaction can occur. In a small microfabricated fuel cell, since the current density will be low under ambient air operation, the conductivity only needs to exceed approximately 1 mS cm<sup>-1</sup> (125 mV IR loss at 50 mA cm<sup>-2</sup> with a 25 μm film). However, this conductivity level must be achievable even at low relative humidities since gas hydration is not feasible in a small passive device. We have established as a working target a conductivity greater than 1mS/cm over the relative humidity range of 15 < RH < 100%.

A typical 5% Nafion®–alcohol solution has too low of a viscosity to print a well-defined film. In addition it has low proton conductivity at low relative humidities as shown in Fig. 4. We modify the commercially available Nafion®–alcohol solution by adding higher boiling

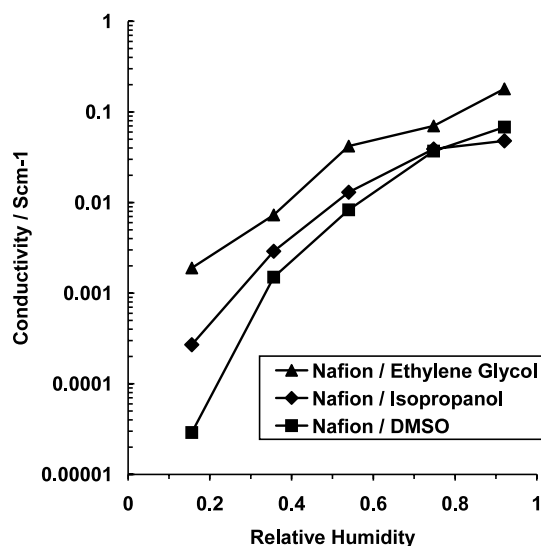


Fig. 4. Conductivity of Nafion® films cast from three different solvents: ethylene glycol, isopropanol, and DMSO. The films were cast, then the solvent subsequently removed in vacuum at 80 °C.

solvents, then concentrating the Nafion<sup>®</sup> solute. Films were cast and the solvent was evaporated under vacuum at about 80 °C. The conductivity of films cast from DMSO and ethylene glycol (EG) are shown in Fig. 4, and the Nafion<sup>®</sup>/EG film meets our conductivity goals. These films were ca. 25  $\mu\text{m}$  thick and were cast from 10 to 15 wt.% solutions, with the majority of the solvent being the higher boiling component.

Another issue is to deposit electrolyte precisely where it is needed. This is necessary to achieve densely packed cells that make the most use of the available area on the substrate and minimize the length of the current collectors. In addition to minimizing current collector lengths, printing patterned electrolyte layers for each cell, as opposed to having several cells sharing a continuous film of electrolyte, eliminates any shunt currents that may otherwise occur in series connected cells.

In Fig. 5a and b are two examples of thick film printing of the modified Nafion<sup>®</sup> solution. The solution used to produce Fig. 5a is clearly superior, the electrolyte films are well-defined, and can be closely spaced. The result shown in Fig. 5b is not acceptable, the

electrolyte film spreads beyond the desired area when printed, and adjacent cells must be further apart. In addition, the film thickness in Fig. 5a is  $\approx 90\ \mu\text{m}$  and uniform across the area of the cell, while in Fig. 5b, the film thickness varies between 5 and 15  $\mu\text{m}$ . While thinner electrolyte films may be preferred to minimize resistive losses, films less than 25  $\mu\text{m}$  thick can lead to excessive hydrogen crossover, particularly for air-breathing devices such as these where operating current densities are low as compared to pressurized macro-size fuel cells. The solution used to cast the film in Fig. 5a consisted of about 40 mg of Nafion<sup>®</sup> and 60 mg of EG with all the alcohol and water of the original 5% Nafion<sup>®</sup>/alcohol solution removed. The solution used to cast Fig. 5b was similar, but without all of the alcohol and water removed. It was of lower viscosity and Nafion<sup>®</sup> density. The actual properties (gel content, viscosity, etc) of the casting solution varied somewhat depending on the processing procedure.

A calculation that estimates the effect of a Nafion<sup>®</sup> 1100 membrane thickness on cross-over is given in Fig. 6. The cross-over rate is also reflected in a lowering of the open circuit potential because of the mixed electrode reaction (hydrogen oxidation coupled with oxygen reduction) at the cathode. These calculations are based on kinetic parameters taken from experimental data of typical conventional PEM fuel cells operated in our laboratories. The drop in OCV as the membrane becomes thinner will be a strong function of the actual catalyst loading. However, as shown, for a water saturated Nafion<sup>®</sup> 1100 film, the cross-over rate increases appreciably for films thinner than 25  $\mu\text{m}$ .

While the Nafion<sup>®</sup>/EG system appears adequate for microfuel cell applications, it still has its limitations. For example, the conductivity at low RH, although acceptable for low current density operation, will limit pulse power capability. Also, these films will swell excessively at 100% RH and the film will delaminate from the substrate thus resulting in failure. Other electrolyte systems are under development in our laboratories, and progress on these approaches are reported elsewhere [10,11].

### 3. Fuel cell performance

The performance of representative microfabricated fuel cells are shown in Fig. 7. These fuel cells are all microfabricated by thick film deposition. The current collection/flowfields are 15  $\mu\text{m}$  thick gold printed using an Ercon ink. The electrodes were printed from a slurry of particles of C/Pt (40 wt.% Pt on XC-72 from Etek Inc.). It was necessary to have thin electrodes (2–5  $\mu\text{m}$ ) to avoid mud-cracking upon drying. The catalyst loading therefore was only 0.2 mg  $\text{cm}^{-2}$  for both electrodes. The Nafion<sup>®</sup> was cast from a Nafion<sup>®</sup>/EG

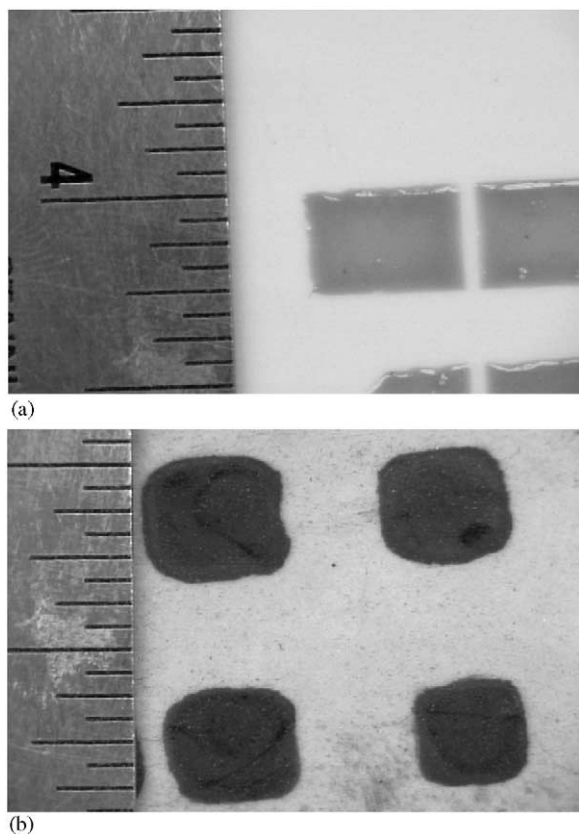


Fig. 5. (A) and (B) Two examples of thick film printing of Nafion<sup>®</sup> electrolyte films on alumina substrates. In (b) the black line squares represents the desired film area as defined by the mask used for printing and the overprinting of the film deposit is clearly present. In (a) the deposit is the same area as the mask. The smallest division on the ruler shown in the figures is 1/16" (0.16 cm).

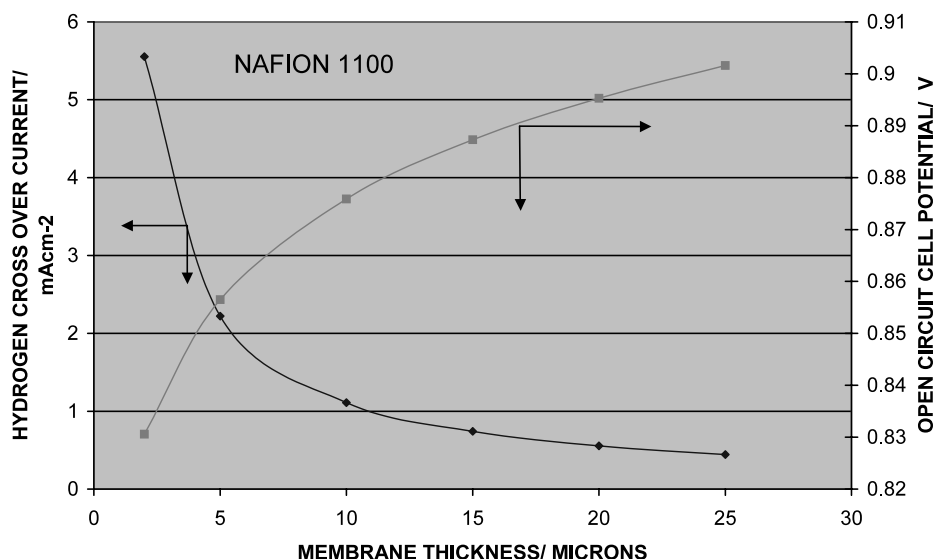


Fig. 6. Calculations that estimate the rate of hydrogen cross-over for a Nafion® 1100 film and that estimate its effect on the open circuit potential based on experimental polarization curves from macro-sized PEM fuel cells. The calculation were based on first calculating the hydrogen cross-over current. A hydrogen permeability of  $5.76 \times 10^{-12}$  was used (e.g. a 10  $\mu\text{m}$  thick film with one atmosphere hydrogen pressure differential yielded a 1.1  $\text{mA cm}^{-2}$  crossover current) This crossover current was then used in the cathode potential expression (based on experimental data) to arrive at the cathode potential under the condition of open circuit with only hydrogen crossover consuming the oxygen. Of course, the cathode potential expression will be strongly related to the platinum catalyst loading and utilization.

solution. The porous substrate was a nylon porous film. The fuel cell was operated in air at 42% RH at 24 °C with humidified hydrogen. The power output at 0.5 V/cell was 2  $\text{mW cm}^{-2}$  continuous, 5  $\text{mW cm}^{-2}$  for 180–300 s durations, and 50  $\text{mW cm}^{-2}$  under a 10 ms pulse. Although long term testing was not carried out, there was no noticeable decay in performance over a 20-h period. Also shown for comparison is the polarization curve from a fuel cell fabricated by applying the inks onto a free-standing Nafion® film. The limiting current

of this polarization curve is due to the diffusion of oxygen through the porous metal current collector.

The pulse capability of this fuel cell is shown in Fig. 8. In this case the air R.H. was at 48%. The duty cycle was 90% at 0.5  $\text{mA cm}^{-2}$  and 10% at a higher current. The pulse width was 10 ms. When the pulse current was 50  $\text{mA cm}^{-2}$  the voltage stayed above 0.5 V for over 600 s of cycling. After about 600 s, the voltage did not recover adequately after each pulse and consequently dropped below 0.5 V after about 600 s. The time to reach the 0.5

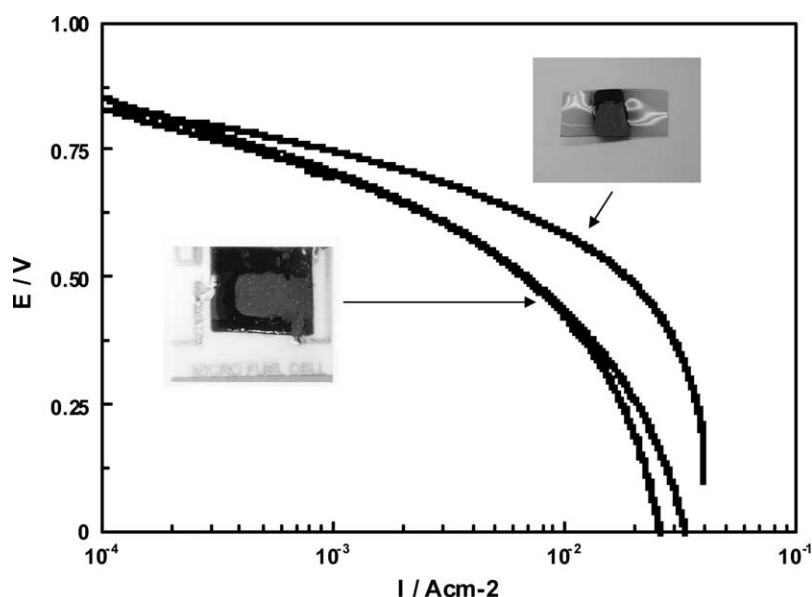


Fig. 7. Polarization curves for two independent micro fabricated fuel cells. Also shown is a polarization curve of a fuel cell fabricated by applying the inks used for the microfabricated fuel cells onto a free-standing Nafion® film.

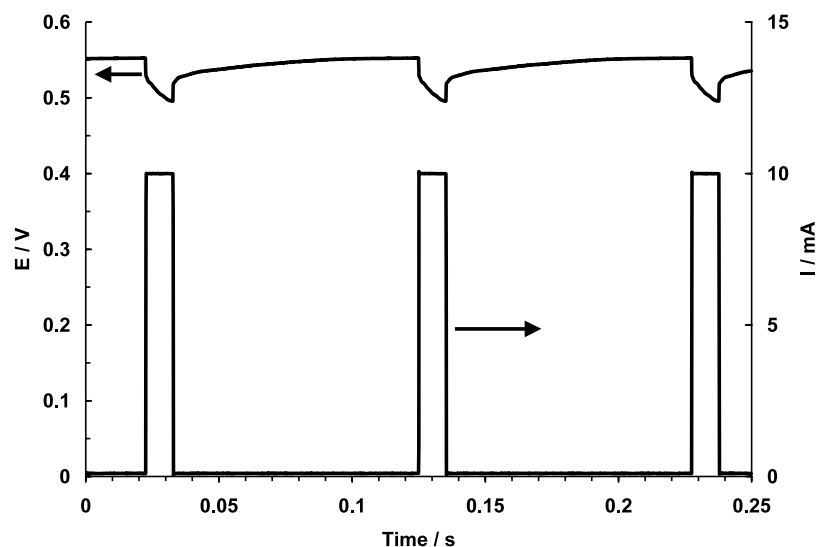


Fig. 8. Example of continuous pulse response of 0.25 cm<sup>2</sup> micro fuel cell. Duty cycle: 10% at 25 mA cm<sup>-2</sup>.

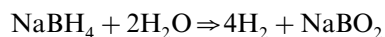
V cut-off was 5400 s for a 25 mA cm<sup>-2</sup> pulse. There was no permanent voltage loss after 50,000 pulses at pulse currents below 25 mA cm<sup>-2</sup>. The cell capacitance was estimated to be 13.5 mF cm<sup>-2</sup>.

The pulse capability will depend strongly on the internal resistance of the cell, which is directly related to the relative humidity. Below 40% RH, the pulse capability is significantly decreased while at over 80% RH, the pulse power capability can double.

#### 4. Hydrogen storage and generation

##### 4.1. Hydrogen generation via decomposition of sodium borohydride solutions

As described, the goal for these microfabricated fuel cells is passive, ambient temperature operation. Hydrogen storage in the form of stabilized aqueous solutions of sodium borohydride (NaBH<sub>4</sub>) is one option that meets these criteria. When sufficient base is added to raise the solution pH to  $\approx 14$ , these solutions are stable at room temperature for several months. However, when brought in contact with a suitable catalyst, they readily decompose according to the reaction:



Sodium borohydride is readily soluble in water, and solutions of over 30 wt.% NaBH<sub>4</sub> can be made at room temperature. For a 30 wt.% solution, stabilized with 10 wt.% NaOH, the following theoretical energy densities can be calculated: 2337 mW h cm<sup>-3</sup> ( $8.41 \times 10^9$  J M<sup>-3</sup>) and 2091 mW h g<sup>-1</sup> (7528 J g<sup>-1</sup>). This is equivalent to  $\approx 7$  wt.% H<sub>2</sub>. The borohydride system also offers distinct advantages compared to the metal hydride systems discussed below. The primary advantage is

that the concentrated solution maintains roughly 35% RH at the fuel cell anode, thus providing a continual source of water vapor to the fuel cell. This has a very distinct benefit in maintaining higher electrolyte conductivity, which is especially important for pulse power delivery.

The simplest design for a hydrogen generator for the microfuel cell consists of a small well (i.e. an opened chamber) etched into a wafer to contain the borohydride solution, which is injected into the well with a syringe when the fuel cell is activated. The decomposition catalyst is printed onto the bottom of the well. The well is capped with the microfuel cell, with the underside of the microfuel cell substrate exposed to the hydrogen that bubbles up from the catalyst at the bottom of the well. A relatively long and small diameter vent through side of the well, above the solution level, allows air to be exhausted when the borohydride solution is injected, and maintains the hydrogen pressure at slightly above ambient, regardless of the relative rates of hydrogen generation by the decomposition reaction and hydrogen consumption by the fuel cell.

Varying the depth of the well for the borohydride solution allows the amount of energy stored to be varied. The obvious drawback of this system is that it is orientation dependent, the fuel cell must be held in an orientation that permits the borohydride solution to contact the decomposition catalyst and that only allows hydrogen and water vapor to be vented to the anode. We are currently working on more advanced designs that would be orientation independent and would incorporate a check valve on the hydrogen vent while remaining completely passive and still be readily manufactured.

A borohydride generator of the simple type was fabricated with a solution volume of 0.6 cm<sup>3</sup>. A

microfabricated fuel cell bonded to the generator was continually operated at 0.5 V for over 90 h on one charge of borohydride solution. (Polarization curves with the attached hydrogen generator were essentially the same as those generated from hydrogen supplied by a tank.) Over this period, the current produced was monitored and integrated. The integrated current produced of 1822 coulombs was over 67% of the theoretical value for complete decomposition of 0.6 cm<sup>3</sup> of the 20 wt.% NaBH<sub>4</sub> solution used. The fuel cell was still operating at the end of the 90-h period; however, the power output had dropped to about 25% of the initial value. Considering that the generator is not sealed, but vents excess hydrogen through a small opening, the fuel utilization achieved in this experiment is very promising. Higher utilizations can be achieved by operating the fuel cell at constant current.

#### 4.2. Hydrogen storage in metal hydrides

The advantages of storing hydrogen in metal hydrides include a high volumetric energy density with no operational dependency on orientation. A major goal of this effort was to produce a metal hydride material that is tailored to this micro fuel cell application, with an equilibrium pressure near atmospheric pressure at room temperature, and that can be applied in a thick film fabrication process. Integrated devices with energy densities on the order of 500 mW h cm<sup>-3</sup> ( $1.8 \times 10^9$  J M<sup>-3</sup>) for a 50 mW h (180 J) storage capacity should be feasible using this approach.

LaAl<sub>0.3</sub>Ni<sub>4.7</sub> hydride material with an additional surface modification has been formulated into a thick film printable ink with very low binder content. A second member of the AB<sub>5</sub> family of hydrides, CaNi<sub>5</sub>, has also been evaluated. For both hydrides, the binder content

was on the order of 1 wt.%, allowing for high volumetric energy density. The surface modification prevents deactivation of the hydride material. Printed inks remained active after over 5 weeks exposure to room air, at which time the tests were stopped. This is an important result because often these materials passivate on exposure to air or water, and can only be re-activated for hydrogen storage by exposure to high hydrogen pressures. As it is impossible to expose material contained within the fuel cell structure to high hydrogen pressures, a non-passivating hydride material is required.

It is also important to show that the hydride material can be repeatedly charged with hydrogen and discharged without loss of capacity. An automated Sievert's apparatus was used for hydrogen sorption/desorption testing of up to six samples simultaneously. Various hydride powders and inks have been subjected to repetitive sorption/desorption testing consisting of 10 minute exposure to  $\approx 133$  kPa (1000 torr) H<sub>2</sub> (sorption step) followed by 600 s exposure to vacuum (desorption, pressure = 1.3 Pa (10 millitorr)). SEM micrographs after 1000 cycles showed no change in particle size, and no change in the adhesion of the ink to the substrate. These tests have been extended to over 4000 cycles without any significant change in the total amount of hydrogen stored, or in the rate at which hydrogen is adsorbed or desorbed. Over the same period, the ink based on the CaNi<sub>5</sub> hydride has lost  $\approx 15\%$  of its original hydrogen storage capacity.

Printed films of the LaAl<sub>0.3</sub>Ni<sub>4.7</sub> ink have been used to provide hydrogen to small, conventionally fabricated fuel cells. In the first experiment, a constant 20 mA current was drawn from the fuel cell, while the cell potential and the hydrogen pressure above the hydride block were monitored, as shown in Fig. 9. Despite the fact that in this experiment, the fuel cell and the hydride

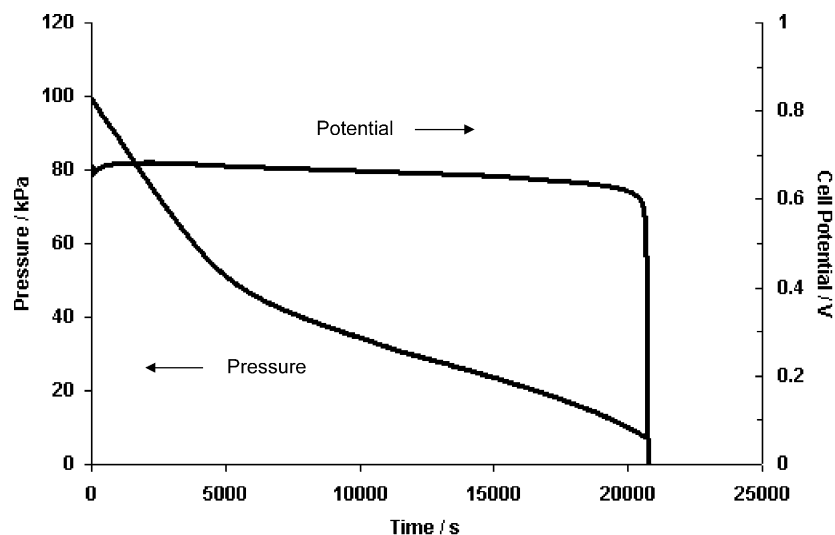


Fig. 9. Small conventional fuel cell potential and pressure above hydride (LaAl<sub>0.3</sub>Ni<sub>4.7</sub>) storage block while maintaining 20 mA current output. The fuel cell is based on a Nafion<sup>®</sup> 117 film, with Pt/C printed electrodes of one square centimeter.

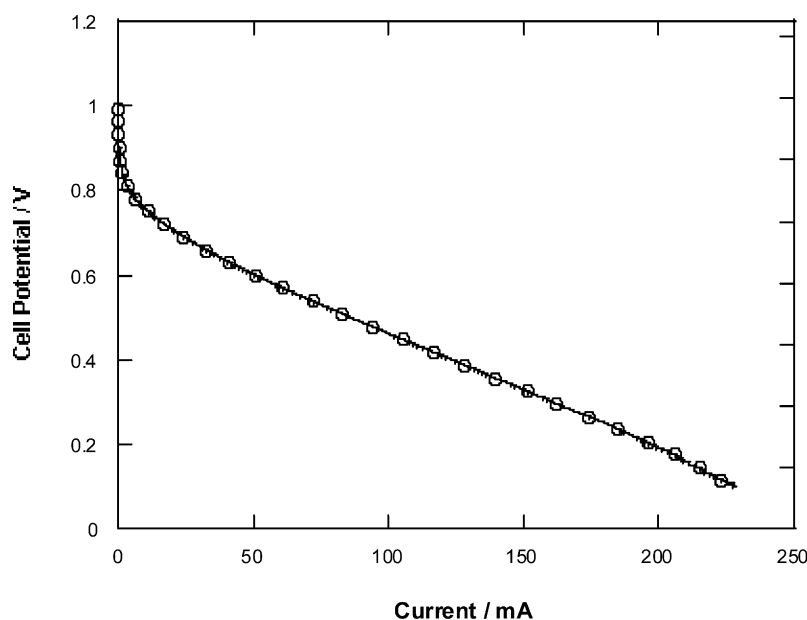


Fig. 10. Polarization curve of the fuel cell described in Fig. 8 coupled to hydride ( $\text{LaAl}_{0.3}\text{Ni}_{4.7}$ ) storage block.

block were connected by  $\approx 5$  cm of 0.32 cm OD tubing, the fuel cell maintained a constant potential until the pressure dropped to  $\approx 8$  kPa (60 torr). The hydrogen consumed during this test represented over 90% of the hydrogen initially stored in the hydride material. With the extremely close coupling of fuel cell and hydride material that will occur in the microfabricated devices, even higher utilizations should be possible. It also is important to note that the potential was essentially constant until the very end of the test; the sloping equilibrium pressure of this hydride material was not reflected in a varying fuel cell performance under these conditions. In Fig. 10, a complete polarization curve for the fuel cell is shown. A current output of over 200 mA was achieved without reaching a limiting current, indicating that the hydrogen desorption rates from this hydride ink are more than sufficient for the microfabricated fuel cell, which is expected to operate at currents on the order of 10 mA.

## 5. Summary

Aspects of the design, materials and fabrication of a microfabricated fuel cell have been presented. An estimate of the performance of these devices is summarized in Table 1, with a comparison to a Li-MnO<sub>2</sub> primary battery of similar voltage, size and energy storage. The interesting advantages of the microfabricated fuel cell as compared to the battery lie in the ability to fabricate the fuel cell on the same substrate as other microelectronic, microelectromechanical or microfluidic devices, in the ability to independently tailor the

design for a desired power and energy storage combination and in the ability to provide peak power.

## Acknowledgements

This report is based on research sponsored by DARPA under agreement no. F30602-97-2-0311. The US Government is authorized to reproduce and distribute reprints for Governmental purposes notwithstanding any copyright notation thereon. The views and conclusions contained herein are those of the authors and should not be interpreted as necessarily representing the official policies or endorsements, either expressed or

Table 1  
Comparison of microfabricated fuel cells and a Li-MnO<sub>2</sub> coin cell

	Micro fuel cell <sup>a</sup>	Li-MnO <sub>2</sub> coin cell Duracell 2016
Nominal voltage	3V	3 V
No. of cells	6	1
Weight	1.7 g	1.8 g
Dimensions	2.7 × 1.8 × 0.2 cm	2 cm dia., 0.2 cm thick
Capacity	60 mA h/cell (216 J/cell)	75 mA h (0.2 mA rate) (270 J) 60 mA h (1 mA rate) (216 J)
Energy	200–300 mW h (720–1080 J)	200 mW h (720 J)
Maximum continuous power	3–15 mW (depends on %RH)	6 mW
Peak power (10 ms pulse)	50–100 mW (depends on %RH)	30 mW

<sup>a</sup> Values for micro fuel cell based on single cell and three cell structures scaled to yield a 3 V device.

implied of DARPA, or the US Government. This work summarizes the combined efforts of a number of students, engineers and postdoctoral researchers over the past 5 years. In particular the authors would like to acknowledge the efforts of Ms. Laurie Dudik, Dr. Arunkumar Venkatesan, John Staser, Andrew Swann, Ms. Lynn Chen, Hyoungh-Juhn Kim, Dr. Snezana Gojkovic, Ms. Liangyuan Chen, Xi Shan and Kenneth Yee, and Professor Joe Payes.

## References

- [1] (a) S.J. Lee, S.W. Cha, Y.C. Liu, R. O'Hayre, F.B. Prinz, in *Micro-Power Sources*, H.Z. Massoud, I. Baumvol, M. Hirose, E.H. Poindexter, Editors, PV200-3, The Electrochemical Society Proceeding Series, Pennington, NJ, (2000).; (b) S.J. Lee, S.W. Cha, A. Chang-Chien, R. O'Hayre, F.B. Prinz, "Factorial Design Study of Miniature Fuel Cells with Micro-machined Silicon Flow Structures", ECS abstract no. 452, San Francisco Meeting, September 2001.
- [2] A. Chang-Chien, S.W. Cha, S.J. Lee, R. O'Hayre, F.B. Prinz, "Planar Interconnections of Multiple Polymer Electrolyte Membrane Fuel Cells by Microfabrication", ECS abstract no. 453, San Francisco meeting, September 2001.
- [3] S.J. Lee, S.W. Cha, Y. Liu, R. O'Hayre, A. Chang-Chien, F.B. Prinz, "Minature Fuel Cells with Non-Planar Interface by Microfabrication", ECS abstract no. 241, Phoenix meeting, October 2000.
- [4] S.C. Kelley, G.A. Deluga, W.H. Smyrl, *AIChE J.* 48 (2002) 1071.
- [5] S.C. Kelley, G.A. Deluga, W.H. Smyrl, *Electrochem. Solid-State Lett.* 3 (2000) 407.
- [6] J.P. Meyers, H.L. Maynard, *J. Power Sources* 109 (2002) 76.
- [7] H. Maynard, J. Meyers, A. Glebov, "Silicon Tunnels for Reactant Distribution in Miniaturized Fuel Cells", ECS abstract no. 60, Toronto Meeting, May 2001.
- [8] J. Meyers, H. Maynard, "Design of Miniaturized Fuel Cells for Portable Power", ECS abstract no. 64, Toronto Meeting, May 2001.
- [9] J.D. Morse, A.F. Jankowski, R.T. Graff, J.P. Hayes, *J. Vac. Sci. Technol. A* 18 (2000).
- [10] H.-J. Kim, M.H. Litt, *ACS Polymer Preprints* 42 (2001) 486.
- [11] C. Genies, R. Mercier, B. Sillion, R. Petiaud, N. Cornet, G. Gebel, M. Pineri, *Polymer* 42 (2001) 5097.